The Physics and Mathematical Theory of Nano-Scaled Ring Resonators and Loop Antennas

Arnold F. McKinley

A dissertation submitted for the degree of
Doctor of Philosophy
The Australian National University

October 2014

Final – 16 October 2014

Final – 16 October 2014

Except where otherwise indicated, this thesis is my own original work.

Arnold F. McKinley
16 October 2014

This Dissertation is dedicated

To my mother who suggested that I join the radio club in high school
so that my father would have something to talk to me about;
and
To my father who talked to me about
Closed Circuit Resonant Loop Antennas (CCRLs).

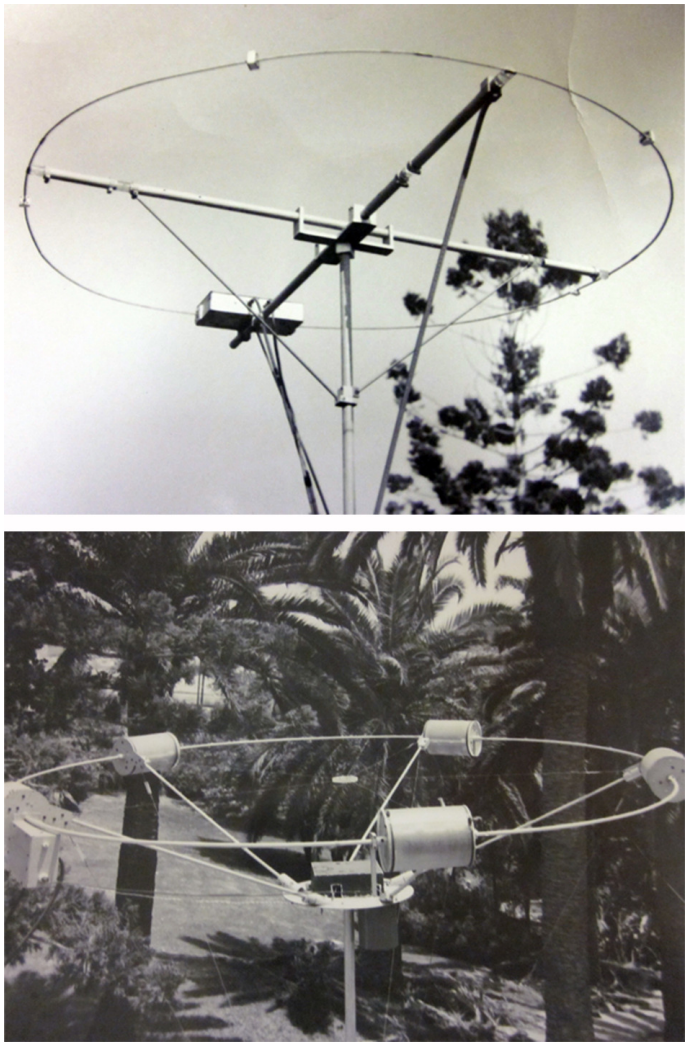

Figure 1: Two CCRLs from 1967; McKinley II [1968c]. The loops used the zero-order mode resonance. They had six sections and operated in the 20 meter amateur band.

Acknowledgments

No one writes a PhD dissertation without support from many people for several years. I have many people to thank.

- Since one doesn't begin doctoral studies without an invitation to do so, I must thank my Supervisor, Dr. Kylie Catchpole, who initiated the invitation in 2009, for the opportunity to work on her team of Research Fellows, Post-Docs, and other PhD students. Her guidance, insights, questions and encouragement throughout the years of study led to some remarkable breakthroughs and discoveries. She taught me how to create detailed, focused, and useful journal papers, and how to think like a nano-photonics expert. I am pleased and thankful also for her financial support.

- I am also very grateful to my second advisor, Dr. Tom White, for his quick understanding of the nuances of my issues and the range and the depth of insight with which he viewed my work. I am greatly impressed with his ability to move easily from nano-photonics physics to electrical engineering and with his ability to gauge the consequences of a hypothesis. I am very grateful for his reviews of my journal papers and his reading of the dissertation. Throughout these past years I have benefited from many of his clever ways of rethinking knotty problems.

- Dr. Angelika Basch, my third advisor, quickly became a close friend and confidant. She arrived at the Centre from Austria on the same day I did in 2010, for a Post-Doc position. She introduced me to Europe and to a wide range of continental friends and continental ideas. I am grateful for her friendship, support, and review of papers and the dissertation.

- I want to thank also the members of Kylie's Nano-photonics group, who supported me with their friendships. My appreciation to Dr. Niraj Lal, who asked some pointed questions in meetings, causing some research work that led to an important insight. I particularly want to thank Dr. Dibakar Chowdhury, who joined us in the last year with a background in meta-materials; he had much to say positively about my work, had useful comments following my presentations, and read the dissertation while in preparation.

- The Nano-photonics group is one group among several within the Centre for Sustainable Energy Systems at the ANU. I want to thank the Director, Dr. Andrew Blakers, for his support and Dr. Igor Skyrabin, who kept telling me not to get distracted on things unrelated to the PhD, as I was so prone to do. There

is a strong academic and technical laboratory team at the Centre, with whom I became close associates and friends. My thanks goes to each of member of the team.

- I particularly want to thank Dr. Andres Cuevas, now the Acting Dean of the Research School of Engineering and Computer Science, for his support throughput the time I was at the ANU. And Dr. Alan McIntosh, Professor of Mathematics at the ANU for his close friendship and help with some mathematical subtleties.

- I also want to thank Dr. David Powell, Dr. Chennupati Jagadish and Dr. Yuri Kivshar within the Research School of Physics and Engineering, who set up a seat for me on the CST simulation software license, used within the School. There were several members of their groups that I need to thank as well: Drs. Andrey Miroshnichenko, Dragomir Neshev, IlyaShadrivov, Ivan Maksymov and Suddha Mokkapati.

- Those marking this dissertation are unknown to me. I appreciate their time and their efforts.

- I want to thank my very good friends, Lachlan Black and Chog Barugkin, who kept me sane through these long years of work.

- I would like to thank my daughter, Alyssa, who keeps life bright for me, and my brothers and sisters, who thought it a marvellous adventure to travel so far away to Australia for study.

- Finally, I would like to thank the Australian Research Council and the Australian Solar Institute for partial funding support.

Abstract

This thesis is based on the realisation that no analytical theory of loop antennas and rings exists that is at once applicable to the Radio Frequency (RF), Micro-wave (MW), TeraHertz (THz), Infra-red (IR), and Optical (OR) regions. Nor is there any Electrical Engineering circuit model, rigorously developed from the results of that theory, that generates results which match numerical simulations and experimental work in the literature across all of these regimes.

This thesis fills that gap.

Maxwell's equations for perfectly conducting, closed circular loops are presented, and then solved, using standard RF and MW antenna theory. The governing equation is then extended to include real, lossy metals with focus on the noble metals, gold, silver and copper. The solution to the extended equation yields results for rings in the THZ, IR and OR. Next, the governing equation is extended to include a single impedance on the periphery. The solution is studied using a capacitive reactance, in particular. These results are compared to simulations of illuminated rings with a single gap, and a relationship is developed between the width of the gap and its capacitive reactance. Primary results are these:

- An analytical set of mathematical functions derived from Maxwell's equations now exist that give the current distribution on closed and single gapped loops at all frequency regimes from the RF through OR, constructed of any metal for which the index of refraction is known.
- A detailed RLC circuit model has been derived from these functions, accurate at all frequency bands, from which the total R, L and C of the loop at any frequency or wavelength, and the R, L and C of any modal resonance, can be calculated. The model yields the functions $R(\omega)$, $L(\omega)$, $C(\omega)$ from which radiation resistance, power loss, radiation efficiency, radar cross-section, and the quality factor (Q) of any resonance can be calculated.
- The input impedance of the circuit model representing the loop can be calculated as a function of wavelength for closed loops and single gap loops.
- The introduction of a single gap in the periphery of a loop will cause a very high-Q resonance in the sub-wavelength region. This is due to the zero-order mode inductance of the loop resonating with a combination of the gap capacitance and the closed loop capacitance. The Q is on the order of several thousand.
- Gap width and capacitance value of the gap are closely related. However, none of the simple models suggested in the literature, such as the flat-plate capacitance model, generates the correct relationship, at least for gaps in rings.

Contents

List of Figures

List of Tables

Part I

Preliminaries

Chapter 1

Preface

Sometimes scientific discovery requires the insights of those who do not see the world through the same perspective lenses as others do. For example, it might be said that everyone teaches themselves what they know; perhaps they learn to distinguish a 'truth' from 'fable' using discretionary criteria that they identified through trial and error or through a personal education. Where the community of modern scientists passes on its truth criteria through a complicated, multi-step, educational process that stresses induction, deduction, and the testing of nature for its final testimony to the facts, there are those who decide on these criteria through some kind of experience. But scientific criteria are difficult to understand; many people not exposed to this education are usually hard pressed to understand the scientific method, let alone employ it.

Yet, there are some particularly gifted people, who, having taught themselves what they know in their own peculiar way, avoid the normal educational process, but employ the scientific method rigorously and rather naturally. One of those persons was my father. In the early 1960s, I was away from home at a distant boarding school, allowed to phone home only once a week. Not liking the restriction, my father built two amateur radio systems and gave one to the school's radio club. He then designed from scratch, over the course of two experiment filled years, a naturally resonant, six-element loop antenna with a very high quality factor, and posted one on his house and one on the roof of the school. I have discovered, through the course of this thesis work, that he had found and exploited the "zero-order mode" resonance of rings. I talked often with him on that ham radio set, and the students talked with people all over the world. It was a marvellous communication system he had invented and it is too bad he never published. He called the antenna a "Closed Circuit Resonant Loop" (CCRL).

I took the design of that loop with me to graduate school in the 1970's and played with it in the Ginzton labs in the Electrical Engineering department at Stanford University, but had no tools to calculate or examine its radiation pattern. Not long afterward, while working at Stanford's Institute for Energy Studies on a study for the US Department of Energy, I thought how useful it would be to shrink the loop down to the incredibly small circumference of an optical wavelength to see how it might capture light and thus enhance energy capture for solar cells.

It turns out that that idea is not far-fetched. Today physicists in the nano-

photonics community are beginning to realize that there may be benefits in applying radio frequency (RF) antenna theory in the THz and optical regions. That viewpoint, applied to solar cells for example, sees nano-particles and nano-structures as light energy capturing devices, which makes them, by definition, antennas. Very simply, in this thesis, I want to apply analytical techniques that I know from RF antenna theory to nano-scaled rings, fabricated for the optical region. Will these nano-scaled rings act the same way as ring antennas do in the RF, and if so, can I design a high-Q, nano-scaled ring that will capture light as effectively as it captures RF energy?

Chapter 2

General Introduction

2.1 Motivation

The closed circular loop never served as an effective antenna for communication at radio frequency during World War II or after, because of its broad, low-Q resonances and its tendency to radiate on multiple harmonics. Small loops were viewed mostly as magnetic sensors. The analytical study of so-called "large loops", those with circumferences on the order of the incident wavelength, was limited in scope to a few papers in the mid-late 20th century; namely, Storer [1956], Wu [1962], and Kanda [1984]. But in 1999, after a modest circuit theory analysis of ring structures, Pendry et al. [1999] suggested that two nested loops, each with a gap, but one twisted 180 degrees with respect to the other, would create, in consort with others in a 3D array, a negative permeability structure, unlike any material found in nature. This effect came to be the identifying mark of meta-materials.

Smith et al. [2000] added to the Pendry ring structure, a cylinder which provided simultaneously a negative permittivity, thereby creating a negative index of refraction material. A 3D structure was built using a square loop as the basis for the meta-material two years later by Shelby et al. [2001] and indeed, it displayed a negative index of refraction at the resonance calculated. Since then, rings with gaps, called "split-rings", have been found useful for high definition imaging, radiation beam control, tiny Fresnel lenses, single photon emitters, medical sensors and a host of other applications.

The central identifying effect is a very high Q resonance in the region where the excitation is greater than double the circumference of the loop; now called the "sub-wavelength" region. All of these authors identified the effect as the resonance of an LC circuit created by the loop, which acted like the inductor (L), and the gap (together with coupling between the loops), which acted like the capacitor (C).

A large number of papers have appeared since then, applying LC circuit models to circular and square rings of varying sizes, attempting to understand the origin of the resonance (see Shamonin et al. [2004, 2005]; Radkovskaya et al. [2005]; Sydoruk et al. [2009]), and in some cases attempting to learn how to tune the resonance (see Aydin and Ozbay [2007]; Zhou and Chui [2006]; Chowdhury et al. [2011b]).

These *LC* models are simple ones, aimed at determining the cause of the sub-wavelength resonance. But the loop is a much more complex beast than such straight-

forward models would imply, and with such recent intensity around the periphery of the subject, it seems time to pursue a direct study of the loop in all of its complex character. The motivation is simply this: to discover where the loop resonates, under what conditions, and how well. How many resonances are there? Is it a broad band or a narrow band antenna? Can the *RLC* circuit model suggest alternative ways of using it at the higher frequencies?

There are several fertile areas of research that will benefit from this work.

2.2 Extending RF Antenna Theory to Nano-photonics

The first reference that uses the word "nano-antenna" seems to have occurred in this century (Lyshevski and Lyshevski [2000]), associated with the field of nano-electromechanical actuators, a field that has been around for some time. It appears in a figure referring to a "nano-switch", constructed with a carbon-nanotube and molecular wire situated above a non-descript entity identified as a "nano-antenna". The usage occurs once in the article and does not occur in any of the cited works.

This is not to say that using the term "antennas" to refer to radiating structures in the optical region does not pre-date the year 2000. Recent papers reviewing the field of "nano-antennas" (Alda et al. [2005]; Gonzalez and Boreman [2005]) cite papers as far back as the mid-1970's. Most of the early modern work, in which wires and similar devices were thought of as optical antennas, appears in the late 1990s in the field of near-field imaging (Novotny [2007b]). Apparently the first application using the scattered light from a nano-sized particle can be attributed to (Synge [1928]). This idea incorporates the idea of capturing incident light and the idea of capturing the reradiated "scattered" light for some use; both of these are functions of antennas. But Synge never used the word "antenna" to refer to the particles involved, nor did any other physicist until 1985. Novotny says that it was John Wessel [1985] who first mentioned the analogy to classical antenna theory.

Alda et al. [2005] suggests that the constant need for broadening communications bandwidth demanded the study of antenna design at higher and higher frequencies and that this improved the fabrication of useful antennas in the micro-wave region. But the development did not continue into the THz and optical regions in a reliable way because semiconductor detectors had made lightwave links possible in free space and along optical fibres. Reliance on classical engineering antenna theory then became unnecessary. Only recently, he suggests, has the need to improve these detectors caused physicists to take another look at the field.

Therefore, treating closed and split-rings as antennas, by applying standard antenna theoretical approaches to light-matter interactions, and by commingling antenna theory with the standard physics of nano-photonics, as this thesis does, contributes to a more broadly applicable understanding of light-matter interactions.

2.3 Nano-Antennas as Tiny Copies of RF Antennas

One obvious first place to bring antenna theory to the optical region is to see what happens when one miniaturizes RF antennas. Several reviews of work performed in the first decade of this century exist: for example, Alda's, Bharadwaj et al. [2009], Novotny and Van Hulst [2011], and Krasnok et al. [2013]. The list of antenna types and of uses to which they have been applied is rather long, and includes single photon emission (Maksymov et al. [2012]), imaging techniques (Koh et al. [2010]), bio-sensors (Larsson et al. [2007]), solar cells (Mokkapati et al. [2011]), and Raman spectroscopy (Fan et al. [2011]).

But since rings have little useful history in RF work, analytical advances more complicated than the simple ring structure were never pursued. The exceptions might be where rings are used as magnetic sensors (Kanda [1984]). Consequently, few researchers expected such rings to be useful if replicated at the higher frequencies. The surprise is that arrays of rings with gaps in them create negative permeability materials, the so called "meta-materials" (Pendry et al. [1999]). Research into what rings could do suddenly flourished in the first decade after the discovery. Now rings, singly and in various array configurations, have been shown to create Fresnel lenses (Memarzadeh and Mosallaei [2011]), tunable antennas in the THz region (Chowdhury et al. [2011b]; Chiam et al. [2010]), and beam shapers (Ahmadi and Mosallaei [2010]). It is only reasonable to expect that a detailed analytical model, describing all magnetic and harmonic resonances of the ring, of various thicknesses, with and without gaps, applicable at all frequencies, would shed some light on new uses and functions of rings. This thesis will fill that gap in understanding.

2.4 Enhancing light capture in solar cells

The most common solar cells are made of crystalline silicon with textured surfaces of small pyramids. When incoming photons hit the surface of a solar cell, they will either enter the cell or be reflected. When they encounter the pyramids, reflected photons are more likely to hit another pyramid rather than escape back into the medium. This enhanced light capture increases the chances of creating hole-electron pairs within the cell's active region thus causing larger currents. Other structures have also worked well. Among those tried have been metal particles (Beck et al. [2010]), gratings of various lengths and period (Heine and Morf [1995]; Yu et al. [2010]; Wang [2012]; and Chong et al. [2012]), nanowires (Lin and Povinelli [2009]), and other plasmonic scatterers (Catchpole et al. [2011]; Mokkapati et al. [2011]).

The natural next question to ask is "What about a resonating ring structure or ring arrays?". If the resonant characteristics of rings were known in detail, could an array of rings be designed that enhances light capture by carefully managing their resonating properties? Could they be used to shape the re-radiated beam out of the internal light-cone to enhance capture? Could their very high Q be used to capture specific regions of the solar spectra? Could nested rings be used in this search for a higher efficiency solar cell? A detailed analytical study of ring resonances should be

able to recognise the options.

Chapter 3

Differing Perspectives on Wave-Matter Interactions

3.1 Introduction

Two different research groups have evolved two different languages for speaking about the underlying physics of wave-matter interactions in two different regions of the spectrum. One region is where low frequency waves interact with antennas for the purpose of communications, the other is where infra-red and optical waves interact with molecular structures forming the surface and bulk of materials. The region in between has formed a sort of "no-man's land", since communications has not been possible there and optical-like phenomena did not occur there. That "no-mans land" thinned and disappeared in the first decade of this century.

Even though each research group begins with the commonly well understood language of Maxwell's equations, differences arise due to scale and to the focus of their research. Indeed, both groups solve Maxwell's equations using the same techniques and the solutions often look nearly the same.

In the case of low frequency radio (RF) and micro-wave (MW) communications, the scale is large, meaning that the wavelengths with which this research group works are on the order of 3 mm and longer. In the case of optics, the scale is small; wavelengths are on the order of 30 μm and less. In the former case, engineers have abstracted their solutions to Maxwell's equations by creating abstract devices that automatically solve certain forms of the equations under certain conditions. These are the resistor R, the inductor L and the capacitor, C. These abstractions have been created in such a way that they can be constructed physically; that is, they have real, physical counterparts and the electrical engineers who use them, build circuits that manipulate and control electric and magnetic fields. In essence these circuits take the place of Maxwell's equations, and some engineers know circuitry but do not know Maxwell's equations. They develop complex results that were never scripted by any written equation at all. The terms these engineers use, such as "voltage" and "current", "input impedance" and quality factor "Q", reflect the behaviour of this large scale phenomenon.

In the latter case, physicists working in non-linear optics give names to the so-

lutions of Maxwell's equations, such as "plasmons", "polaritons", or "evanescent waves". Light is "scattered", "reflected from", and "transmitted through" substances. Electrons and other particles are affected by light waves, raising their "energy state" and "jumping a band-gap"; these particles have a "lifetime" and a "decay-rate". These physicists want to know, for example, how the "index of refraction" affects all of these phenomena.

Recently electrical engineers have become interested in communication possibilities at THz frequencies, while non-linear optics physicists have become interested in the MW behaviour of negative index of refraction meta-materials. Since no-mans land is thinning, the two languages are meeting head-on and causing some confusion.

In one way, this thesis is a meeting of two cultures. Low frequency antenna theory, the language of electrical engineering at low frequencies, will be used to speak about short wavelength optical phenomena. This chapter explains some of the similarities and differences between the two approaches, so that the reader will have a sense of the two bases that underlie the work.

The language and perspective of low frequency antenna theory has always been the language of electrical engineers, because it is they who tamed electromagnetic theory for the express purpose of low frequency communications. As a consequence, the diagrams, analysis and perspective of antenna theory incorporates large amounts of electronic circuit theory, which relies heavily on simplified versions of Maxwell's field equations. Indeed, [Kraus and Carver, 1973, See Chapter 9.] show how Maxwell's equations are generalizations of basic circuit theory concepts, such as Ohm's Law and Kirchoff's Laws.

The language and perspective of optical physicists has remained with Maxwell's field theory. Their work began with the optical response behavior of materials, particularly relating to refraction, absorption, scattering, and transmission phenomena and continues today as they study many new phenomena, such as negative-index of refraction materials and surface plasmons, and new uses, such as single photon emission.

Recently, though, the two worlds have become intertwined. Communications engineers have moved into the microwave (MW) region and now seek to move into the Terahertz (THz) region (Akyildiz et al. [2014]). Physicists have found ways of producing "optical-like" effects at microwave frequencies in configurations of circular and square loops, called "meta-materials" (Smith et al. [2000]). One of these effects, by which a meta-material object becomes invisible to incident wavelengths, would have many practical applications if brought to the optical wavelengths. As yet, this remains an unachieved goal in the optical regime.

As the regions between engineering communications and optical applications grows tighter, it would be beneficial for engineers and physicists to converse and to share the languages and perspectives of both regions for the purpose of improving understanding and control of the physical behaviour of material objects.

This section aims to highlight the work that has been done over the last fifteen years to bring the methods engineers use to study wave-matter interactions to the op-

tical region and to show similarities and differences with the methods physicists use to study nano-photonic phenomena. This section is important because the engineering methods discussed here will be applied throughout the thesis, and a physicist needs to know the way of thinking that leads to this attempt at characterising nano-scaled rings.

3.2 Wave-Matter Interactions from the Perspective of Engineering

3.2.1 The Engineering View of Particles and Fields

As history goes, electromagnetic fields were discovered and explained mathematically in the mid 1800s, about 40 to 50 years before the electron was discovered. Faraday's experiments in the 1840's and 1850's showed that interactions occurred between currents and magnetic phenomena. In the 1860's, Maxwell translated Faraday's idea of lines of flux into electric and magnetic fields and developed a set of equations, which also incorporated work by Ampere and Gauss, that showed explicitly how these fields interacted with current flowing in materials. But no one knew what constituted currents until the early 1900s when atomic theories of particles showed that electrons moved and carried with them a negative charge. By that time, engineers had invented models of large scale, wave-particle, phenomenon, which had, as a convention, a direction of positive current flow with respect to driving voltage that was opposite to the actual direction of electron flow. In other words, conventional current flows in the opposite direction from that which constitutes the phenomenon.

The simplest of these models are used regularly in engineering circuit design. They are the resistor (R), which describes the basis for energy loss in a system (essentially Ohm's Law); the inductor (L), which describes the basis for current and magnetic interactions in a system (essentially Faraday's Law of magnetic induction); and the capacitor (C) which describes the basis for electric charge storage in a system (essentially Gauss' Law of electric flux).

With these tools in hand, it is only natural then that engineers would think almost exclusively in terms of voltage and current flow control, as the primary means of attaining selected goals. Voltage and current are, for engineers, the real thing now, not Maxwell's equations. These circuit elements are no longer considered idealisations, or a short-hand, for Maxwell's equations, since they can be constructed to behave nearly linearly and to follow the mathematical specifications of Maxwell's equations. Rather, circuit elements are thought of as manipulators of voltage and current. This is true, even though real resistors, inductors and capacitors all have non-linear aspects when pushed to the boundary of their material and construction limits.

3.2.2 Circuit theory Applied to RF Communications

In communications, the primary goal of circuit design has been the transmission and delivery of information over long distance without the need of wires. The means for

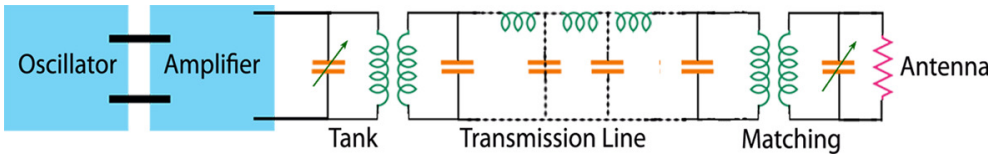

Figure 3.1: A design of a tank circuit, transmission line, and antenna. The impedance on the right end represents the antenna. One varies the capacitance of the tank and sometimes of the matching circuit at the antenna in order to get resonance and best energy flow.

doing this was the manipulation of electromagnetic waves, first by modulating the amplitude of carrier waves (AM) and later by modulating the frequency of the carrier waves (FM). These discoveries were nothing short of genius.

Three of the more important ideas that enabled these means; (1) the mastery of the phenomenon of resonance, (2) the transmission line, and (3) mastery of impedance matching and wave matching; that is, determining the conditions under which a wave travelling down a wire matches to free space. In the first, current and voltage are set oscillating at some frequency in pre-amplifying circuits of the transmitter, amplified, then handed to a circuit consisting of an inductor in parallel with a capacitor (see Fig 3.1). This is called a "tank" circuit, because, if the frequency matches the resonance condition of the LC circuit, energy rises within the magnetic and electric fields of the inductor and capacitor and the tank circuit acts like a storage device. This rise continues until the rate of energy loss, due to resistive heat loss and to extraction by a transmission connected at the other end, matches the incoming flow rate of the energy.

The transmission line removes energy from the tank circuit best under the condition that the ratio of voltage to current remains in the same "balance" as in the tank circuit. That ratio is critical to successful energy transfer down to the antenna. The balance is called the transmission line's characteristic impedance. A typical value is 50 ohms.

The antenna provides wave matching. The word "antenna" was coined, apparently, by the Italian inventor, Guglielmo Marconi, during experiments in the Swiss Alps in 1895. He used the word to refer to a wire he dangled from a vertical pole. In Italian, the central pole holding up a tent is called 'l'antenna centrale' (Gardiol and Fournier [February 2006]). The antenna is usually seen as a wavelength matching device, in the sense that the wavelength coming off the transmission line needs to be reformed into something that can become an electromagnetic wave in free space ([Balanis, 2005, See for example, Chapter 1, page 1]). This makes the antenna a sort of "transition" device. For example, dipoles open up the transmission line to couple the electric component of the wave to free-space. Vee and Rhombics do the same thing more cleverly. Horns open up the mouth of a waveguide allowing the microwave to match itself to free space. Alternatively, antennas can be thought of as transferring the balance between voltage and current to the $\vec{E}$ and $\vec{H}$ fields of free-space. The dominant view of the antenna as a wave-matching device has proven quite successful.

Circuit theory can be applied from the tank circuit through the transmission line to the antenna. The tank and the antenna can be modelled using lumped elements, while the transmission line is modelled using distributed elements. A lumped element occupies one position in a circuit and carries a distinct value; it performs a distinct task. A distributed element is expressed in terms of density, eg. ohms per meter, and represents a section of the circuit spread over some distance. The antenna, which is our interest here, is treated as an impedance, usually as a series RLC circuit, where the R represents the radiation resistance.

The use of distributed elements to represent the antenna is not often done in the RF region, but work has been done on the ring at THz and optical frequencies which uses distributed elements (for example, see Shamonin et al. [2004]). It is natural to try distributed elements, particularly when lumped elements do not seem to apply, usually when the wavelength is roughly the same size as the antenna.

There are two ways of energizing an antenna: either by connecting it directly to a voltage or current source, or by illuminating it with an ambient wave. Connecting it to a source, such as a transmission line, causes the antenna to transmit energy. Illuminating the antenna with a plane wave causes currents to flow in the antenna and energy to be transferred to the transmission line in reverse of transmit, in such a way that the line moves energy to a receiver. The position of a switch on the transmit/receive side of the line decides whether the antenna is in transmit or receive mode (Collin [2003]).

3.2.3 Scattering and Absorption From an Electrical Engineering Perspective

The quality of an antenna shows up in its radiation capabilities, given in terms of several important measures: gain, directivity, radiation patterns, power pattern, polarisation, effective aperture and the radar cross-section. Many of these are directly determined by the current distribution over the surface (and bulk, if the material is lossy) of the antenna. Generally, the larger the current, the better the quality measures.

The term "radar cross-section" (RCS) comes, as one might imagine, from the early days of world War II, when early knowledge of airborne attacks was crucial to effective response. A transmitter sent a directed plane wave toward an area of interest, and if an aircraft was present, the wave would reflect back to the source as an echo. The time between transmission and receipt would give an indication of how far away the aircraft was and its speed. The "cross-section" refers to the effective area presented by the aircraft to the incident plane wave; the larger in area the reflection, the larger the cross-section. There are two RCS modes: (1) mono-static and (2) bi-static. In the first, the receiving radar is in the same location as the transmitting radar. In the second, it is not.

RCS is, by definition,

$$RCS = \frac{\text{Power scattered to receiver per solid angle}}{\text{incident power density / } 4\pi} = \lim_{r\to\infty} 4\pi r^2 \frac{P_{sc}}{W_i} \tag{3.1}$$

where a spherical shell of radius r encircles the target. The incident power density, W_i, is that which is usually given for an illuminating wave per unit square meter of the plane determined by the cross product of the incident electric and magnetic fields, $\vec{E}_i$ and $\vec{H}_i$. It is sometimes called the power intensity. Hence the reason for the units of m^2 for the cross-section. The resulting cross-section has an area that grows as the size of the target grows, unless the target has been engineered to hinder reflections, particularly in the direction of the receiver. One would expect the RCS of a human to be about 1 m^2, for example, or a fighter aircraft perhaps 100 m^2.

RCS is not an easy calculation if done by hand, since the incident and scattered waves interfere. The rate with which energy density passes through the surface of the sphere depends on the absorption, because if there were no absorption, the same amount of energy would scatter outward as inward and the total net power density flow would be zero. In fact, this means that the net power density flow, W_T, through the surface, S, is excess inward and therefore exactly the negative of the amount absorbed.

$$W_{abs} = -\int_S \vec{W}_T \cdot d\vec{S} \tag{3.2}$$

The net power density is given by the sum of the incident power density, $W_i = \frac{1}{2}\mathrm{Re}(\vec{E}_i \times \vec{H}_i^*)$, the scattered power density, $W_{sc} = \frac{1}{2}\mathrm{Re}(\vec{E}_s \times \vec{H}_s^*)$, and the power density due to the interfering terms, $W_{int} = \frac{1}{2}\mathrm{Re}(\vec{E}_i \times \vec{H}_s^* + \vec{E}_s \times \vec{H}_i^*)$.

If inward is taken positive and outward negative, then the second of the four terms (the scattered power term) will be negative. Bringing it to the left side will leave three terms on the right, one representing the incident power and two representing the interference. The result is called the "extinction", W_{ext}.

$$W_{ext} = W_{abs} + W_{sc} = \frac{1}{2}\mathrm{Re}(\vec{E}_i \times \vec{H}_i^* + \vec{E}_i \times \vec{H}_s^* + \vec{E}_s \times \vec{H}_i^*) \tag{3.3}$$

In illuminating an antenna structure, one expects to find the incident plane wave inducing currents. Usually the current is drawn off the antenna into receiving circuitry, but if that is not done and the energy is left in the loop, it re-radiates, giving rise to forward and backward scattering, as shown in Fig. 3.2. If the frequency of illumination matches one of the loops resonances, where more current occurs than at some other frequency, one would expect a higher scattering cross-section. One would further expect to see a higher cross-section when receiving along its radiation beam than not. All of these factors go into accounting for the RCS of an antenna.

The illuminating beam induces current flow in the antenna, part of which is then absorbed in the material resistance as a loss, W_{abs}, and part of which is re-radiated as scattered energy, W_{sc} out of phase with the incoming beam. The latter occurs in the radiation resistance. We have

$$W_{sc} = \frac{1}{2}I^2 R_{rad} \quad \text{and } W_{abs} = \frac{1}{2}I^2 R_{loss} \tag{3.4}$$

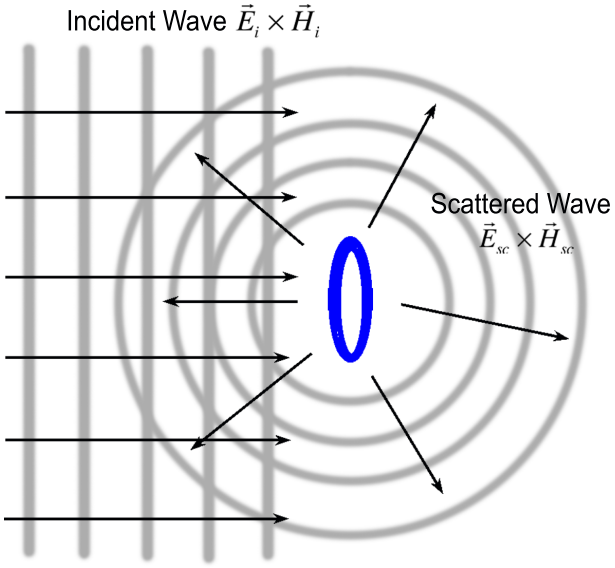

Figure 3.2: The relation between fields during scattering off a loop antenna.

The RCS and the Absorbed Cross-section (ACS), then are

$$RCS = \lim_{r\to\infty} 2\pi r^2 \frac{I^2 R_{rad}}{W_i} \quad \text{and } ACS = \lim_{r\to\infty} 2\pi r^2 \frac{I^2 R_{loss}}{W_i} \tag{3.5}$$

When a numerical simulator such as MWS[1] is used to calculate the radar cross-section of the loop in Chapter 10, the results will be proportional to the square of the current times the radiation resistance. We expect to see cross-sections about the size of the square area of the ring; about πb^2, where b is the radius of the ring. If $b = 1um$, the cross-section ought to be about $3.14 \times 10^{-12} m^2 \approx 3\mu m^2$.

3.3 The Language and Perspective of Nano-Photonic Physics

3.3.1 Reflection, Refraction, Absorption, and Transmission From a Physics Perspective

Standard experimental tests of surface phenomena employed by physicists use plane wave illumination, even in simulations. There is no concept of a voltage or current source; there is no way, in fact, on the nano-scale to employ such a thing. The physicist's first impulse is to illuminate a target to see what happens, rather than model it. Engineers tend to do the reverse. Consequently, if one wants to energise a ring structure of some sort on the surface of a solar cell, for example, the standard approach is simply to illuminate it and measure the resulting reflection and transmission spectra. Some light will reflect from the surface, some will be absorbed, and some will

[1]See Appendix A

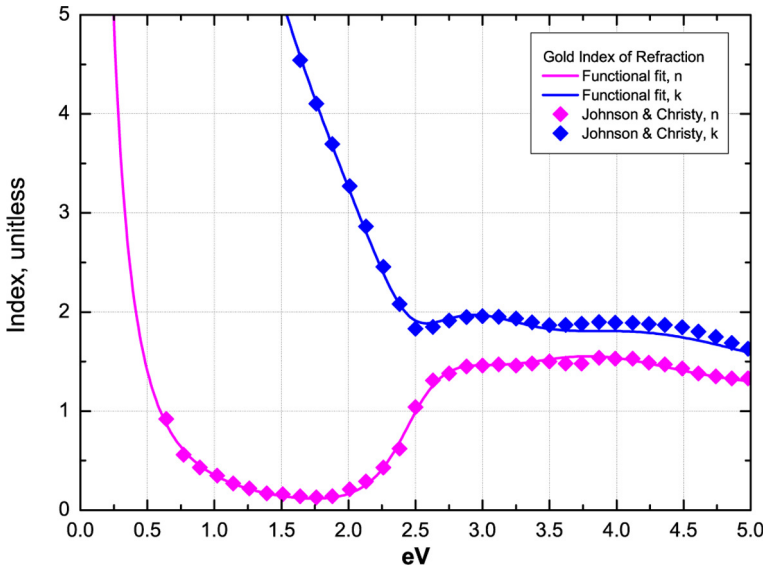

Figure 3.3: The index of refraction of gold, as given by Johnson and Christy [1972]. The inter band transitions are seen in the abrupt change in both the real and imaginary parts of the index.

escape the other side as a transmitted wave. The degree to which each occurs can be calculated and is represented by a decimal value between 0 and 1.

Since light refracts when passing through bulk material, the effects of a material on the refraction of light forms a central focus of study. Since refraction is characterised as an complex index, which varies by material and varies over frequency, it describes amplitude and phase changes throughout the bulk quite handily. It is so important that the index plays a central role in calculations of reflection, absorption, and transmission. The latter have a smooth variation for the most part from low to high frequency, until the optical region, where the index suddenly experiences rapid fluctuations. They are due to sudden influxes of electrons into the conduction band from the upper band states of the bulk material when hit by the incident photons. These fluctuations are called "inter-band transitions". Figure 3.3 shows the index of refraction for gold against photon energy (eV). The smooth curves on the left abruptly divert in the middle of the visible region because of the inter-band transitions. This change appears in the higher reflection of photons in the the higher energy part of the spectrum beginning from orange through UV.

In physics, the scattering cross-section is thought of in the same way as in engineering with, however, the lack of a 4π.:

$$SCS = \lim_{r\to\infty} r^2 \frac{P_{sc}}{W_i} \quad \text{and } ACS = \lim_{r\to\infty} r^2 \frac{P_{abs}}{W_i} \tag{3.6}$$

Consequently, characterising a nano-scaled ring using an illuminated plane wave makes sense to a physicist, and the measures will have the same meaning. This correspondence is particularly easy to understand, since antenna radiation in the

far-field has dipole moments, just like scatter from illuminate particles do (Jackson [1999]). The characterisation will be done in Chapter 10.

3.4 General Conclusions on the Differences in Perspectives and Language

Two close encounters between engineering and nano-photonics have occurred, both beginning in the early 2000s. The first follows a line through the literature from Pendry et al. [1999]'s use of RLC circuit elements to describe meta-materials in the MW to a large number of articles treating nano-particles and other nano-structures in the THz and optical region as nano-antennas, with characteristics also to be understood using RLC circuit models (Alda et al. [2005]; Bharadwaj et al. [2009]; Mokkapati et al. [2011]; Novotny and Van Hulst [2011]; Agio [2012]). The second follows a line from Engheta et al. [2005]'s search for nano-circuit elements to Staffaroni et al. [2012]'s development of RLC circuit elements for plasmonic behaviour.

The time is ripe therefore, for applying low frequency antenna theory, using RLC circuit elements, to a loop or ring, a nano-structure which hasn't yet been used for many nano-photonic applications. The effort would tie together the first and second threads noted above, show how antenna theory elucidates ring behaviour in meta-materials, and test whether engineering design methods developed at low frequencies can be applied to nano-photonic applications in the optical region.

Chapter 4

The General Theory of Resonance

4.1 Introduction

Resonance is a general physical phenomenon, in which a system oscillates in response to a driving signal such that more energy is stored in the system than is dissipated. The loss may occur as heat loss or radiation loss. The phenomenon occurs over a range of frequencies, called the “bandwidth", and some systems typically show wider bandwidths than others.

The phenomenon is handled in electrical engineering using *RLC* circuit elements. A system’s resonances are governed by specific combinations of these, of which there are two primitives, the series *RLC* circuit and the parallel *RLC* circuit. This chapter presents these primitives because the loop antenna, and the nano-scaled ring, at any given frequency, can be represented by combinations of either. I select the series circuit representation and give reasons for that choice in Chapter 8. This chapter serves as foundation material for Chapter 5 and for the rest of the thesis.

The general theory of resonance is discussed first, followed by its application to electrical circuits. The next chapters apply these results to the ring.

4.2 The Theory of Resonance

4.2.1 Governing Equation of Resonance

Systems described by the following differential equation oscillate and will resonate:

$$y = m\frac{dx}{dt} + \gamma x + k\int_0^{t'} x dt' \tag{4.1}$$

where m, γ and k are constants and the forcing function is a constant amplitude oscillation, $y = Y_0 e^{i\omega t}$, with initial conditions of the system having no first or second derivative and $x(0) = X_0$. One can eliminate the integral by differentiating through to create a second order differential equation, but the solution is straightforward in

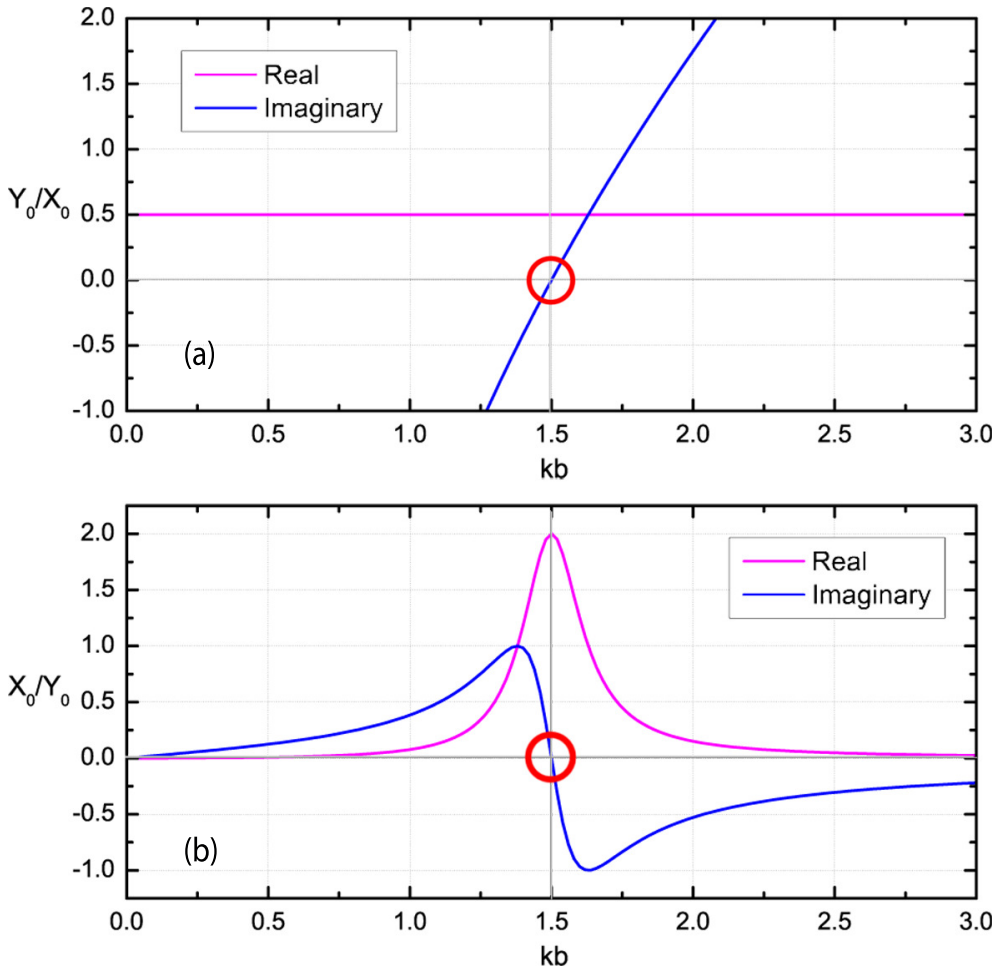

Figure 4.1: The two forms of resonance, (a) $\frac{Y_0}{X_0}$ and (b) $\frac{X_0}{Y_0}$ with $\gamma = .5, m = 2, k = 4.5$. The red circles mark the resonance, in this case 1.5 radians/sec.

either case. Substituting $x(t) = X_0 e^{i\omega t}$ and arranging,

$$Y_0 e^{i\omega t} = \left[i\omega m - i\frac{k}{\omega} + \gamma \right] X_o e^{i\omega t} \tag{4.2}$$

This is examined in its two forms:

$$(A) \quad \boxed{\frac{Y_0}{X_0} = \gamma + i\left[\omega m - \frac{k}{\omega}\right]} \quad \text{and} \quad (B) \quad \boxed{\frac{X_0}{Y_0} = \frac{1}{\gamma + i\left[\omega m - \frac{k}{\omega}\right]}} \tag{4.3}$$

These are simply inverses of each other, but the literature examines both forms when noting resonances. The real and imaginary parts of both forms are shown in Fig. 4.1.

The action occurs where the imaginary part equals zero; this is the "resonant" frequency; in Fig. 4.1, $\omega_0 = \sqrt{k/m} = 1.5$ radians/sec. Below resonance, $\omega < \omega_0$, the system element represented by k dominates the imaginary term, making the

imaginary part negative. Above resonance, the element represented by m dominates and the imaginary part is positive. In the case of (A) the real part is constant. In the case of (B), the real part rises to a peak then falls off again to zero at high frequencies.

The peak of the real part in form (B) is found by taking the derivative and setting it equal to zero in the standard way:

$$\frac{d}{d\omega}\left[\frac{X_0}{Y_0}\right] = \frac{1}{\gamma}\frac{d}{d\omega}\left[\frac{(\omega\omega_d)^2}{(\omega\omega_d)^2 + (\omega^2 - \omega_0^2)^2}\right] = 0 \tag{4.4}$$

where $\omega_d = \gamma/m$ is called the damping frequency, due to the damping constant, γ. Solving gives the peak: $\boxed{\omega_{pk} = \omega_0}$. That is, the peak occurs at resonance. The peak value itself comes from a substitution of this into (4.3)(B):

$$\left.\frac{X_0}{Y_0}\right|_{\omega_0} = \frac{1}{\gamma} \tag{4.5}$$

As γ goes to zero, the peak goes to infinity. It is this constant that limits the peak.

4.2.2 Energy and Quality Factor

The quality of resonance, Q, was originally applied to electrical resonances, and later to mechanical and other physical systems, and in that forum, Q refers to the ratio of energy stored during one cycle with respect to energy dissipated in that cycle. That is,

$$Q = 2\pi\frac{\text{Energy stored at resonance}}{\text{Energy dissipated per cycle at resonance}} = 2\pi\frac{E_{stored}}{E_{dissipated}} \tag{4.6}$$

In such systems, the energy stored at any moment at any frequency is given by the sum of the energies in the elements described by m and k. The element m is called the kinetic element, because in physical systems it is related to the momentum: $p = m(dx/dt) = m\dot{x}$. The k element is called the potential element because it is related to restoring forces in the system: $f = -kx$. Since $x = X_0 e^{i\omega t}$ and bearing in mind that since it is a complex number, the real part describes real behaviour, the energies corresponding to the two elements at resonance are:

$$\begin{aligned} E_m &= \frac{1}{2}m\mathrm{Re}(\dot{x}^*)\mathrm{Re}(\dot{x}) = \frac{1}{2}m\omega_0^2\left|X_0\right|^2\ \sin^2(\omega t) = \frac{1}{2}\frac{\omega_0\sqrt{km}}{\gamma^2}\left|Y_0\right|^2\ \sin^2(\omega t) \\ E_k &= \frac{1}{2}k\mathrm{Re}(x^*)\mathrm{Re}(x) = \frac{1}{2}k\left|X_0\right|^2\ \cos^2(\omega t) = \frac{1}{2}\frac{\omega_0\sqrt{km}}{\gamma^2}\left|Y_0\right|^2\ \cos^2(\omega t) \end{aligned} \tag{4.7}$$

The total energy in the system is:

$$E_T = E_m + E_k = \frac{1}{2}\omega_0\sqrt{km}\left|X_0\right|^2 = \frac{1}{2}\frac{\omega_0\sqrt{km}}{\gamma^2}\left|Y_0\right|^2 = E_{stored} \tag{4.8}$$

It can be seen that E_m and E_k have the same magnitude, but vary by the $\cos^2(\omega t)$ and $\sin^2(\omega t)$, so that the total energy, E_T, is constant in value and equal to either $|E_m|$ or $|E_k|$. In other words, the energy E_T flows from element k to element m and back again. At resonance the total does not change, which means that no energy enters or leaves the domain of the two elements. This is the energy stored, E_{stored}, in the resonant system. The magnitude of the energy depends only upon the factor $\sqrt{km}/\gamma^2$. If there is no damping, the energy goes to infinity.

The rate of energy dissipation is given by $\gamma \dot{x}^* \dot{x}$ (Goldstein [1980]). The energy lost over one cycle at resonance, therefore, is the integral

$$\begin{aligned} E_{lost} &= \int_0^{T=2\pi/\omega_0} \gamma \, \mathrm{Re}(\dot{x}^*) \, \mathrm{Re}(\dot{x}) dt = \int_0^{T=2\pi/\omega_0} \gamma \omega_0^2 \, |X_0|^2 \, \sin^2(\omega t) dt \\ &= \pi \omega_0 \gamma \, |X_0|^2 = \pi \frac{\omega_0}{\gamma} \, |Y_0|^2 \end{aligned} \tag{4.9}$$

Substituting Eqns. 4.8 and 4.9 into 4.6, the quality factor becomes:

$$Q = 2\pi \frac{E_{stored}}{E_{lost}} = \frac{\sqrt{km}}{\gamma} = \frac{\omega_0}{\omega_d} \tag{4.10}$$

Using Q, the total energy, (4.8), becomes:

$$E_T = \frac{1}{2} \omega_0 \gamma Q \, |X_0|^2 = \frac{1}{2} \frac{\omega_0}{\gamma} Q \, |Y_0|^2 \tag{4.11}$$

The solutions (4.3) to the differential equation (4.1), then take the form:

$$(A) \quad \frac{Y_0}{X_0} = \gamma \left[1 + iQ \left(\frac{\omega}{\omega_0} - \frac{\omega_0}{\omega} \right) \right] \quad \text{and} \quad (B) \quad \frac{X_0}{Y_0} = \frac{1}{\gamma \left[1 + iQ \left(\frac{\omega}{\omega_0} - \frac{\omega_0}{\omega} \right) \right]} \tag{4.12}$$

When damping is low, ω_d is small, as noted above, and $\omega \approx \omega_0$. Then the peak of the real part of (B) may then be approximated by $1/\gamma$.

Squaring X_0 taken from (B) leads to

$$|X_0|^2 = \frac{|Y_0|^2}{\gamma^2} \left[\frac{1}{1 + Q^2 \left(\frac{\omega}{\omega_0} - \frac{\omega_0}{\omega} \right)^2} \right] \tag{4.13}$$

The two frequencies, one on either side of the peak, at which this squared value reaches one-half the peak, are called the "half-power" points, because the power is related to this square. Setting Eqn. 4.13 to 1/2 and solving for the frequencies gives,

$$\omega_+, \omega_- = \pm \frac{\omega_0}{2Q} + \frac{\omega_0}{2Q} \sqrt{1 + 4Q^2} \tag{4.14}$$

The difference between these is

$$\omega_+ - \omega_- = \frac{\omega_0}{Q} = \pm\omega_d \tag{4.15}$$

Alternatively,

$$Q = \frac{\omega_0}{(\omega_+ - \omega_-)} \tag{4.16}$$

4.3 Electrical *RLC* Circuit Models

In general, electrical circuits in electrical engineering are represented by a characteristic “input impedance", which represents the balance between the voltage and the current at the point where energy enters a circuit. When mathematically simplified, the impedance is a complex number; the real part representing the resistance (the absorption, if you will, in physics terms), and the imaginary part representing the reactance of the system (the phasing). The reactance is either positive or negative, and if positive, the system acts inductively; if negative, it acts capacitively.

Resonance occurs in an electrical circuit whenever the reactance of a system can be modelled at its input with an inductor (L) and a capacitor (C); both must be present. The inductor models the effects of the changing magnetic vector potential, that is, any Faraday Law behaviour in the system. The capacitor models the effects of the changing electric potential of the system, that is any Coulomb or Gauss' Law behaviour. At resonance the inductor and capacitor work 180 degrees out of phase with each other, so that when energy enters the inductor, it leaves the capacitor, and vice-versa. The energy remains within the two devices, increasing, until at resonance, the energy increases to infinity. In real systems, heat and radiation losses occur to limit the energy increase. These are modelled using a resistor. Once the rate of dissipation in the resistance of the system matches the rate of energy input from the driving source, the energy buildup ceases, and “steady-state” is achieved.

While many combinations of R, L, and C generate resonances, each of the resonances can be built from two primitives: the series and the parallel circuits shown in Fig. 4.2 (A) and (B). That is, a system with many resonances will have a number of inductors and capacitors, some in series, some in parallel, but when the analysis is complete, each of the resonances will consist of some mathematical combination of the inductors to produce one inductance, and of some mathematical combination of the capacitors to produce one capacitance.

Both primitives are governed by a differential equation that looks like (4.1), therefore they resonate. As with the generic resonant system of section 4.2, the energy at resonance in the inductor and in the capacitor are equal and the total energy within the two LC elements is constant with time. Since no energy enters or leaves the LC combination, the series combination does not add or subtract from the circuit current flow, which means that the two elements may be replaced by a simple wire at resonance and the circuit will behave the same; that is, the circuit will act like a

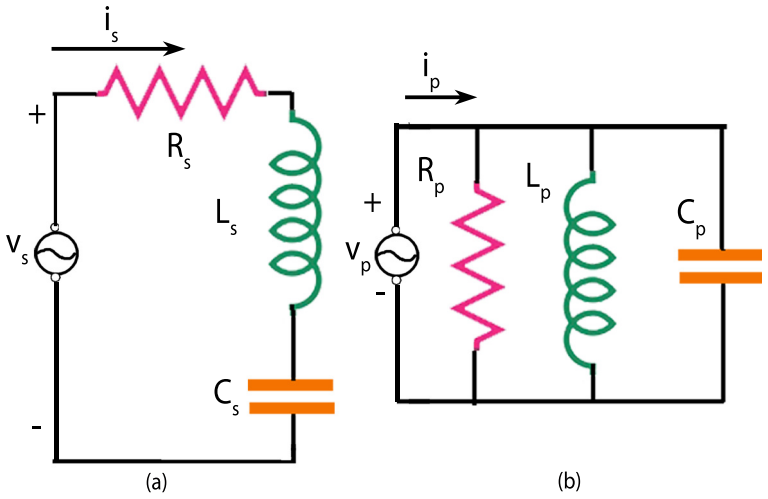

Figure 4.2: (a) A series resonant *RLC* circuit (b) A parallel resonant *RLC* circuit

simple resistor. The series circuit is therefore often called a "short-circuit" resonance. Similarly, the *LC* combination may be removed from the parallel circuit at resonance without effect to the behaviour of the system, since no current enters the *LC* combination and the circuit will act like a simple resistor. The parallel circuit is therefore often called an "open-circuit" resonance.

Since a loop antenna or ring can resonate, it can be modelled using various combinations of these two primitives. Exactly which models the ring best is the subject of Chapter 8. The following sections describe resonant *RLC* circuit models in enough detail that ring behaviour can be understood over the entire useful spectrum from Radio Frequency (RF) through the optical region.

The series resonant circuit is governed by the linear differential equation (A); the parallel resonant circuit by (B)

$$(A) \quad v_s = L_s \frac{di_s}{d} + R_s i_s + \frac{1}{C_s}\int_0^{t'} i_s dt' \qquad (B) \quad i_p = C_p \frac{dv_p}{dt} + \frac{1}{R_p} v_p + \frac{1}{L_p}\int_0^{t'} v_p dt' \tag{4.17}$$

Under the transformation

$$v_s \to i_p; \quad i_s \to v_p; \quad R_s \to \frac{1}{R_p}; \quad L_s \to C_p; \quad C_s \to L_p \tag{4.18}$$

both have the same form, that of a damped harmonic (resonant) oscillator. In this sense they are "duals".

4.3.1 The Series Resonant Circuit

Comparing (A) with (4.1), the transformation

$$y \to v_s; \quad x \to i_s; \quad m \to L_s; \quad \gamma \to R_s \quad \text{and} \quad k \to \frac{1}{C_s} \tag{4.19}$$

makes section 4.2 relevant to the series circuit. Applying those results,

$$\omega_0^2 = \frac{1}{L_s C_s}; \quad \omega_d = \frac{R_s}{L_s}; \quad \text{and } Q_s = \frac{\omega_o}{\omega_d} = \frac{\sqrt{L_s/C_s}}{R_s} \tag{4.20}$$

The two forms given in (4.3) appear as:

$$(A) \quad \boxed{\frac{V_0}{I_0} = R_s + i\left[\omega L_s - \frac{1}{\omega C_s}\right] \equiv Z_s} \quad \text{and} \quad (B) \quad \boxed{\frac{I_0}{V_0} = \frac{1}{R_s + i\left[\omega L_s - \frac{1}{\omega C_s}\right]} \equiv Y_s} \tag{4.21}$$

Z_S is called the "Impedance" of the circuit and Y_s the "Admittance". Note that they both represent the balance of input voltage and input current, one the inverse of the other. The units are "ohms" and "siemens", respectively. The real and imaginary parts are shown in Fig. 4.3. These are the same as in Fig. 4.1. Below resonance, the capacitor manages the circuit current and the reactance is negative; the circuit behaves capacitively. Above resonance, the inductor manages the circuit current and the reactance is positive; the circuit behaves inductively.

Using Q_s, the impedance can be reformed to

$$Z_s = R_s + i\left[\omega L_s - \frac{1}{\omega C_s}\right] = R_s\left[1 + iQ_s\left(\frac{\omega}{\omega_0} - \frac{\omega_0}{\omega}\right)\right] \tag{4.22}$$

4.3.2 The Parallel Resonant Circuit.

In similar fashion, the differential equation (B) of (4.17) leads to

$$y \to i_p; \quad x \to v_p; \quad m \to C_p; \quad \gamma \to \frac{1}{R_p} \quad \text{and} \quad k \to \frac{1}{L_p} \tag{4.23}$$

$$\omega_0^2 = \frac{1}{L_p C_p}; \quad \omega_d = \frac{1}{R_p C_p}; \quad \text{and } Q_p = \frac{\omega_o}{\omega_d} = \frac{R_p}{\sqrt{L_p/C_p}}$$

The two forms given in (4.3) appear as:

$$(A) \boxed{\frac{V_0}{I_0} = \frac{1}{R_p + i\left[\omega L_p - \frac{1}{\omega C_p}\right]} \equiv Z_p} \quad \text{and} \quad (B) \boxed{\frac{I_0}{V_0} = \frac{1}{R_p} + i\left[\omega C_p - \frac{1}{\omega L_p}\right] \equiv Y_p} \tag{4.24}$$

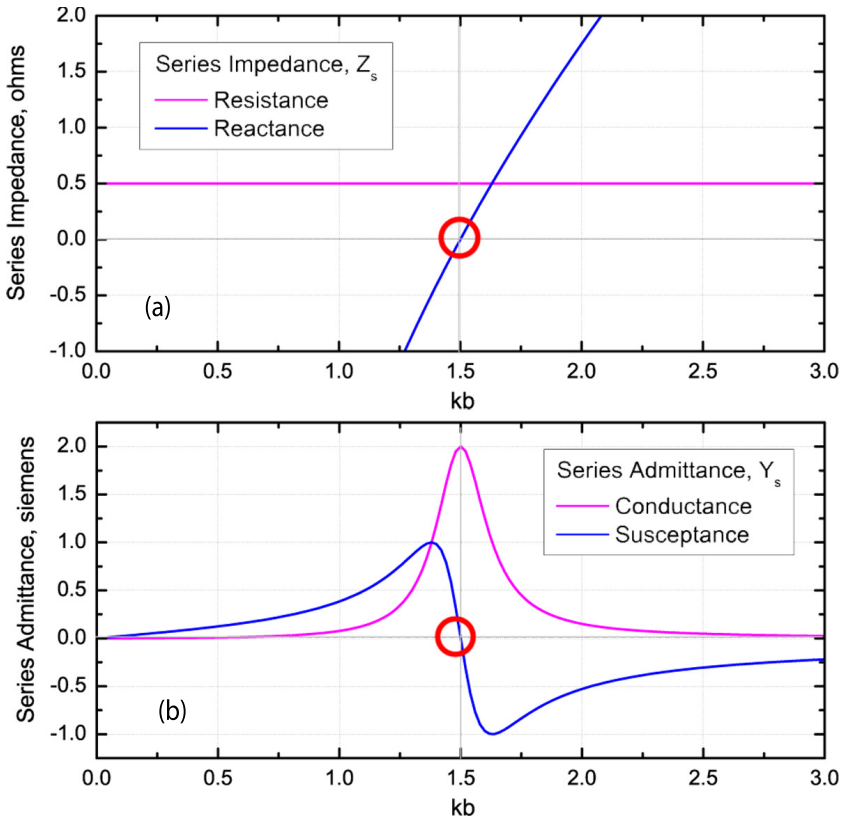

Figure 4.3: Series impedance (a) and admittance (b) for $R_s = 0.5, L_s = 2$, and $1/C_S = 4.5$. The red circles mark the resonance, in this case 1.5 radians/sec.

Z_p is the "Impedance" of the circuit and Y_s is the "Admittance". Note that they have the opposite behaviour of the impedance and admittance of the series resonant circuit. The real and imaginary parts are shown in Fig. 4.4. Below resonance, the inductor manages the circuit current and the reactance is positive; therefore the circuit behaves inductively. Above resonance, the capacitor manages the circuit current and the reactance is negative; the circuit behaves capacitively.

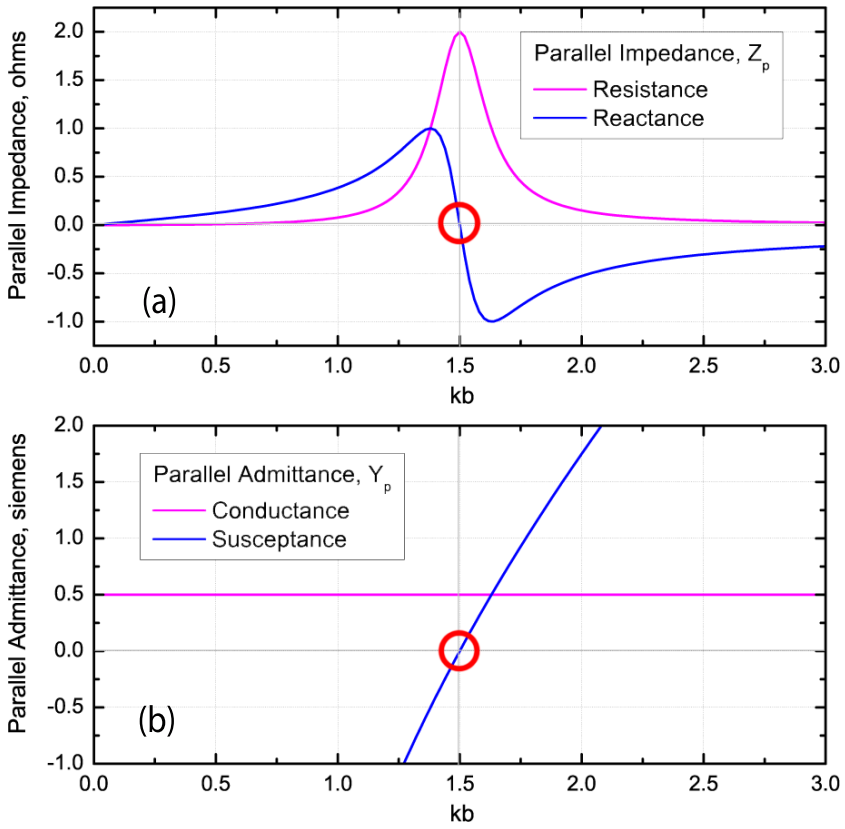

Figure 4.4: Parallel impedance (a) and admittance (b) for $1/R_p = 0.5, C_p = 2$, and $1/L_p = 4.5$. The red circles mark the resonance, in this case 1.5 radians/sec.

Using Q_p, the admittance can be reformed to

$$Y_p = \frac{1}{R_p} + i\left[\omega C_p - \frac{1}{\omega L_p}\right] = \frac{1}{R_p}\left[1 + iQ_p\left(\frac{\omega}{\omega_0} - \frac{\omega_0}{\omega}\right)\right] \tag{4.25}$$

4.4 Resonances and Anti-Resonances

4.4.1 True Resonance

In the remaining chapters of this thesis, the behaviour of rings will be described first and foremost by their input impedance and admittance. Depending on incident wavelength, this impedance and this admittance will show characteristics of either

the series *RLC* circuit or the parallel *RLC* circuit or both. Indeed, the general *RLC* model of rings will be shown to be quite complicated, since the values of these three parameters vary with frequency, unlike conventional *RLC* circuits where the elements have fixed, constant values. In other words, the R, L and C of loop antennas and nano-scaled rings are functions of frequency: $R = R(\omega)$, $L = L(\omega)$, and $C = C(\omega)$. But despite the complications, a ring can be described, at any given frequency, as a simple *RLC* circuit, with constant values, values which will also be reasonably correct in the vicinity of that frequency.

One may therefore appeal to Fig. 4.2 for a rather accurate understanding of ring behaviour at any given frequency. At some frequencies, Fig. 4.2 (A) will be more representative of ring behaviour than (B). In that case, the impedance and admittance in the region around the resonance will behave like that in Fig. 4.3:

- The ring will behave capacitively just below the resonance and inductively just above.
- At resonance, the input current ring current will reach a maximum as described above by (4.4).
- At resonance, the *LC* combination will look like a short circuit and the impedance will be real; the ring will behave only like a resistor.

Consequently, when this occurs, the resonance is called a "short-circuit" resonance, or "true" resonance (since the current is larger than at any other nearby frequency).

4.4.2 Anti-Resonances

At some frequencies, Fig. 4.2 (B) will be more representative than (A). In that case, the impedance and admittance in the region around the resonance will behave like that in Fig. 4.4:

- The ring will behave inductively just below the resonance and capacitively just above.
- At resonance, the input ring current will reach a minimum, usually zero.
- At resonance, the *LC* combination will look like an open circuit.

Consequently, when this occurs, the resonance is called an "open-circuit" resonance, or "anti-resonance" (since the current is smaller than at any other nearby frequency).

Both resonances and anti-resonances appear in the impedance of loops. Where they occur in the frequency spectrum will be distinct. They will also be quite evident in the plot of the input impedance.

Part II

Prior Work

Chapter 5

Prior Work on Closed Circular Rings at Radio Frequencies (1 MHz to 1 GHz)

5.1 Introduction

This chapter reviews prior work on loop antennas in the radio frequency (RF) region. It is “classical" work, in the sense that it approaches the analytical study of loops in the same way that engineers approached the study of dipoles and other types of antennas in the early days of antenna design. For loops that are small compared with wavelength, it is sufficient to assume a constant current distribution. In Chapter 10, I shall call this the “zero-order" mode and there shall be a resonance associated with this mode that crops up when one adds a capacitor to the closed loop. The first section here, Section 5.2, on small loop analysis is all that was known about loops prior to 1938.

Four works are of fundamental importance in establishing the basis for loops with circumferences on the order of the exciting wavelength, which is the work of this thesis: the papers by Hallen [1938], Storer [1956], Wu [1962], and Iizuka [1965]. Studies prior to Hallen a single sinusoidal current distribution on the loop. Hallen took the bold step of using a delta function voltage generator at one point in the periphery of the loop, so that all modes of the loop would be stimulated. This results mathematically in the establishment of a differential equation that is solved using a Green’s function. The delta function has within it, mathematically, an infinite number of modes and therefore a delta function generator would generate a small voltage for each mode. This approach manages to overthrow the simplistic sinusoidal assumption.

Following Hallen’s approach, Storer solved the differential equation and found the current distribution for all harmonic modes; the solution unfortunately did not converge. He did, however, produce, an approximation, which provided an excellent solution for the first four harmonic modes. Wu questioned the validity of the approximation and instead, suggested a small change to the differential equation, which produced a tidy closed form for the coefficients. This is the solution for the closed

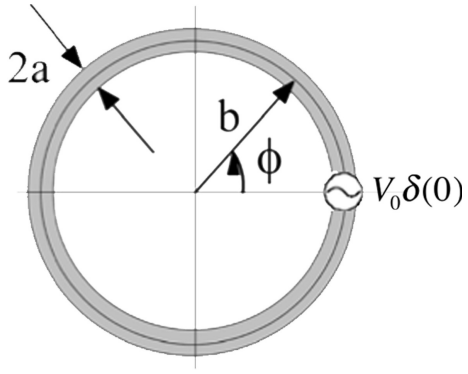

Figure 5.1: The geometry of the ring for purposes of the derivation. b is the ring radius. a is the wire radius. The size of the loop is given effectively by $\Omega = 2\ln(2\pi b/a)$

loop in the RF region that I use in Chapter 8. Iizuka suggested that impedances could be introduced into the periphery of the loop if one accounted for phasing properly. I use his suggestion in Chapters 10 to produce the current distribution for single and multiple gaps in nano-scaled rings.

Prior work on loops and rings at higher frequencies is examined in the next chapter.

5.2 Small, Perfectly Conducting Rings

Loops that are small with respect to the wavelength of incident radiation are relatively straightforward to understand, but the analysis is fairly complex. A derivation of the far-fields appears in [Balanis, 2005, sec 5.2]. A "small" ring is, by definition, one for which the current, as a function of the angle around the circumference, is constant. This constancy assumption applies when the circumference, given by $2\pi b$ in Fig. 5.1, is much less than the wavelength, λ, of interest, say about $1/10\lambda$. It is assumed that the material of construction is perfectly conducting, meaning that it has no resistance and therefore no heat loss.

The result is that the far-field of a small ring, looks like a magnetic dipole[1]. In the same way that an electric dipole is used to measured the charge of an external body brought close, so a small ring can be used to measure the strength of a magnet brought close. Just as the electrical dipole moment is given by $p = I_0 l$, where I_0 is the current running along a short wire of length l laying along the z axis, so the ring magnetic moment is given by $m = I_0 S$ where S is the area of the ring and I_0 the constant current flowing around the ring.

The far-field for the electric dipole is defined as the field in the region $kr \gg 1$, where k is the wavenumber, $2\pi/\lambda$ and r is the radial distance from the centre of the

[1]The near-fields have no importance in the work of the thesis, so they are neglected. The near-field power is reactive. Not so the far-field, where the power is real, as shown below.

loop:

$$H_r = H_\theta = E_\phi = 0; \quad H_\phi = ip\frac{k\sin(\theta)}{4\pi r}e^{-ikr} \tag{5.1}$$
$$E_r = b_x p\frac{\cos(\theta)}{2\pi r^2}e^{-ikr}; \quad E_\theta = ib_x p\frac{k\sin(\theta)}{4\pi r}e^{-ikr}$$

while the far-fields for the small ring are the duals

$$E_r = E_\theta = H_\phi = 0; \quad E_\phi = b_x m\frac{k^2\sin(\theta)}{4\pi r}e^{-ikr} \tag{5.2}$$
$$H_r = im\frac{k\cos(\theta)}{2\pi r^2}e^{-ikr}; \quad H_\theta = -m\frac{k^2\sin(\theta)}{4\pi r}e^{-ikr}$$

Here, ϵ_0 is the electric permittivity and μ_0 is the magnetic permeability of free space, such that $b_x = \sqrt{\mu_0/\epsilon_0} = 376.73$ is the balanced reactance of free-space, commonly called the intrinsic or characteristic impedance of free space. Notice that in the far-field H_r decreases much faster than either E_ϕ or H_θ and that $E_\phi/H_\theta = b_x$.

The radiated power is given by the complex Poynting vector.

$$\vec{S} = \frac{1}{2}\left(\vec{E}\times\vec{H}^*\right) = \frac{1}{2}\left[(E_\phi\hat{e}_\phi)\times(H_r^*\hat{e}_r + H_\theta^*\hat{e}_\theta)\right] \tag{5.3}$$
$$= \frac{1}{2}\left(-E_\phi H_\theta^*\hat{e}_r + E_\phi H_r^*\hat{e}_\theta\right)$$

The average is given by integrating $\vec{S}$ over a spherical shell surrounding the ring at a large distance. Again, the condition taken is $kr \gg 1$. The second term yields 0 since the $\sin\theta$ and $\cos\theta$ are orthogonal. The result, using the definitions for $m = I_0 A$ as above, is along the radial only, indicating outward power flow in the amount

$$P_r = \frac{1}{12}b_x k^4 m^2 = \frac{1}{12}b_x k^4(\pi a^2)^2|I_0|^2 \tag{5.4}$$

The constancy of the current magnitude in a ring with circumference much less than the incident wavelength gives rise to an inductance that depends on its radius and on the thickness of the wire.

$$L = \mu_0 b l_\mu \text{ where } l_\mu = \left[\ln\left(\frac{8b}{a}\right) - 2\right] \tag{5.5}$$

The important point to note is that the inductance changes with the thickness of the loop, b/a. There is no capacitance, since the charge is the same at every point along the length of the ring. Resonances simply do not occur. This is an important result because any analysis of large loops must converge to this answer in the approximation of small rings. Moreover, the addition of a capacitor will resonate with this inductance, and that is the basis of a zero-order resonance studied in Chapter 10.

5.3 Large, Perfectly Conducting Rings

5.3.1 Preliminary

Loops with circumferences about the length of the incident wavelength are much more difficult to analyse than small loops. Hallen [1938]'s approach, which eventually proved successful in determining the current distribution, was to use a delta function generator across a gap, which mathematically could be made infinitesimally small and therefore allow for a lumped voltage source approach. One would expect such an approach to stimulate all resonating modes.

There is, in the historical annals of physics, a similarly occurring phenomenon with rings. In 1913, Neils Bohr produced an analysis which suggested that electrons, as waves, circulated around the nucleus of an atom in such a way as to quantise its angular momentum. In 1924, Louis deBroglie found that these waves fit exactly the circumference of the orbits which they occupied. That is, the electron was resonant to its corresponding orbit. That idea was critical to the development of the quantum view of particle physics. Fig. 5.2 shows the idea. Similarly, a good guess for current distribution on a closed circular loop is to say that a current wave in such a loop, reinforces itself when its wavelength exactly matches the circumference of the loop; namely, when $\lambda = 2\pi b \equiv \lambda_b$, where b is the radius of the loop. In fact, one might further guess that the wave reinforces itself as long as the current wavelength is some integer fraction of the fundamental wavelength; $\lambda = \lambda_b/n$, for n an integer. This expectation replicates the "deBroglie" conditions mentioned above. The frequency associated with $n = 1$ is called the "fundamental"; those associated with the integers $n > 1$ are called "harmonics" of the fundamental. Hence the circumference of the loop is an extremely important parameter when discussing the behaviour of circular loops.

The opposite phenomenon, namely cancellation due to wave interference occurs generally at the half integer wavelengths, $\lambda = \lambda_b/(n/2)$. These are called "anti-resonances". No current flows in the loop at such frequencies, because the current wave is $n/2$ times longer than the circumference and continually cancels itself out since it reaches a full passage around the circumference on the half cycle. In such a case, it is impossible for energy to enter, let alone accumulate.

5.3.2 Derivation of the Current and of the Driving Point Impedance and Admittance of the Ring.

The parameters of the circular ring are shown in Fig. 5.1. A delta function voltage generator, $V_0\delta(\phi)$, is located across an infinitesimal gap at $\phi = 0$. This is appropriate since the differential equations later encountered are linear in the variables and therefore the impulse response is a Green's function, which, when convolved with any other linear input such as a plane wave, will generate the corresponding modal response of the ring. The delta function requires $E_\phi = 0$ except at $\phi = 0$, where it

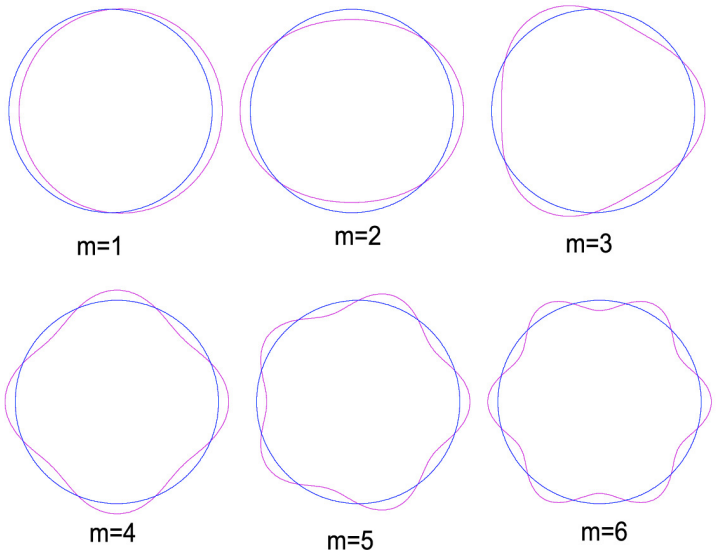

Figure 5.2: The deBroglie conditions for model resonances, m, on a loop.

becomes infinite, but in such a manner that

$$\int_{-\Delta g/2}^{\Delta g/2} E_\phi d(b\phi) = -V_0 \tag{5.6}$$

where b is the radius of the ring and Δg is the width of the gap. This imposed electric field generates a scalar potential, Φ, and a vector potential, $\vec{A}$, according to $\vec{E} = -\vec{\nabla}\Phi - \partial\vec{A}/\partial t$. Expanding in cylindrical coordinates, and using $e^{i\omega t}$, gives:

$$\frac{V_0\delta(\phi)}{b} = \frac{1}{b}\frac{\partial\Phi}{\partial\phi} + i\omega A_\phi \tag{5.7}$$

The potentials at the element $bd\phi$ are

$$\begin{aligned}\Phi &= \frac{1}{4\pi\epsilon_0}\int_{-\pi}^{\pi} q(\phi')W(\phi-\phi')d\phi' \\ A_\phi &= \frac{\mu_0}{4\pi}\int_{-\pi}^{\pi} I(\phi')W(\phi-\phi')\cos(\phi-\phi')d\phi'\end{aligned} \tag{5.8}$$

where $q(\phi)$ is the charge distribution in Coulombs (C) and $I(\phi)$ is the current distribution in amperes (A). $W(\phi-\phi')$ is the standard Green's weighting function,

$$W(\phi-\phi') = \frac{1}{2\pi}\int_{-\pi}^{\pi}\frac{e^{-ik_0bR(\phi-\phi')}}{R(\phi-\phi')}d\psi$$

where R is the Euclidean distance between two points on the surface of the ring, (ϕ, a, θ) and (ϕ', a, θ') normalised by the radius of the loop (see Fig. 5.3 for the co-

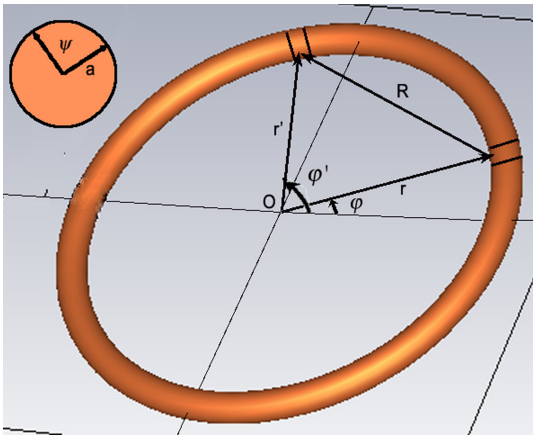

Figure 5.3: The function given in (5.9) "weights" the charge and the current to account for the delayed effects of one element of the ring on another. The element $\{\phi, a, \psi\}$ affects the element $\{\phi', a, \psi'\}$. ψ measures the angle around the internal circumference of the wire $2\pi a$.

ordinate geometry of the derivation). ψ is an angle inside the wire in the toroidal direction.

$$R(\phi - \phi') = \sqrt{4^2 \sin^2 \frac{(\phi - \phi')}{2} + \left(\frac{a}{b}\right)^2} \tag{5.9}$$

The complex propagation constant of the medium is taken as

$$k = \beta + i\alpha/2 \tag{5.10}$$

and, with $\beta = \omega/c = 2\pi/\lambda; \alpha = 0$, $k \equiv k_0$ throughout this thesis, unless specified otherwise. λ is the driving or illuminating wavelength. In a perfectly conducting wire, the current moves everywhere to create an electric field which exactly cancels any imposed electric field. This is the source of the modal currents in the loop. Therefore the driving field, E_ϕ, appears only in the gap. As a result, a boundary condition for the solution of Eq. (5.7) is that the total electric field, given by the sum of the imposed field and the reactive field, is zero on the surface of the wire; ie., the surface impedance, $Z_s = 0$. The surface impedance in this case must have units of surface density, Ω/m^2.

Using continuity, $\vec{\nabla} \cdot \vec{J} = \partial J_\phi / b\partial\phi = -\partial\rho/\partial t = -i\omega\rho$, where $J(\phi)$ is the surface current density (A/m^2), and ρ is volume charge density (C/m^3). The assumption that the current flows through the wire only in the ϕ direction is called the "thin-wire approximation" since in thick wires, the current has components in the radial direction, r, and in the "toroidal" direction, θ, as well. The thin wire approximation assumes that the current flows over the full cross-sectional face of the wire in the longitudinal direction, which isn't the case for thick wires, due to the "skin depth" effect, where the current remains near the surface. The approximation may be stated more clearly as $a^2 \ll b^2$.

Using this continuity equation, the charge is thereby converted to current and we have

$$\Phi = \frac{i}{4\pi\omega\epsilon_0 b}\int_{-\pi}^{\pi}\frac{\partial I(\phi')}{\partial\phi'}W(\phi-\phi')d\phi' \tag{5.11}$$

and

$$\frac{\partial\Phi}{\partial\phi} = \frac{ib_x}{4\pi k_0 b}\int_{-\pi}^{\pi}\left[\frac{\partial I(\phi')}{\partial\phi'}\frac{\partial W(\phi-\phi')}{\partial\phi}\right]d\phi'$$

Since $\partial W(\phi-\phi')/\partial\phi = -\partial W(\phi-\phi')/\partial\phi'$, we have by partial fractions:

$$\begin{aligned}\frac{\partial\Phi}{\partial\phi} &= -\frac{ib_x}{4\pi k_0 b}\int_{-\pi}^{\pi}\left[\frac{\partial}{\partial\phi'}\left(I(\phi')\frac{\partial W(\phi-\phi')}{\partial\phi'}\right) - I(\phi')\frac{\partial^2 W(\phi-\phi')}{\partial\phi'^2}\right]d\phi' \\ &= \frac{ib_x}{4\pi k_0 b}\int_{-\pi}^{\pi} I(\phi')\frac{\partial^2 W(\phi-\phi')}{\partial\phi'^2}d\phi'\end{aligned} \tag{5.12}$$

Substituting into (5.7),

$$\begin{aligned}V_0\delta(\phi) =& \frac{ib_x k_0 b}{4\pi}\int_{-\pi}^{\pi} I(\phi')W(\phi-\phi')\cos(\phi-\phi')d\phi' \\ &+ \frac{ib_x}{4\pi k_0 b}\int_{-\pi}^{\pi} I(\phi')\frac{\partial^2 W(\phi-\phi')}{\partial\phi^2}d\phi'\end{aligned} \tag{5.13}$$

Rearranging,

$$V_0\delta(\phi) = \frac{ib_x}{4\pi}\int_{-\pi}^{\pi} M(\phi-\phi')I(\phi')d\phi' \tag{5.14}$$

where the new kernel becomes

$$M(\phi-\phi') = \left[k_o b\cos(\phi-\phi') + \frac{1}{k_0 b}\frac{\partial^2}{\partial\phi^2}\right]W(\phi-\phi') \tag{5.15}$$

A solution of Eqn. (5.14) is obtained by expanding the kernel in a Fourier series,

$$W(\phi-\phi') = \sum_{m=-\infty}^{\infty} K_m e^{-im(\phi-\phi')} \tag{5.16}$$

Substituting this into Eqn. (5.15) and the result into Eqn. (5.14) leads to

$$V_0\delta(\phi) = \frac{ib_x}{4\pi}\sum_{m=-\infty}^{\infty}\left[k_0 b\left(\frac{K_{m+1}+K_{m-1}}{2}\right) - \frac{m^2 K_m}{k_0 b}\right]\int_{-\pi}^{\pi} I(\phi')e^{-im\phi'}d\phi' e^{im\phi} \tag{5.17}$$

Expanding the current in a Fourier series leads to

$$I(\phi') = \sum_{m=-\infty}^{\infty} I_m e^{im\phi'},\ \text{for which}\ I_m = \frac{1}{2\pi}\int_{-\pi}^{\pi} I(\phi')e^{-im\phi'}d\phi' \tag{5.18}$$

and so we have:

$$V_0\delta(\phi) = \frac{ib_x}{2}\sum_{m=-\infty}^{\infty} a_m I_m e^{im\phi} \tag{5.19}$$

where

$$a_m = a_{-m} = k_b\left(\frac{K_{m+1}+K_{m-1}}{2}\right) - \frac{m^2}{k_b}K_m \quad \text{and } k_b \equiv k_0 b \tag{5.20}$$

The coefficients K_m are the only parameters yet undetermined. The introduced term, $k_b = 2\pi b/\lambda$ = circumference/wavelength, is a unit-less variable, which will allow the equations to speak for many different sizes of rings. Eqn. (5.19) is a Fourier series for which the coefficients are found in the standard way, so that

$$\frac{ib_x}{2}a_m I_m = \frac{1}{2\pi}\int_{-\pi}^{\pi} V_0\delta(\phi)e^{-im\phi}d\phi = \frac{V_0}{2\pi} \tag{5.21}$$

Using (5.18), the current then becomes

$$\begin{aligned} I(\phi) &= \sum_{m=-\infty}^{\infty} I_m e^{im\phi} = \frac{V_0}{i\pi b_x}\sum_{m=-\infty}^{\infty}\left[\frac{e^{im\phi}}{a_m}\right] \\ &= \frac{V_0}{i\pi b_x}\left[\frac{1}{a_0} + \sum_{m=1}^{\infty}\frac{2\cos(m\phi)}{a_m}\right] \end{aligned} \tag{5.22}$$

The last step occurs because the a_m and the exponential are even functions of m. The impedance and admittance at the gap are defined as follows:

$$Z \equiv \frac{V_0}{I(\phi=0)} = i\pi b_x \Big/ \left[\frac{1}{a_0} + 2\sum_{m=1}^{\infty}\frac{1}{a_m}\right]; \quad Y \equiv \frac{1}{Z} \tag{5.23}$$

Storer evaluates the K_m coefficients in an Appendix, arriving at a recursive relation for the $K's$:

$$\begin{aligned} K_0 &= \frac{1}{\pi}\ln\frac{8b}{a} - \frac{1}{2}\int_0^{2k_b}\left[\Omega_0(x) + iJ_0(x)\right]dx \\ K_{n+1} &= K_n + \Omega_{2n+1}(2k_b) + iJ_{2n+1}(2k_b) \end{aligned} \tag{5.24}$$

$\Omega_m(x)$ and $J_m(x)$ are the Lommel-Weber function and the Bessel function of the first kind respectively.

$$\begin{aligned} \Omega_m(x) &= \frac{1}{\pi}\left[\int_0^{\pi}\sin(x\sin\theta - m\theta)d\theta\right] \\ J_m(x) &= \frac{1}{\pi}\left[\int_0^{\pi}\cos(x\sin\theta - m\theta)d\theta\right] \end{aligned} \tag{5.25}$$

5.3.3 The Divergence Problem.

Hallen had shown that, for large m, the coefficients a_m approach the value

$$a_m = \frac{m^2}{\pi k_b}\left\{\ln(\frac{2b}{a}) - \gamma - \ln m\right\} \tag{5.26}$$

where $\gamma = .5772$, Euler's constant, which means that as m increases, a_m approaches 0, and the series sum runs into a singularity near

$$m \to m_0 \approx \frac{2b}{a}e^{-\gamma} \tag{5.27}$$

To handle this problem, Storer truncates the series at $m = 4$ and approximates the remaining terms using

$$\Psi = \frac{2\pi}{\ln(m_o/4.5)}\frac{k_b}{4.5}\left[\mathcal{J}_1(\phi) + (\frac{k_b}{4.5})^2\mathcal{J}_2(\phi)\right] \tag{5.28}$$

where $\mathcal{J}_1$ and $\mathcal{J}_2$ are integral functions of the angle ϕ.

$$\begin{aligned}\mathcal{J}_1(\phi) &= \int_1^\infty \frac{\ln(m_o/4.5)}{\ln(m_o/4.5) - \ln x}\frac{\cos(4.5x\phi)}{x^4}dx \\ \mathcal{J}_2(\phi) &= \int_1^\infty \frac{\cos(4.5x\phi)}{x^4}dx\end{aligned} \tag{5.29}$$

At $\phi = 0$, the values are

$$\begin{aligned}\mathcal{J}_1(0) = \{0.47, 0.9, 1.25, 1.4, 1.4\} \text{ and } \mathcal{J}_2 \approx 1/3 \\ \text{for } \Omega = 2\ln\left(2\pi\frac{b}{a}\right) = \{8, 9, 10, 11, 12\}\end{aligned} \tag{5.30}$$

Ω is a measure of the thickness of the ring, with larger numbers referring to thinner wire rings. This use of Ψ to substitute for most of the sums in the series significantly speeds the calculation. Storer's series sum now appears as

$$Z = i\pi b_x / \left[\frac{1}{a_0} + 2\sum_{m=1}^{4}\frac{1}{a_m} - \Psi\right] \tag{5.31}$$

Since the input impedance requires the current at angle $\phi = 0$, only the values of the integrals there, namely as given by Eq. (5.30), are needed for their calculation. But a calculation of the current at any other angle in the ring requires a computation involving the integrals of (5.29).

Wu questioned the validity of the approximation in Eqn. 5.28. One that something is wrong with the printed version of the integral for $\mathcal{J}_1$ in (5.29), since the denominator has a divergence at $x = m_0/4.5$ within the bounds of the integration. Wu notes that the divergence problem is a consequence of the approximations used

to simplify the original differential equations, specifically in regard to the formation of the distance R in (5.9). Wu instead suggests the form

$$R(\phi - \phi') = \sqrt{4\sin^2\frac{(\phi - \phi')}{2} + \frac{4a^2}{b^2}\sin^2(\psi/2)} \tag{5.32}$$

Then, Storer's recursive K_m coefficients (5.24) are replaced with

$$\begin{aligned} K_0 &= \frac{1}{\pi}\left\{\ln\frac{8b}{a}\right\} - \frac{1}{2}\int_0^{2k_b}\left[\Omega_0(x) + iJ_0(x)\right]dx \\ K_m &= K_{-m} = \frac{1}{\pi}\left\{\mathcal{K}_0(\frac{ma}{b})\mathcal{I}_0(\frac{ma}{b}) + C_m\right\} - \frac{1}{2}\int_0^{2k_b}\left[\Omega_{2m}(x) + iJ_{2m}(x)\right]dx \\ C_m &= \ln(4m) + \gamma - 2\sum_{m=0}^{m-1}(2m+1)^{-1} \end{aligned} \tag{5.33}$$

$\mathcal{I}_0(x)$ and $\mathcal{K}_0(x)$ are modified Bessel functions of the first and second kind respectively. They may be approximated to first order in the parameter x when $x \ll 0$ ([Stegun and Abramowitz, 1964, See particularly page 375, Eq. 9.6.12 and 9.6.13]), giving

$$\begin{aligned} \mathcal{I}_0(x) &= 1 + O(x^2) \approx 1 \\ K_0(x) &= -\mathcal{I}_0(x)(ln(x/2) + \gamma) + O(x^2) \approx -ln(x/2) - \gamma \end{aligned} \tag{5.34}$$

The series now converges and there is no need for Storer's extra term, Ψ. Consequently the full treatment reverts to Storer's original form for the impedance, equation (5.23).

5.3.4 Interpretation of the Impedance and Admittance Curves.

The input impedance at the source, given by (5.23), may be evaluated against the variable $k_b \equiv k_0 b = \omega/c = 2\pi b/\lambda$, where λ is the wavelength of the driving source voltage. This variable is a unit-less ratio of the circumference of the ring over the driving wavelength. The horizontal axis of most figures hereon will feature this variable. Fig. 5.4 suggests two ways of interpreting the axis.

The results of the evaluation apply to any loop at any frequency, where the material from which the ring is made acts like a perfect conductor (*i.e.* where its resistivity is 0). Storer gave plots of the input impedance and admittance as a function of k_b, of current as a function of the angle ϕ, and of the first five a_m coefficients for rings of sizes $\Omega = \{8, 9, 10, 11, 12\}$. Recall that the definition of $\Omega = 2\ln\left(2\pi\frac{b}{a}\right)$, is given in Eqn. 5.30. These are repeated in King [1969] and in Balanis [2005]. Storer provided some minimal experimental results using a half loop above a ground plane, but no experimental or simulation work has been done since Storer's paper to show the accuracy of the derivation. A section on the accuracy of these results follows Section 5.3.5.

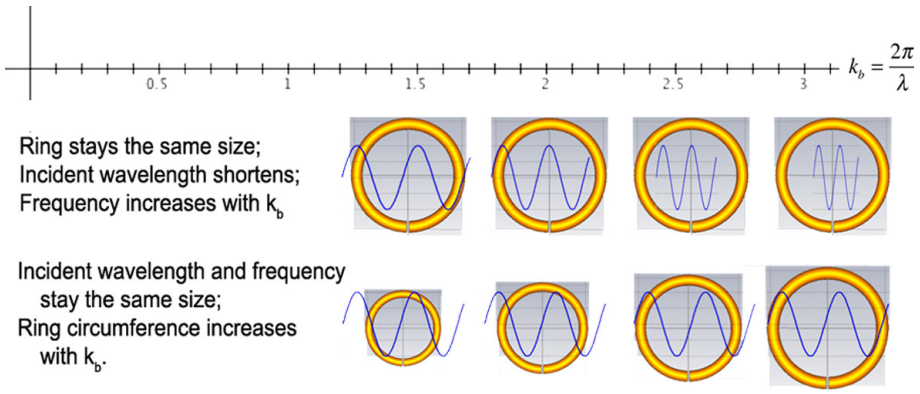

Figure 5.4: Two interpretations of the variable k_b.

5.3.5 Resonances and Anti-Resonances

The input impedance is complex, $Z = R + iX$; the real part indicating the resistance of the loop, the imaginary part indicating the reactance of the loop. The most important feature of these curves is where the ring resonates and "anti-resonates". These occur when the reactance crosses through $k_b = 0$. These “zero-crossings (ZC)" are marked in Fig. 5.5 (a). The resonances and anti-resonances of the loop are distinguishable by looking at their form near the zero-crossings and comparing those forms to Figs. 4.3 and 4.4. Note that the first and second true resonances occur near $k_b = 1$ and $k_b = 2$. These are the fundamental and second harmonic of the loop. The anti-resonances occur at about half those values. The resistance shows expected peaks at the anti-resonances; “expected" because the input current goes to a minimum in a parallel resonant circuit and this imp lie a high resistance.

The next important feature of these curves is the position of peaks of the real part of the admittance in Fig. 5.5(b). If V_0 is taken to be 1 volt, Eqn. (5.23) indicates that the admittance ($Y = G + iB$) and the input current at the input ($I(0)$) are equivalent in both real and imaginary parts; that is, the admittance curves may also be considered current curves. The real part, called the “conductance”, shows peaks just to the left of the resonances. The imaginary part, called the “susceptance", also shows the resonances and anti-resonances, but with the ZC reversed from those in the impedance curves. Both conductance and susceptance are measured in “milli-Siemens" (mS).

Table 5.1 shows measures for the first two sets of ZC resonances and anti-resonances for rings of size $\Omega = 8$, 9, 10, 11 and 12. Note that the resistance at every k_b is the radiation resistance of the ring. This is because the rings are perfectly conducting and therefore have no heat losses.

5.3.6 Accuracy of the Results

When evaluating the accuracy of (5.23) using a calculational engine such as MATLAB, a matter arises regarding the number of modes to include in the summation. Fig. 5.6 shows loops of three thicknesses, $\Omega = 8$, 10, and 12. For each, the resistance and

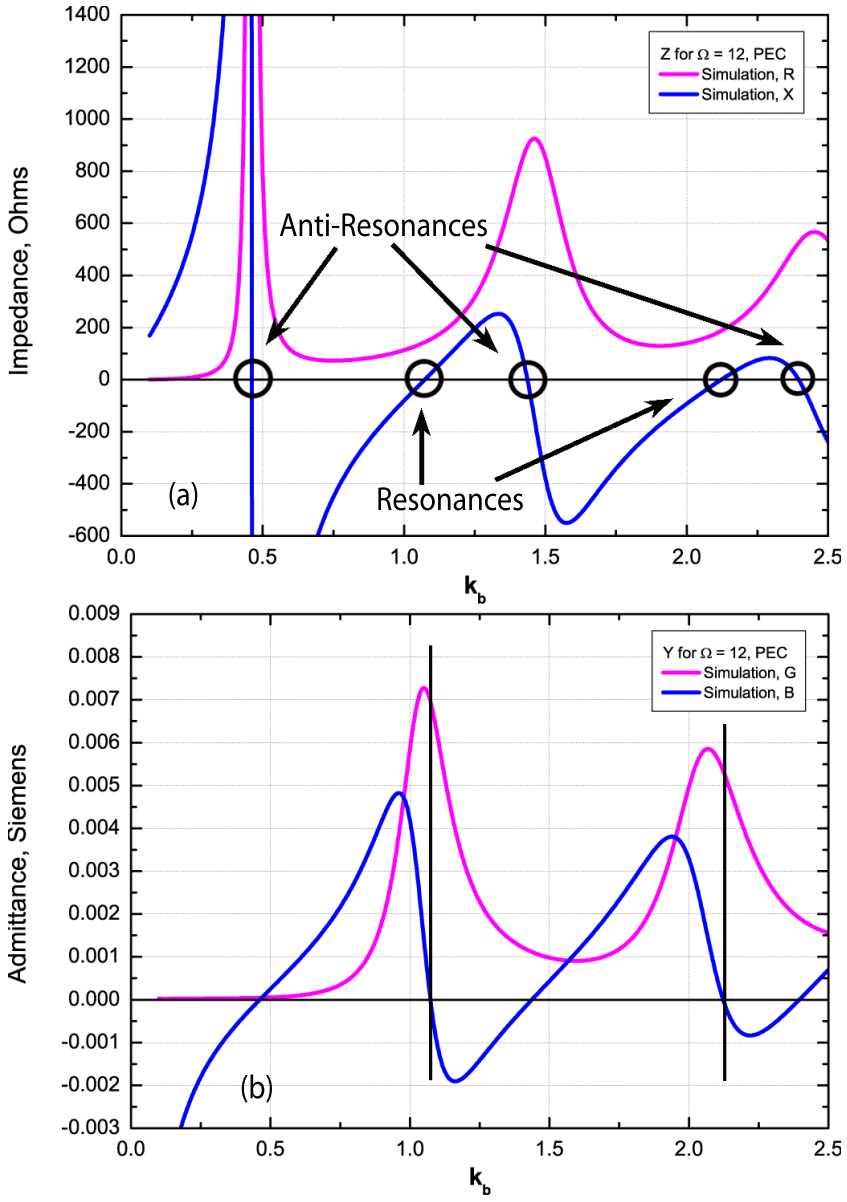

Figure 5.5: The impedance (a) and admittance (b) of a size $\Omega = 12$ ring; $b/a \approx 64.2$. Resonances and anti-resonances are marked by circles in (a). Notice that the peaks of the admittance are to the left of the true resonances.

Table 5.1: Details of zero-crossing resonances and anti-resonances from (5.23) for PEC rings. The thicker loops do not have some zero-crossings (marked as '-'), but they do have admittance peaks, nevertheless, albeit broader, hence lower Q than the thinner loops.

	Resonances			$\|I\|^2$		Anti-Resonances		
Ω	#	ZC	R	Peak		#	ZC	G
		k_b	ohms	k_b	$(mA)^2$		k_b	mS
12	1	1.09	147	1.04	53	1	0.47	0.35
	2	2.14	195	2.06	34	2	1.46	1.0
11	1	1.11	152	1.05	54	1	0.46	0.05
	2	2.22	127	2.06	36	2	1.43	1.51
10	1	1.15	165	1.05	56	1	0.45	0.06
	2	-	-	2.06	40	2	-	-
9	1	-	-	1.05	62	1	0.43	0.07
	2	-	-	2.06	54	2	-	-
8	1	-	-	1.03	180	1	0.31	0.04
	2	-	-	2.08	300	2	-	-

reactance are plotted in three ways: (1) following Storer and summing to mode 4 with the PSI term (using (5.23)), (2) following Wu and summing to mode m_0, defined in (5.27) without the PSI term, and (3) simulating in CST's MWS (see Appendix A). In the second case, trial and error shows that the sums converge rapidly and that the inclusion of modes up to mode m_0 is adequate for thicknesses at least to $\Omega = 8$. The results of the comparison are the following:

- In general, Wu's method replicates the simulation results better than does Storer's method.
- In general, both methods blue-shift the harmonic anti-resonances from the simulation results as the thickness increases. This may be due to the thin-wire approximation used in theory.
- In general, the first anti-resonance does not shift and the resonances do not shift, except for Storer's method for $\Omega = 8$.
- In general, the analytical model gives higher magnitude peaks for the resistance of the harmonic anti-resonances than those given by numerical simulation.

The conclusion is that Wu's method is reliable, but the analytical theory weakens as one approaches $\Omega = 8$ thicknesses and thicker. Therefore this is clearly a thin-wire model, but one that does give good estimates of the first ZC anti-resonance and ZC resonance if that is all that is required, such as for a quick estimate during a design process. Limiting the summation to mode m_0 creates a considerably fast calculation in MATLAB that will yield results much faster than modelling the loop

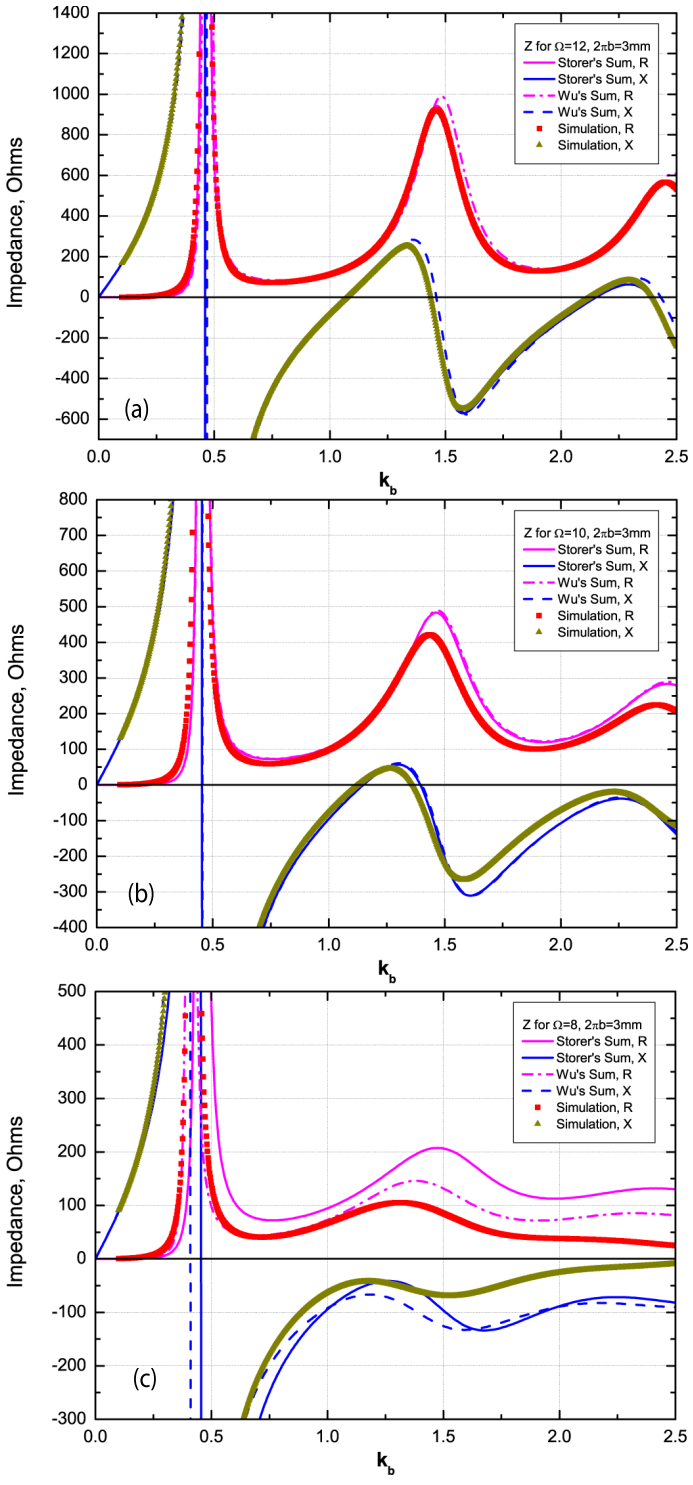

Figure 5.6: A comparison of Storer summation method and Wu's summation method with simulation results for $\Omega =$ (a) 12, (b) 10 and (c) 8 rings. Equation (5.23) matches simulation results less and less as the ring becomes thicker, due to assumptions of the derivation. In (a0 and (b) Storer and Wu results are on top of each other. For (c), Wu's method is more accurate than Storer's.

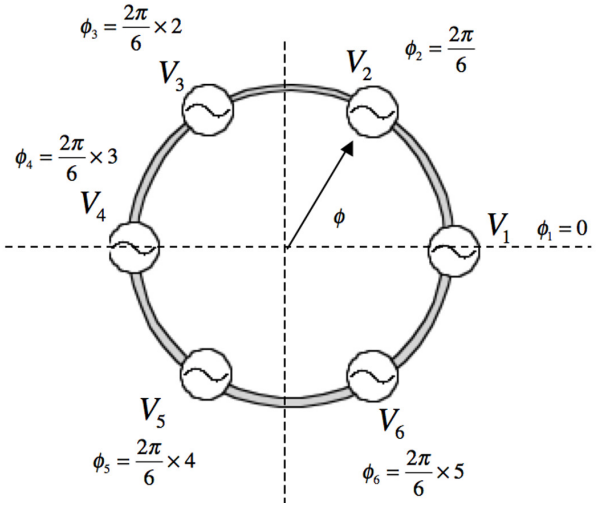

Figure 5.7: Loop geometry used by Iizuka. The voltage sources marked, V_p are evenly spaced around the ring. In this case, $M = 6$. Their general form must be a delta function generator in series with an impedance; *viz.*, $\left(V_{0p} - I(\phi_p)Z_p\right)\delta(\phi_p)$

in a simulation tool. The analytical model also allows us to interpret the behaviour of loops in terms of their underlying modes.

5.4 Multiple Impedances in the Periphery of a Perfectly Conducting Ring

In 1965, not long after Wu provided a solution to the convergence problem, Iizuka [1965], found a simple method for including impedances in the periphery of the ring. This was an important advance because current phasing around the ring can be controlled using inductors and capacitors in the right places, thus effecting a control over the major radiation beam of the ring. Moreover, one can expect such inductors and capacitors to change the resonance and the quality factor of the ring.

The method is also important because it will be used to extend the theory of the closed loop to a theory of split-rings, that is, rings with multiple gaps, in Chapter 10.

5.4.1 Derivation of the Current in the Ring

The derivation proceeds by replacing the Storer/Wu delta-function voltage source (see section 5.3.2) with the same voltage source in series with a lumped impedance; that is, with $V_0\delta(\phi) \rightarrow [V_0 - I(0)Z_0]\,\delta(\phi)$, which allowed Iizuka then to use the Storer/Wu derivation for the ring's current. Iizuka then went one step further and spaced a number of voltage/impedance combinations evenly around the ring, separated by an angle $2\pi/M$ where M is the number of impedances. Suppose $M = 6$; the sources are then at the angles $\phi_p = 2\pi(p-1)/6, p = \{1, ..., 6\}$. The current in the ring results

from a superposition of the currents due to all of the voltage sources. Using (5.22),

$$I(\phi) = \sum_{q=1}^{M} I_q(\phi) = \frac{1}{i\pi b_x} \sum_{q=1}^{M} \left(\sum_{m=-\infty}^{\infty} \frac{e^{-im(\phi - 2\pi(q-1)/M}}{a_m} \right) V_q = \sum_{q=1}^{M} Y(\phi, q) V_q \tag{5.35}$$

Note that at the source, p, the angle is $\phi_p = 2\pi(p-1)/M$, leading to

$$Y\left(\frac{2\pi}{M}(p-1), q\right) = \frac{1}{i\pi b_x} \sum_{m=-\infty}^{\infty} \frac{e^{-im(2\pi(p-q)/M)}}{a_m} \equiv Y_M(p,q) \tag{5.36}$$

This lends itself to matrix notation. The term $Y_M(p,q)$ is the p^{th} horizontal vector with M elements, or, alternatively, a square, $M \times M$ matrix, where p is the row counter and q the column counter. Hence, $Y_M(p,q) \rightarrow [Y_{pq}]$. The $Y(\phi, q)$ becomes a horizontal vector, $Y_q(\phi)$. Then (5.35) becomes

$$I(\phi) = [Y_q(\phi)]\,[V_q] \tag{5.37}$$

In order to include impedances, the voltage sources are turned into delta function voltage generators with series impedance, as noted above. This appears as:

$$V_q \rightarrow V_q - \sum_{q=1}^{M} Z_q I_q \tag{5.38}$$

The term V_q refers to the voltage generator at q. Setting it to 0 eliminates the generator leaving only the impedance. The term $[Z_q I_q]$ cannot work in matrix notation. The alternative is to set Z_q to a diagonal $M \times M$ matrix with the periphery impedances on the diagonal, and then multiply. The result is

$$Z_q I_q \rightarrow [Z_{qk}]\,[I_k] \tag{5.39}$$

where $[I_k]$ is a vertical vector. This is Iizuka's intention, as can be seen from his equation (14). This provides enough information to find the current at each impedance node. Setting $\phi = 2\pi(p-1)/M$, (5.37) becomes

$$\begin{aligned} I_p = [Y_{pq}]\,[V_q] = [Y_{pq}]\left([V_q] - [Z_{qk}][I_k]\right) = [Y_{pq}[V_q] - [Y_{pq}][Z_{qk}][I_k] \\ I_p + [Y_{pq}][Z_{qk}][I_k] = [Y_{pq}][V_q] \\ \left(\mathcal{I}_{pk} + [Y_{pq}][Z_{qk}]\right) I_k = [Y_{pq}][V_q] \end{aligned} \tag{5.40}$$

The term $\mathcal{I}_{pk}$ is the diagonal identity matrix. To simplify the notation, define

$$[f_{pk}] \equiv \mathcal{I}_{pk} + [Y_{pq}][Z_{qk}] \tag{5.41}$$

This results in

$$I_k = [f_{pk}]^{-1}[Y_{pq}][V_q] \tag{5.42}$$

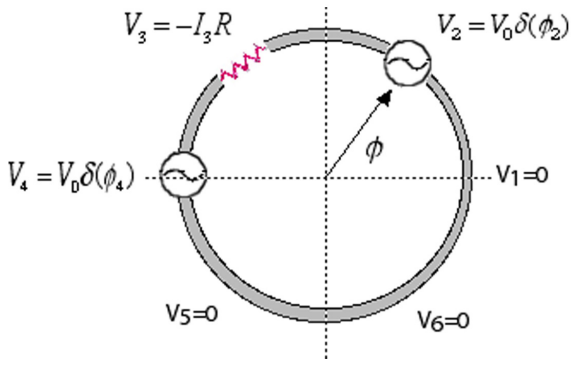

Figure 5.8: An example given by Iizuka to illustrate the use of (5.44). One must create an even distribution of loads around the ring by giving some of them the value 0.

where the inverse of the matrix f_{pk} has been taken. When (5.41) and (5.42) are substituted into the sum (5.37), the current at any angle in the ring results:

$$\begin{aligned} I(\phi) = \left[Y_q(\phi)\right]\left[V_q\right] &\rightarrow \left[Y_q(\phi)\right]\left(\left[V_q\right] - \left[Z_{qk}\right]\left[I_k\right]\right) \\ &= \left[Y_q(\phi)\right]\left[V_q\right] - \left[Y_q(\phi)\right]\left[Z_{qk}\right]\left[I_k\right] \\ &= \left[Y_j(\phi)\right]\left[V_j\right] - \left[Y_q(\phi)\right]\left[Z_{qk}\right]\left[f_{pk}\right]^{-1}\left[Y_{pl}\right]\left[V_j\right] \end{aligned} \tag{5.43}$$

The last line requires a change in the counter notation so that similarly named counters from the previous line and from the substitution are not confused. The second group of q's has been changed to j's. This allows the common voltage generator term to be removed.

$$I(\phi) = \left(\left[Y_j(\phi)\right] - \left[Y_q(\phi)\right]\left[Z_{qk}\right]\left[f_{pk}\right]^{-1}\left[Y_{pj}\right]\right)\left[V_j\right] \tag{5.44}$$

Equation (5.44) corresponds to Iizuka's equation (13), except that Iizuka set $V_j = V_0$ for $j = 1$ and $V_j = 0$ for $j > 1$. He also set $Z_1 = 0$. This represents the first of his results.

Notice the difference between (5.44) and (5.35). V_j refers to the voltage generator at j, while V_q refers to both the voltage generator and the impedance. Iizuka's other results are not pertinent to the current thesis.

5.4.2 Derivation of the Driving Point Impedance and Admittance of the Ring

Iizuka finds the driving point impedance and admittance for several example rings. Such an impedance occurs when there is only one driving source; his example put the source at $\phi = 0$, but that is completely arbitrary due to symmetry; the source can be at any of the M number of angles spread evenly around the ring. Taking it at $\phi = 0$, the impedance and admittance are calculated by dividing the source voltage, $V_1 = V_0$, by the current at $\phi = 0$:

$$Z \equiv \frac{V_0}{I(0)} = \Big([Y_1(\phi)] - [Y_q(0)][Z_{qk}][f_{pk}]^{-1}[Y_{p1}] \Big)^{-1} \equiv \frac{1}{Y} \tag{5.45}$$

5.4.3 Examples of Circular Rings with Selected Impedance Loads

Iizuka first gives an example of a ring driven by two generators loaded by a resistor, offset around the ring in a peculiar way, as shown in Fig. 5.8. His approach is to distribute three more generators for a total of six, in order to balance the other three around the ring, and then set them to 0, so they add nothing to the computation. He shows no results for this ring.

His first fully worked example puts a driving source generator at $\phi = 0$ and a load impedance, Z_L, at $\phi = \pi/2$. In this case, $M = 4$ voltage sources with $V_1 = V_0$, $V_2 = -IZ_L$, $V_3 = V_4 = 0$. The results match an unpublished calculation by King and Harrison [Iizuka, 1965, reference 4].

5.5 Conclusion

The work of Storer and Wu laid the foundation for an understanding of loop behaviour as a resonant system with many modes. Their model gives the current distribution and the characteristic input impedance of loops at low frequency when constructed of perfect conductors. Iizuka extended their model further to include impedances in the periphery of the loop. Their work remained essentially in this form all through the rest of the century. The point of the thesis is to extend their work to the optical region and to include gaps in the periphery. First, though, it is important to see what work has been done on circular rings, by physicists in the MW and optical regions. These are the topics of the next two chapters.

Chapter 6

Prior Work on Circular Rings at Microwave Frequencies (1-100 GHZ, 3-300 mm)

6.1 Introduction

Prior work on rings at high frequency focuses on circular and square rings that are used in meta-materials, beginning with work at the turn of the century in the MW region where metals still behave like conductors rather than dielectrics. Veselago [1968] had suggested that negative index of refraction materials could physically exist and if constructed would show novel optical effects. Such a material would be "left-handed", in the sense that the vectors $\vec{E}, \vec{H}$, and $\vec{k}$ would follow a left-handed rule of orientation rather than a "right-handed" rule. This result would create optical effects such as strange Doppler effects, Vasilov-Cerenkov effects, and negative refraction behaviour at the boundary with right-handed materials.

Three seminal papers form the core of efforts to design and build such negative index materials: the works by Pendry et al. [1999], Smith et al. [2000], and Shelby et al. [2001]. After examining and calculating the permeability of various configurations of metallic cylinders and rolled metallic sheets, Pendry's group decided on the flat disk, nested split-rings, shown in Fig. 6.1, as the fundamental building block of a 3D structure, which they thought would show a region of negative permeability at 13.5 GHz. In 2000 they suggested it could be used to create a perfect lens (Pendry [2000]). The Smith group included a small cylinder, just above the ring, to add a negative permittivity to the structure and thus create the negative index of refraction. The Shelby group built the structure shown in Fig. 6.2 and showed that it did indeed yield negative index phenomena (see Fig. 6.3). They used square loops instead of circular for ease of fabrication.

Pendry's group modelled the system using *RLC* circuit theory. They considered the individual ring as a single lumped inductor and approximated the mutual capacitance between two nested ring configurations in the 3D array by assuming that they acted like infinite metallic sheets. These are gross approximations at best, but did the trick to show the negative permeability of the system. In 2004, Shamonin

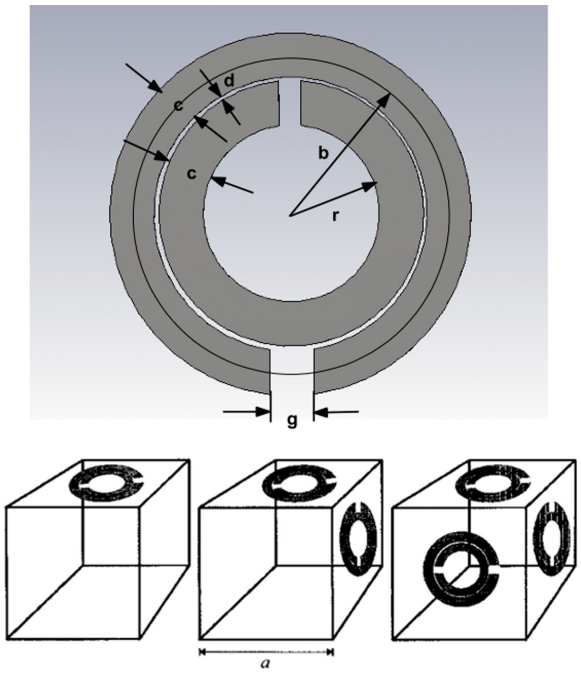

Figure 6.1: Pendry et al. [1999] design of ring and 3D structure. $a = 10.0$ mm; $c = 1.0$ mm; $d = 0.1$ mm; $l = 2$ mm; $r = 2$ mm. Consequently, the middle radius of the outside ring is $b = r + d + 1.5c = 2.6$ mm.

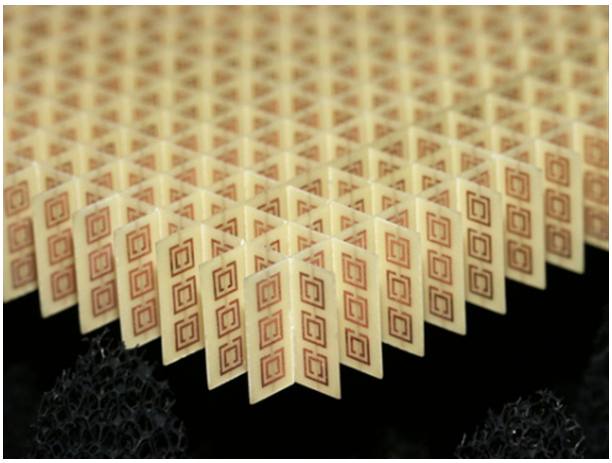

Figure 6.2: The Shelby meta-material structure using flat disk square loops. From Shelby et al. [2001]

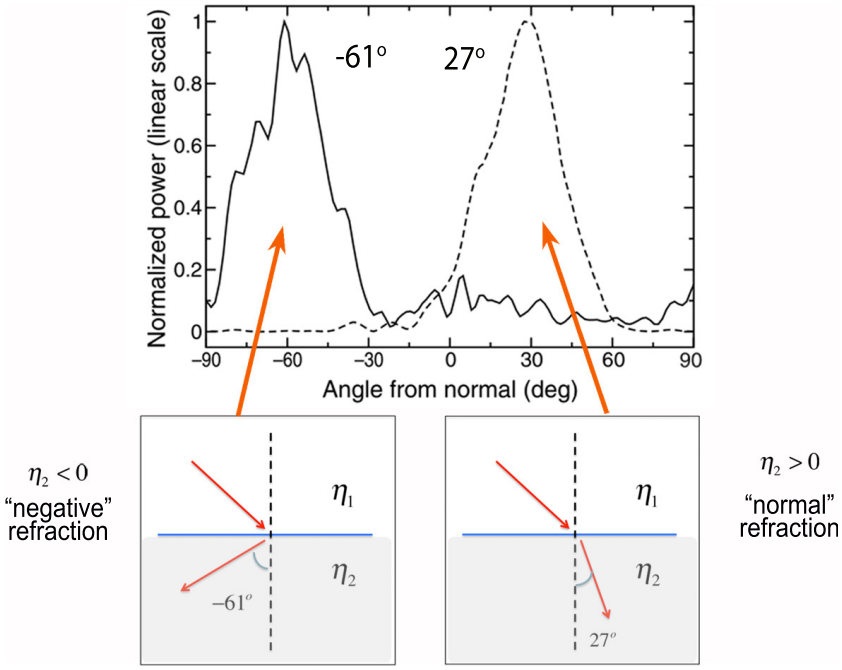

Figure 6.3: Effects of the negative Index of refraction on incident waves. The waves bend away from the normal at a negative angle, instead of toward the normal at a positive angle. From Shelby et al. [2001]

et al. [2004] set up a model which used an infinite number of lumped *LC* circuits in a circular transmission line configuration, where a lumped capacitance was taken for the gap. This allowed them to establish transmission line differential equations relating the voltage and current. They were able to show how the first, second and third harmonic resonances varied with gap widths.

A few years later, Zhou and Chui [2006] claimed more accurate results, finding that Shamonin had left out important capacitances of the system. They used instead a "Quasi-static Approximation (QSA)" of Maxwell's equation, which they claim takes into account the inductive and capacitive effects of the system completely and finds the elements rigorously, rather than empirically. QSA is an assumption specifically meant for structures that are small compared with the incident wavelength. The assumption makes their analysis inherently weaker than that used by Storer and Wu when applied to rings that are large compared to wavelength. Hence their method is analytically strong for low k_b and weaker for, say, $k_b > .6$.

I examine the Pendry paper because it shows the traditional approach an engineer would take to matter-wave interactions in the MW region. The group used *RLC* circuit principles to design a model and from that predict, design, then redesign until the desired behaviour is achieved. The paper is a fascinating study in the technique. I then review a paper by Shamonin et al. [2004] which attempted to find a more accurate *RLC* model of the same ring, but of different dimensions, using a distributed element, transmission line approach. The transmission line approach had

been used a bit earlier by Hsieh and Chang [2002] to extract lumped *RLC* elements for the closed ring and split-ring, from that determining the Q. That study presents a very different approach to transmission line models, but just as standard, and the results are just as useful. I review one of these papers to show the ideas involved. Two papers follow by S. T. Chui's group: Zhou and Chui [2006] and Zhan and Chui [2014]. Although 8 years apart, they use first principles of antenna theory in both, not to calculate the impedance using *RLC* theory as engineers would do, but to calculate the t-spectra (transmission and reflection coefficients), as physicists would have done. They do, however, calculate the L and C for every mode and therefore have all of the resonances determined by a circuit model. Results from the 2006 paper are used as partial verification of the analytical model in this thesis in Chapter 10. Their 2014 paper shows an approach that combines engineering circuit theory with methods used by physicists as they determine the t-spectra of structures. Their example is a split-ring, and they find the zero-order resonance described in Chapter 10.

6.2 Magnetism from Conductors and Enhanced Nonlinear Phenomena

Pendry et al. [1999] discovered two effects in their nested split-ring structure. The first was a very strong resonant enhancement, which, coupled with a very strong E-field within the gap, led to a high energy density storage system; the second was the exhibition of negative permeability by arrays of these loops. Fig. 6.1 shows a planar view of the single structure and a 3-dimensional view of the array. Although later rings used in meta-materials are much shorter than the incident wavelength and therefore called "sub-wavelength", this loop is not (see Problem #4 in Chapter 11). Nor is it a toroidal ring, since it is thin, broad and flat, more like a round disk.

The Pendry group's approach was to calculate an effective permeability of the structure by taking the ratio of the $\vec{B}$ field to the $\vec{H}$ field. The $\vec{B}$ field is a magnetic flux density in Webers/m^2, while the $\vec{H}$ field is the magnetic field intensity in Amperes/meter. Their ratio gives the magnetic permeability $\mu = \vec{B}/\vec{H} = \mu_{eff}\mu_0$ in Henries/meter. Here μ_0 is the permeability of free space, namely, $4\pi \times 10^{-7}$ H/m and μ_{eff} is the effective permeability to be calculated. Their approach was to calculate an average $\vec{B}$ and an average $\vec{H}$ over the unit cell.

This led to the result

$$\begin{aligned}\mu_{eff}(\omega) &= 1 - \frac{\pi r^2/a^2}{\left(1 + i\frac{1}{\omega}\frac{2l\sigma}{r\mu_0} - \frac{1}{\omega^2}\frac{3lc_0^2}{\pi \ln(2c/d)r^3}\right)} \\ &= 1 - \frac{1}{\left(\gamma - i\left(\omega m - \frac{k}{\omega}\right)\right)}\end{aligned} \tag{6.1}$$

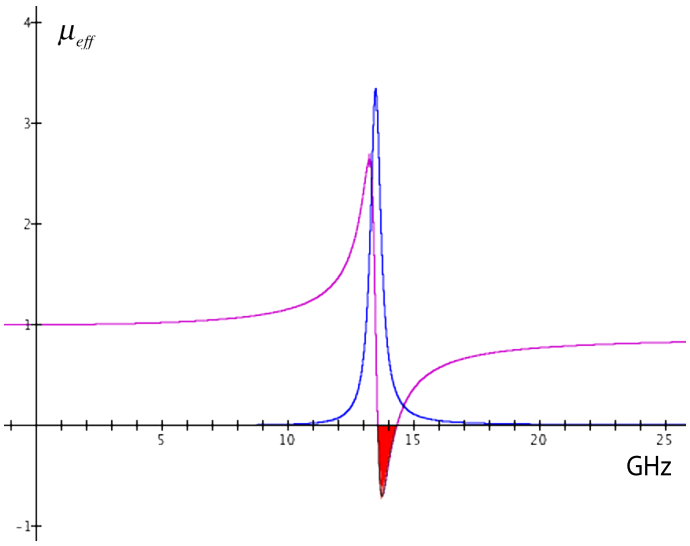

Figure 6.4: Pendry et al. [1999] constants: a=10.0 mm; c=1.0 mm; d=0.10 mm; l=2.0 mm; r=2.0 mm; $\sigma = 2000$ leading to the standard constants, $m = 2.5 \times 10^{-7}$, $\gamma = 796$, and $k = 1.8 \times 10^{15}$.

where

$$m = \frac{1}{\Pi} = \frac{a^2}{\pi r^2}; \quad \gamma = \frac{2lc_o m}{r\mu_0}; \quad \text{and} \quad k = \frac{klc_0^2 m}{\pi \ln(2c/d)\, r^3} \tag{6.2}$$

and σ is the sheet resistance of the material ring around the circumference; c_0 is the speed of light.

Equation (6.1) is in the standard form for a resonance given by (4.12), except for the 1 in front, which simply shifts it upward along the vertical axis. The resulting function appears in Fig. 6.4 and shows a strong resonance at 13.47 GHz for the given parameters.

The rather extraordinary thing that opened up the field of meta-materials was the discovery that part of the permeability curve was negative. The lower boundary of that negative piece is given by the resonant frequency; the upper boundary is defined by the second zero crossing. Pendry's group called the latter the "magnetic plasma frequency".

6.3 Properties of a metamaterial element: Analytical solutions and numerical simulations for a singly split double ring

In the mid-decade, researchers in Germany and the UK came together on two papers in which they developed a transmission line *RLC* equivalent model of the Pendry split-ring configuration, with and without a gap in the inner loop (Shamonin et al. [2004] and Shamonin et al. [2005]). Using the model they calculated a very strong

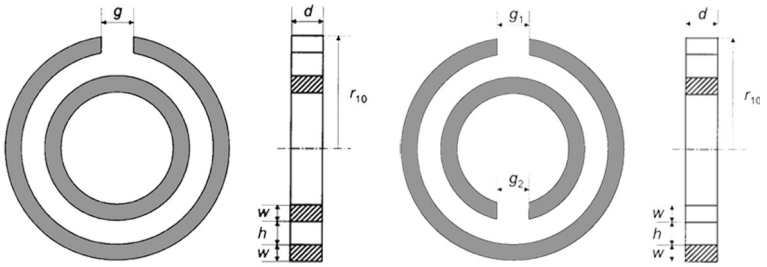

Geometry, mm			
r_{10}	9.0	d	2.5
w	0.5	h	1.0
Inductances, nH/rad			
L_1	4.96	L_2	3.83
L_a	3.36	M	2.79
Inter-ring Capacitance pF/rad			
C	0.27		

Figure 6.5: The configuration of the two ring systems studied by the Shamonin group. (a) from Shamonin et al. [2004] Fig. (1) and (c) from Shamonin et al. [2005] Fig. 1.

resonance, reminiscent of the sub-wavelength resonance found by Smith et al. [2000] (see Problem #4 in Chapter 11), which I shall call in Chapter 10, the "zero-order resonance". The configurations of the two systems with their corresponding *RLC* values for their model appears in Fig. 6.5.

The model for the first configuration with a gap only in the outer loop is shown in Fig. 6.6. In Fig. 6.5(a), the inner gap capacitance is set to infinity, while in (b) it is given a finite value.

A standard solution of the transmission line equations in the angle, ϕ, yields enough equations to solve for all unknown constants. Note that the angular coordinate runs in the clockwise direction to match the transmission line current. An equivalent circuit of one angular element of the loop, $d\phi$, is shown in Fig. 6.7.

For system (a), the results are:

$$
\begin{aligned}
V &= V_0 \sin(k(\phi - \pi)) \qquad (6.3)\\
V_0 &= \frac{\gamma_C}{D}\frac{Z_C}{\omega L_a}(G_2\xi_M - G_1\xi_2) \quad \text{and} \quad k^2 = \omega^2 C L_{eq}\\
I_0 &= i\frac{V_0}{Z_C}\frac{\sin(k\pi)}{k\pi}\frac{L_{eq}}{L_a}\gamma_L^{1/2} + -i\frac{1}{\omega L_a}\left[G_2(\xi_1 - \xi_M) + G_1(\xi_2 - \xi_M)\right]\\
I_1 &= i\frac{V_0}{Z_C}\left[\cos(k(\phi - \pi) + \gamma_1\frac{\sin(k\pi)}{k\pi}\right] - i\frac{1}{\omega L_a}\left(G_1\xi_2 - G_2\xi_M\right)\\
I_2 &= I_0 - I_1\\
\gamma_C &= \frac{C}{C_G}, \quad Z_C = \sqrt{\frac{L_{eq}}{C}}, \quad L_a = \sqrt{L_1 L_2 - M^2}, \quad L_{eq} = L_1 + L_2 - 2M
\end{aligned}
$$

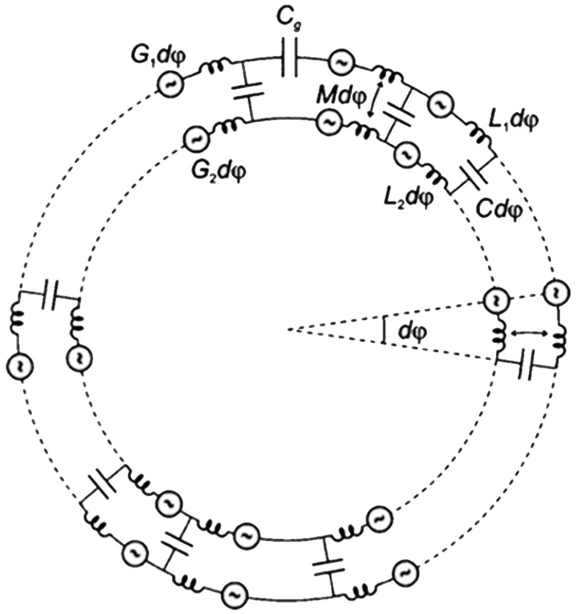

Figure 6.6: The corresponding transmission line model for (a) in Fig. 6.5. From Shamonin et al. [2004], Fig. 2.

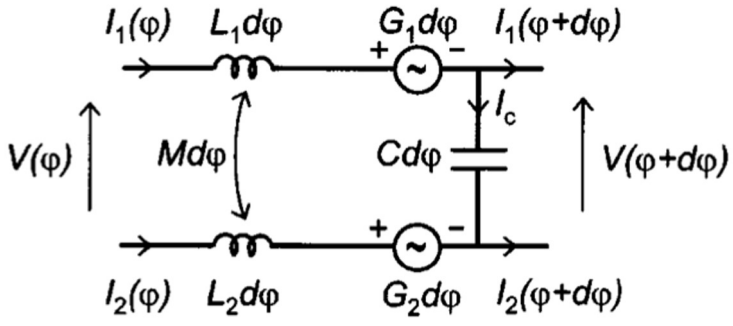

Figure 6.7: A section, $d\phi$, of the Shamonin transmission line model. From Shamonin et al. [2004], Fig. 3.

$$\xi_1 = \frac{L_1}{L_a}, \quad \xi_2 = \frac{L_2}{L_a}, \quad \xi_M = \frac{M}{L_a}, \quad \gamma_L = (\xi_2 - \xi_M)^2$$
$$D = \frac{(\sin(k\pi)}{k\pi}(2\pi k^2 - \gamma_C\gamma_L) - \gamma_C \cos(k\pi)$$

Note that L_{eq} is the equivalent inductance of the two loops taken together per unit angle. The results are similar for system (b) with an extra gap capacitance[1].

Resonances occur when $D = 0$, which leads to multiple roots. These can be determined once all of the inductances and capacitances are known. This is the difficult part of the exercise and probably the least accurate. Their method is to use tables constructed by Grover [1981] and by Hammond and Sykulski [1994] to determined the *LC* element values. There are several problems with this approach:

(1) The tables were generated for low frequency applications and are not applicable when the material changes its behaviour at higher frequencies. This makes the results meaningless much above 100 GHz. Fortunately, Shamonin et al. are applying their work at 1 to 20 GHz, but their work cannot be extended to the optical region.

(2) Using the tables forces values on the inductances and capacitances instead of elucidating values, in the sense of a method that generates values as results. In other words, the loop ought to be yielding the functions $R = R(\omega)$, $L = L(\omega)$, and $C = C(\omega)$, from which resonances can be calculated.

(3) The geometries selected from the tables are similar to the ring, but do not represent the ring exactly.

Nevertheless, their calculated resonances match simulated resonances well, and their transmission line approach is a step toward a more accurate *RLC* model than the approach of Pendry et al. [1999].

Shamonin's group examined a number of the resonances, but I will focus on the lowest mode resonance as an example of their method, because it corresponds to the zero-order mode analysed in Chapter 10. They call this their "fundamental" mode. The first example uses configuration (a). They give $\omega^2 = (1 + \gamma_L)/(2\pi C_g L_{eq})$, their Eqn. (20), as the resonance condition. The resonances are determined by the gap capacitance, C_g, and the equivalent inductance of the loop $L_{eq} = L_1 + L_2 - 2M$, which includes the significant mutual inductance between the rings. The capacitance for a gap width of 2.5 mm is $16.5 \times 10^{-15} F$. They calculate resonance at 2.72 GHz.

The next step is important. They calculate that the fundamental resonance comes from a half wavelength current distribution around the loop. This is very true, as Chapter 10 notes. The gap capacitance, in conjunction with the zero-order mode inductance of the loop, causes this resonance of rings to occur near the half-wavelength. But it is not due to a fundamental half-wavelength resonance, as sometimes happens in physical systems. The gap size is the important parameter and large gap widths

[1]It is likely that γ_1 in I_1 is a typography error and is probably γ_L.

bring the resonance closer to $k_b = 0.45$ than do smaller gap widths (see Chapter 10 for more details). So this is not a half-wavelength resonance, as they suspected.

The second example comes from their July 2005 paper, in which the inner ring also has a gap with the same capacitance value as the gap in the outer ring. Here the lowest resonance is again sub-wavelength but this time determined by (6.4). The configuration table in Fig. 6.6 still applies.

$$\omega_0^2 = \frac{1}{L_{av}\left(\frac{2\pi C}{4} + C_{g1} + C_{g2}\right)}, \quad L_{av} = \frac{L_1 + L_2}{2} \tag{6.4}$$

They give the resonances in their Fig. (3) (a), and it appears again to be very close to 2.7 GHz. Apparently the gap in the second ring does not greatly affect this mode.

The important point to draw from their work is that they use *RLC* circuit theory to establish the resonances of the ring, they recognise the existence of the many harmonic modes of the ring, and they have a way of calculating them. The model is certainly not an easy one, and they neglect loss in the material, which is a reasonable assumption for the MW region, but not for the optical.

6.4 Eigenmodes of metallic ring systems: A rigorous approach

A year or so following the two Shamonin papers, Zhou and Chui [2006] suggested an analytical model based on first principles that yielded an *RLC* model of the thin ring in approximation. They used it to calculate all modal resonances of the ring and named them based on even and odd symmetric principles. The approximation is called the "Quasi-static Approximation" [Jackson, 1999, see Sec. 5.18], in which the the system is small compared to the wavelength associated with the dominant time-scale of the problem. In other words, the system is sub-wavelength to the incident signal. This allows Zhou and Chui to neglect the displacement current in the fundamental differential equation derived from Maxwell's equations that describes the system. It is an assumption which allows signals within the system to propagate at the speed of light.

The analysis, consequently cannot be applied in the optical region where the material is not a good conductor. Nevertheless, their efforts do produce a model that gives the radiation resistance, inductance and capacitance of the loop and all of the modal resonances within these conditions. The method is therefore worth understanding.

They give the "inductive Electric field" as:

$$\vec{E}_L(\vec{r}) = -\frac{\partial \vec{A}}{\partial t} = -\omega\mu_0 \frac{\int \vec{j}(r')d\vec{r}'}{4\pi|\vec{r} - \vec{r}'|} \tag{6.5}$$

and the "capacitive Electric field" as:

$$\begin{aligned}\vec{E}_C(\vec{r}') &= -\nabla V(\vec{r}') = -\nabla \frac{1}{4\pi\epsilon_0}\int \frac{\rho_e(\vec{r}')d\vec{r}'}{|\vec{r}-\vec{r}'|} \\ &= \frac{1}{i\omega}\frac{1}{4\pi\epsilon_0}\nabla \int \frac{[\nabla'\vec{j}(\vec{r}')]d\vec{r}'}{|\vec{r}-\vec{r}'|}\end{aligned} \tag{6.6}$$

The solutions to these are obtained by firstly assuming the "thin-wire" approximation, in which the radius of the metal wire is taken to be considerably smaller than the radius of the ring, secondly by expanding the current as a Fourier series in the azimuthal angle ϕ, and thirdly by expanding the term $1/(|\vec{r}-\vec{r}'|)$ in spherical harmonics. The first simplifies the calculations by assuming that the current flows at the center of the wire, even though it actually flows at the boundary, and that the current is not toroidal. The second is the same approach taken by Storer (see (5.18)). The third is a standard expansion to determine the far-field components of a radiating field and in this, they follow [Jackson, 1999, Sec. 3.5].

The solutions are:

$$E_L^m = -i\omega L_m I_m \quad \text{and} \quad E_C^m = i\frac{1}{\omega C_m} I_m \tag{6.7}$$

where

$$\begin{aligned} E_L^m &= \frac{1}{2\pi}\int_0^{2\pi} \vec{E}_L \cdot \vec{e}_\phi e^{-im\phi} d\phi \quad \text{and} \quad L_m = \mu_0 \frac{(A_{m-1}+A_{m+1})}{4} \\ E_C^m &= \frac{1}{2\pi}\int_0^{2\pi} \vec{E}_C \cdot \vec{e}_\phi e^{-im\phi} d\phi \quad \text{and} \quad C_m = \epsilon_0 \frac{2R(R-a)}{m^2 A_m} \\ A_m &= \sum_{l=|m|}^{\infty} \frac{(l-m)!}{(l+m)!}\alpha^j \left[P_l^m(0)\right]^2 \quad \text{and} \quad \alpha = \frac{R}{R+a} \end{aligned} \tag{6.8}$$

in which P_l^m is the associated Legendre function. This is a remarkable result, since the model gives inductance and capacitance values for the ring for every mode for perfectly conducting metals. According to the authors, the external field, which includes the incident and re-radiated fields plus the inductive and capacitive fields, drives the current distribution through the resistance of the material from which the ring is made and the resistance of the gap. $\bar{\rho}(m-m')$ is the Fourier component of resistivity normalized by the area through which the current passes: $\rho(\phi)/S$.

$$E_{ext}^m + E_L^m + E_C^m = \sum_{m'} \bar{\rho}(m-m') I_{m'} \tag{6.9}$$

$$E_{ext}^m = \sum_{m'} \left(\bar{\rho}(m-m') I_{m'} + (i\omega L_m I_m - i\frac{1}{\omega C_m})\delta_{mm'} I'_m \right) = \sum_{m'} H_{mm'} I_{m'} \tag{6.10}$$

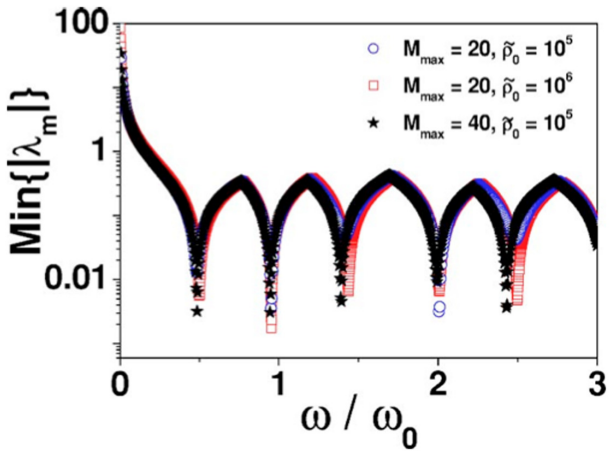

Figure 6.8: Resonances given by Zhou and Chui for their example 1 ring: ring radius $R =$ 4mm, wire radius $a =$ .1mm, and gap width $\Delta = \pi/40$; from Zhou and Chui [2006] Fig. 2.

where

$$H_{mm'} = \bar{\rho}(m - m') + i\omega L_m \left(1 - \frac{\omega_m^2}{\omega^2}\right) \delta_{mm'} \quad \text{where} \quad \omega_m^2 = \frac{1}{L_m C_m} \tag{6.11}$$

The eigenvalues of $H_{mm'}$, found by diagonalizing $H_{mm'}$, are recognizable as the modal impedances (see (4.22)):

$$\lambda_m = \bar{\rho}_m \left(1 + iQ \left(\frac{\omega}{\omega_m} - \frac{\omega_m}{\omega}\right)\right) \quad \text{where} \quad Q = \frac{\sqrt{L_m/C_m}}{\bar{\rho}(m)} \tag{6.12}$$

Consequently, Zhou and Chui also have recognized a method for calculating the quality factor of the loop and have ascertained that the loop acts like a series resonant circuit at a given frequency.

They present the resonances calculated for two open-ring structures similar to the Pendry outer ring. Both example rings have a gap of angular width $\pi/40$. The first ring has an $\alpha = .99$, which corresponds to a Storer Ω value of 12.87. Fig 6.8 reproduces their Fig. 2. They call the resonances near 0.96 and 2.0 "even-numbered", while those near .5, 1.42, and 2.48 "odd-numbered resonances". It should be noted that the even-numbered resonances can be calculated using their formula for resonances noted above; namely, $\omega_m^2 = 1/(L_m C_m)$. This does not work for the odd-numbered resonances and they suggest that these resonances are perhaps created by the gap. They are not; according to Storer, they are the anti-resonances (see discussion in section 5.3.5).

Zhou and Chui's second ring has ring radius $R = 4$ mm and wire radius $a = .1$ mm, equivalent to a Storer $\Omega = 11$. They present the transmittance of a 2D planar structure, in which the xy plane is tiled with these rings, using a lattice constant 16 mm in both directions. Again they find even and odd-numbered resonances at about

the same places as in their prior figure: .5, .96, 1.4, 2, and 2.48.

The importance of their work is that they produce a rigorous *RLC* circuit theory for the ring. The inductances and capacitances for each mode are readily found, and the model is not cumbersome, although complicated.

6.5 t matrix of metallic wire structures

Very recently, Zhan and Chui [2014] extended their group's previous work, discussed in section 6.4 above, to provide an *RLC* circuit theory model in which retardation effects are taken into account for metallic wire structures. This provides the current within the structure making it straightforward to calculate the scattered field and hence the transmission matrix of the structure. They illustrate their method using the split-ring resonator.

In their method an incident plane wave is expressed in terms of spherical Bessel and Hankel wave functions.

$$E^o(\vec{r}) = \sum_{n=1}^{\infty} \sum_{m=-n}^{n} a^o_{Emn} N^{(1)}_{mn}(k\vec{r}) + a^o_{Hmn} M^{(1)}_{mn}(k\vec{r}) \tag{6.13}$$

The coefficients, a^o, depend upon the polarization and propagation direction of the wave. The scattered field may be expressed in the same way, and its coefficients are related to the incident coefficients through the 't' or transmission matrix.

$$a^s_{Pmn} = \sum_{n'=1}^{\infty} \sum_{m=-n'}^{n'} t_{Pmn,Pm'n'} a^o_{Pm'n'} \quad \text{for} \quad P = E, H \tag{6.14}$$

Scattering depends on the interaction of the incident wave with the metallic structure which in turn depends upon the currents induced, so it is important to have a good modal representation of that current. Zhan and Chui look for a set of basis functions that will accomplish this for the given structure. The general form they introduce is

$$I_m = \sum_{n'=1}^{\infty} \sum_{m=-n'}^{n'} Y_{m,m'} E^o_{m',n'} \tag{6.15}$$

where Y is an effective admittance. $E^o_{m,n}$ are the expansion coefficients of the incident wave in terms of the spherical basis functions mentioned above.

$$E^o_{mn} = \xi_{Emn} a^o_{Emn} + \xi_{Hmn} a^o_{Hmn} \tag{6.16}$$

The scattered field is calculated from the induced current by using the dyadic Green's function and carrying out some integrations. The coefficients are then given in terms of the current:

$$a^s_{Emn} = \eta_{Emn} I_m \quad \text{and} \quad a^s_{Hmn} = \eta_{Hmn} I_m \tag{6.17}$$

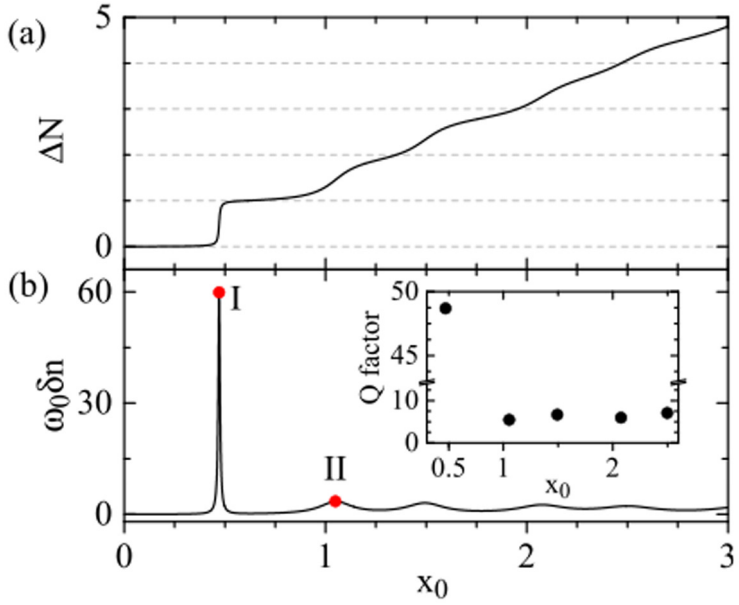

Figure 6.9: Integrated density of states top) and density of states (bottom) calculated from Zhan and Chui [2014], Fig. 2. Note the very high, zero-order resonance, marked "I", at $x_o = kr_o = .47$. Also note the resonance marked "II" at $x_0 = 1.06$

The t-matrix is then given by

$$[t] = [\eta][Y][\xi] \tag{6.18}$$

Under various assumptions the scattering cross-section and the absorption cross-section can be calculated from the transmission matrix.

In applying their model to the ring resonator, they introduce an RLC circuit model of the following form. Consider a ring of radius r_0 and wire radius $a = .01r_0$ with a small gap at the origin in air. Fourier current components, I_m are induced in the ring by the incident wave, where m is the modal number of the wave. The ring itself is composed of modal impedances, where (using $e^{-i\omega t}$)

$$Z_m = \rho_c - i(\omega L_m - \frac{1}{\omega C_m}) \tag{6.19}$$

The term ρ_c is the resistivity of the wire. The gap resistivity, ρ_g, is assumed to be very large. Applying (6.8), they arrive at a closed form for the t matrix for the split-ring. Fig. 6.9 shows their main results of the calculation. A large resonance appears at about $x_o = 0.47kr_o$ and minor resonances follow at higher frequencies. Note that $k = 2\pi/\lambda$ the wavenumber. This large resonance is the zero-order resonance and again, as in Shamonin, it appears near the half-wavelength mark. They calculate a quality factor, $Q = 48.7$. The source of this extra resonance is attributed to the zero-crossing of the imaginary part of, what they call, the "effective" impedance of the

loop, given as

$$Z_e = 1/\left(\sum_m \frac{1}{Z_m}\right) \tag{6.20}$$

They cite McKinley et al. [2012] for this effective impedance.

The important point to take away from their results is that the *RLC* models of rings are becoming more sophisticated, are using many Fourier modes, and can be used as the basis for calculating scattering cross-sections. The Zhan and Chui model, however, does not yet incorporate a sophisticated model of the ring material and therefore is not useful for the THz and optical regions.

6.6 Conclusions

This is where things stand now with regard to attempts at finding accurate *RLC* models of rings. There have been many alternative suggested, but all in the same vein as those reviewed here. The search has been for less complicated and faster computational models. Prior work performed in this regard at the optical frequencies follows in the next chapter.

The work of this thesis in Chapters 8 and 9 advances the models of this chapter in three ways:

- finding a more accurate *RLC* model at low frequencies,
- adding material characteristics to the low frequency model so that it becomes useful at high frequencies, and
- discovering that the resulting model provides a fast computation of the current, resonances, and other characteristics of the loop that are very close to simulated and experimental results.

Chapter 7

Prior Work on Circular Rings at TeraHertz and Optical Wavelengths (3-400 nm)

7.1 Introduction

This chapter reviews prior work in the TeraHertz (THz), Infra-red (IR), and Optical (OR) regions. Of the many developments related to rings that have occurred during the last decade and a half, the following are relevant to this thesis:

- the modelling of nano-particles and nano-particle systems as nano-resistors, nano-inductors and nano-capacitors (see, for example, the seminal work by Engheta's group, including Engheta et al. [2005]);
- the modelling of plasmons using *RLC* elements (see, for example, the seminal works by Yablonovitch's group, including Staffaroni et al. [2012]);
- combining the two approaches, the most recent work along these two lines (see work at IMRE in Singapore by Zhu et al. [2014]);
- the use of simple *RLC* models to understand various meta-material ring configurations at the higher frequencies (see, for example, Linden et al. [2004]; Zhou et al. [2005]; Tretyakov [2007]; Soukoulis et al. [2007]; Delgado et al. [2009]; Elhawil et al. [2010]);
- applications of RF antenna theory to rings specifically designed for the optical region (see in particular, Locatelli [2011]).

This is not to say there have been no other developments with rings. For example, very interesting work has been done with loop arrays for light focusing (Memarzadeh and Mosallaei [2011]), beam shifting (Ahmadi and Mosallaei [2010]), imaging (Xu et al. [2010]), nested rings (Chowdhury et al. [2011b,a], and optical properties from the point of view of plasmonics (Aizpurua et al. [2003]; Dutta et al. [2008]). Moreover, there has been considerable work on the fabrication of nano-scaled rings (Linden et al. [2004]; Clark and Cooper [2011]; Cai et al. [2012]; Halpern and Corn [2013];

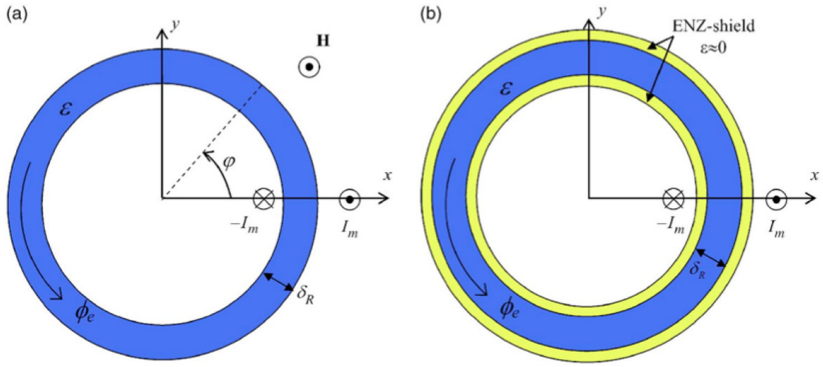

Figure 7.1: Silveirinha et al. [2008]'s design (their Fig. 2) of a nano-circuit using a ring to close the circuit loop. Note the transformer coupling for exciting the ring.

Wang et al. [2014]) and on the imaging of plasmons in rings (Larsson et al. [2007]; Koh et al. [2010, 2011]). But these studies were not informed by low frequency circuit theory. The focus here is on ring research using *RLC* circuit models.

7.2 Nano-particles as *RLC* Circuit Elements

A series of papers appeared in the mid-2000s from a group at the University of Pennsylvania in conjunction with a group at the University of Rome Tre in Rome, Italy (Engheta et al. [2005]; Salandrino et al. [2007]; Alu et al. [2007]) in which the goal was to treat nano-particles as lumped *RLC* circuit elements; "nano-elements". They were successful in constructing nano-scaled circuit representations of spherical nano-particles, connecting these elements in series and parallel configurations, creating a nano-circuit in the form of a ring, and even synthesising circuits from various nano-structures. There does not appear to have been any extension of the ideas since then, except for the idea of using a ring as a way to construct series and parallel interconnections of nano-capacitors and nano-inductors in a closed-loop (see Silveirinha et al. [2008]). The rings shown in Fig. 7.1 are excited using a transformer coil carrying current.

This work is important because it explores nano-particle configurations that would work as tiny circuits; it explores the resistive, inductive, and capacitive behaviour of these particles, not as plasmons, but as circuit elements. It also explores means of interconnecting them. The use of Maxwell's equations appears in the quasi-static approximation and is therefore is limited to perfectly conducting materials ([Jackson, 1999, see Sec. 5.18]).

7.3 Plasmons as RLC Circuit Elements

An alternative to the idea that nano-particle structures, as objects, can be modelled by RLC circuits is the idea that the behaviour of plasmons themselves can be modelled by distributed RLC circuits, as in transmission lines. In a seminal paper Staffaroni et al. [2012], provided descriptions for bulk plasmons, single surface plasmons and parallel-plate waveguide plasmons, by which the authors meant simple circuits representing plasmons induced in certain configurations of metallic materials. Bulk plasmons, as they describe them, occur in the bulk of, say, a rectangular metal bar. Single surface wave plasmons occur on the surface between a metal and free-space. Parallel-plate plasmons are guided in some direction by the parallel plates.

The simple circuits created in this paper capture most of the physics, so the authors claim, of behaviour in the optical region for these three types of plasmons. They can, for example, reproduce frequency vs wave function (f vs k) dispersion relations and provide a characteristic impedance for the parallel-plate plasmonic waveguide. For each new plasmonic configuration, the distributed inductance and capacitance need to be recalculated, and this calculation depends greatly on something called the "kinetic inductance" or "self-inductance" of electrons.

Kinetic inductance arises from the inertia of electrons. Since electrons have mass, they have an inherent hesitation to accelerate and decelerate that all massive bodies do. This phenomenon doesn't warrant any attention at low frequencies because electron mass is so small that the reluctance is almost nil. But at THz and optical frequencies, when the incident $\vec{E}$ field alternates on the order of 10^{12} to 10^{15} times per second, the electrons simply can't keep up. First they go out of phase with the $\vec{E}$ field and second, they lose kinetic energy to radiation (since electrons radiate when they accelerate and decelerate).

The effect is seen in metals by the arising of a complex imaginary term in the conductivity. The Drude model for the conductivity characterises metals in the optical region (see section 9.2.1):

$$\sigma = \frac{\omega_p^2 \epsilon_0}{2\Gamma + i\omega} = \omega_p^2 \epsilon_0 \left(\frac{2\Gamma}{(2\Gamma)^2 + \omega^2} - i \frac{\omega}{(2\Gamma)^2 + \omega^2} \right) \tag{7.1}$$

where Γ is the damping frequency, ω_p a very large frequency called the plasma frequency, and ϵ_0 is the permittivity of free-space. The imaginary term becomes more important as the frequency increases. The real and imaginary parts are equal when $\omega = 2\Gamma$, so the imaginary term becomes important at about $1/10$ of that, which for gold is about $.0013eV = 330$ GHz. This fundamentally explains the difficulties in bringing meta-material behaviour to the THz and IR regions from the MW region. The electrons can't keep up with the incident fields.

Kinetic inductance attempts to take this effect into account in an easy way. In a conventional inductor, a changing magnetic field produces an electromotive force (emf) that causes a current which opposes the original change in the field. This is called "reactance". In kinetic inductance, inertia prevents charge from responding

immediately to an impressed electric field, and the effects with respect to the current are the same as that described above in an inductor; the current behaves in the same way, with a phase shift and a magnitude change. In a straight wire the kinetic inductance is found by setting the kinetic energy of the electrons to the energy stored in an inductor, the kinetic inductor. The number of electrons in a length, l of wire with a cross-sectional area, A, is nlA, where n is the free electron concentration, $\#/m^3$. The current passing is $I = nAev$. Then,

$$\frac{1}{2}mv^2(nlA) = \frac{1}{2}L_kI^2 \quad \text{giving} \quad \boxed{L_k = \frac{ml}{ne^2A}} \tag{7.2}$$

Kinetic inductance then is a simple way of introducing an inductive element to handle the Drude characteristics of a metal at THz frequencies and above. This inductance is simply added to the Faraday inductance, which it dominates at these frequencies. In fact the wire will now carry a complex impedance given by $1/\sigma \times l/A$. This will have a real term, the resistance giving heat loss, and an imaginary term, the reactance, giving the phase differences.

The model is a remarkably simple way of thinking about electron behaviour at optical frequencies, and the Staffaroni paper shows that it is about right in its correspondence to actual behaviour for the three types of plasmons studied.

The work is important because it recognises the important way that the Drude model affects metals at high frequencies and gives a simple circuit model for handling it. This work has so far not been applied to metallic rings. I review the paper because I use an expanded Drude model in Chapter 9 to extend low frequency antenna theory of rings to the optical region.

7.4 Combining the Previous Two Approaches

An extension of the above approaches appears in a paper by the IMRE Singapore group in Zhu et al. [2014]. They worry that the previous work does not lead to a sufficiently intuitive understanding of the underlying physics. They therefore seek to expand it using thermodynamic principles in which the underlying energy phenomena are associated with corresponding nano-elements. In particular they seek some predictive results from the modelling. Their effort is rewarded with an *RLC* circuit model of a nano-rod plasmonic resonator which produces the correct spectral response, including the main resonance and Q. The model includes the kinetic and Faraday inductances, ohmic losses, radiation loss and capacitance due to the potential energy. They include a term for free-electron conduction that apparently isn't included in the previous work above. They apply the approach also to a metal nanosphere and to a square split-ring, modelling the zero-order mode resonance, found in all of the meta-material split-rings, with a simple L and C.

The work is important because it attempts to ground the *RLC* nano-circuit ideas developed in previous work with energy principles that can be applied to generic configurations of plasmonic structures.

7.5 *RLC* Models of Meta-material Ring Configurations

Given the success of meta-materials to effect negative index behaviour in the MW, it would be natural to attempt an extension to the THz, IR and OR. Physicists and engineers, both, moved in that direction almost immediately, but found that the Drude behaviour of metals caused substantial losses and limited their effectiveness (Stockman [2006]).

As part of that effort, several groups have turned to the development of equivalent *RLC* circuit models that would take the Drude effects into account, and their method of doing so was to employ the kinetic inductance term, then look for other sources of capacitance that might affect the resonance of loops, such as capacitance between the ring and the substrate and between coupled rings (Elhawil et al. [2010]). Some looked at multiple gaps in the square ring to see how the addition of gaps might affect the placement of the resonance, with the extra gaps also being modelled by capacitors (Soukoulis et al. [2007]; Delgado et al. [2009]). Most of these efforts focused on square rings, instead of circular rings but the results make little difference. All of these studies found that the material caused a saturation of the zero-mode resonance frequency determined by their simple LC circuit.

One way to show this saturation is to look at a plot of resonance vs some scaling factor; that is, some representative size parameter of the ring, usually the radius of the ring. Fig. 7.2 shows saturation curves given by Zhou et al. [2005]; Tretyakov [2007], and Delgado et al. [2009]. The bending of the curves show a non-linear response to scaling, and an eventual saturation in the resonances, so that at frequencies above some limit, the dipole or ring will not resonate.

These works are important because they have found a way to include Drude effects simply, using the kinetic inductance, but they were then able to use this new inductance with new capacitive effects to predict how resonances would change as the Drude phenomena played itself out at the optical wavelengths; namely, as resonance saturation.

Chapter 9 of this thesis elucidates resonance saturation with a more detailed and accurate *RLC* model for toroidal rings and a more detailed Drude model for the optical region that takes into account inter-band transitions in the metals.

7.6 Applications of RF Antenna Theory to Rings in the Optical Region

Beginning in 2009 a group at the University of Brescia, Italy, wrote two papers with the express goal of applying low frequency antenna theory to the optical region. They began with a standard center-fed wire dipole of optical length (Locatelli et al. [2009]), by employing an integral approach. They recognised immediately that the normal assumption of the perfectly conducting wire would not hold and instead added a surface impedance that was dependent on the characteristics of the metal. They borrowed the functional form of the surface impedance from a very early work

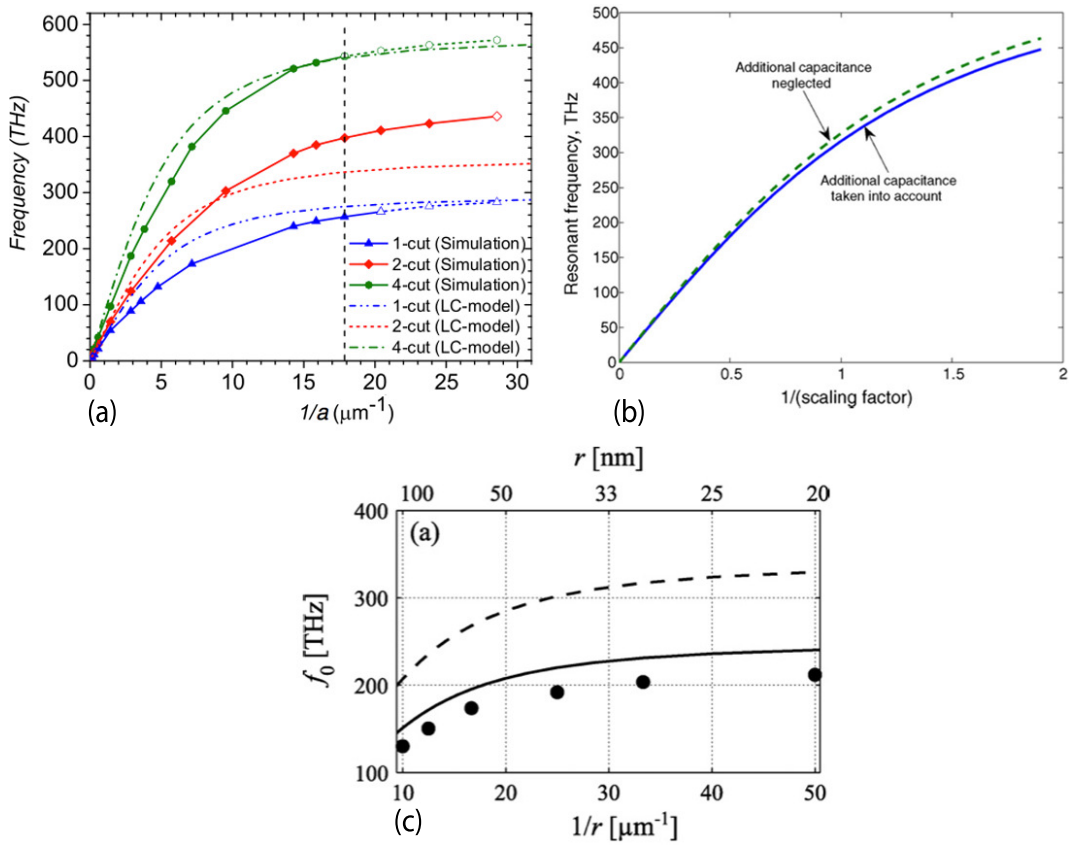

Figure 7.2: Resonance saturation and wavelength scaling as given by (a) Zhou et al. [2005] Fig. 2, (b) Tretyakov [2007] Fig 3, and (c) Delgado et al. [2009] Fig. 3a. The scaling factor, a or r, is the radius of the ring. Scaling is evident from the bending of the curve and saturation occurs when the curve goes flat.

by Stratton [1941], recently made more relevant by its application to IR and optical dipole antennas by Hanson [2006].

The surface impedance term they used is:

$$Z_s = \frac{\gamma J_0(\gamma a)}{2\pi a \sigma J_1(\gamma a)} \tag{7.3}$$

where J_0 and J_1 are Bessel functions of order 0 and 1, a is the radius of the wire, σ is the conductivity of the material, and γ is the characteristic complex wave function in the material, given as $k = \beta + i\alpha/2 = \beta = 2\pi/\lambda = \omega/c$ in the review of Storer's work, (5.10), but here $\alpha \neq 0$. Instead,

$$\gamma = k = \frac{\omega\eta}{c} = \frac{\omega}{c}\sqrt{1 - i\frac{\sigma}{\omega\epsilon_0}} \quad \text{if using } e^{-i\omega t} \tag{7.4}$$

where η is the index of refraction of the material. The governing equation for the

cylinder is

$$(\partial_z^2 + k_0^2)A_z = i\frac{\omega}{c}\eta\,(E_z - I(z)Z_s) \tag{7.5}$$

Locatelli's group forms the vector potential $\vec{A}$, as was done by Storer (5.8), but for the cylindrical wire.

$$\begin{aligned} A_z &= \frac{\mu_0}{4\pi}\int_{-L/2}^{L/2} I(z')K(z-z')dz' \quad \text{where} \\ K(z-z') &= \frac{1}{2}\int_0^{2\pi} \frac{e^{-ik_0R}}{R}d\phi \quad \text{and} \\ R &= \sqrt{(z-z')^2 + \rho^2 + a^2 + 2\rho a\cos(\phi')} \end{aligned} \tag{7.6}$$

The point (x, y, z) is the observation point and (x', y', z') is the position of the source element located on the wire surface at $\rho = a$. This result, Eqn. 7.5, is Pocklington's equation as it applies to a cylindrical wire in the optical region.

The group continued by simulating Eqn. (7.6) using a Method of Moments to find the current distribution on the wire. A 1 volt delta function across the gap drives the loop, the method used by Storer (see (5.6)). They then calculated the input impedance, as would normally be the case in applied antenna theory. They produced plots of the input resistance and reactance, showed how they could remove the effects of the gap used in the simulation scheme, and determined the radiation resistance and the loss resistance. Fig. 7.3 shows the impedance curves from their paper.

The second paper was written singly by Locatelli [2011], and focused on the optical properties of rings. He simply took the cylindrical wire and brought the ends almost together to form a ring with a small gap. The results from the first paper for cylindrical wires apply. He was able to develop the input impedance, which showed the fundamental and several of the harmonic modes (see Fig. 7.4). He pointed out the integer and half-integer resonances. He shows that the radiation efficiency, given by $R_{rad}/(R_{loss} + R_{rad})$ peaks at the fundamental (see Fig 7.4). He shows some stunning simulations of the current distribution at the integer and half-integer resonances, Fig 7.5 showing that indeed the half-integers are anti-resonances in which very little current flows, as was determined by Storer (see Section 5.3.5). Finally, he was able to show wavelength scaling and resonance saturation for rings.

It is worth pointing out his note that the gap did not affect the position of the resonances but did affect the position of the anti-resonances.

The work by the Brescia group is important because it provided, for the first time, standard RF antenna theory principles and design procedures to the optical region, arriving at significant results. The work of this thesis uses many of their ideas and extends their results by creating a full *RLC* circuit model of the loop applicable at all frequencies, which is the topic of the next Part "New Work".

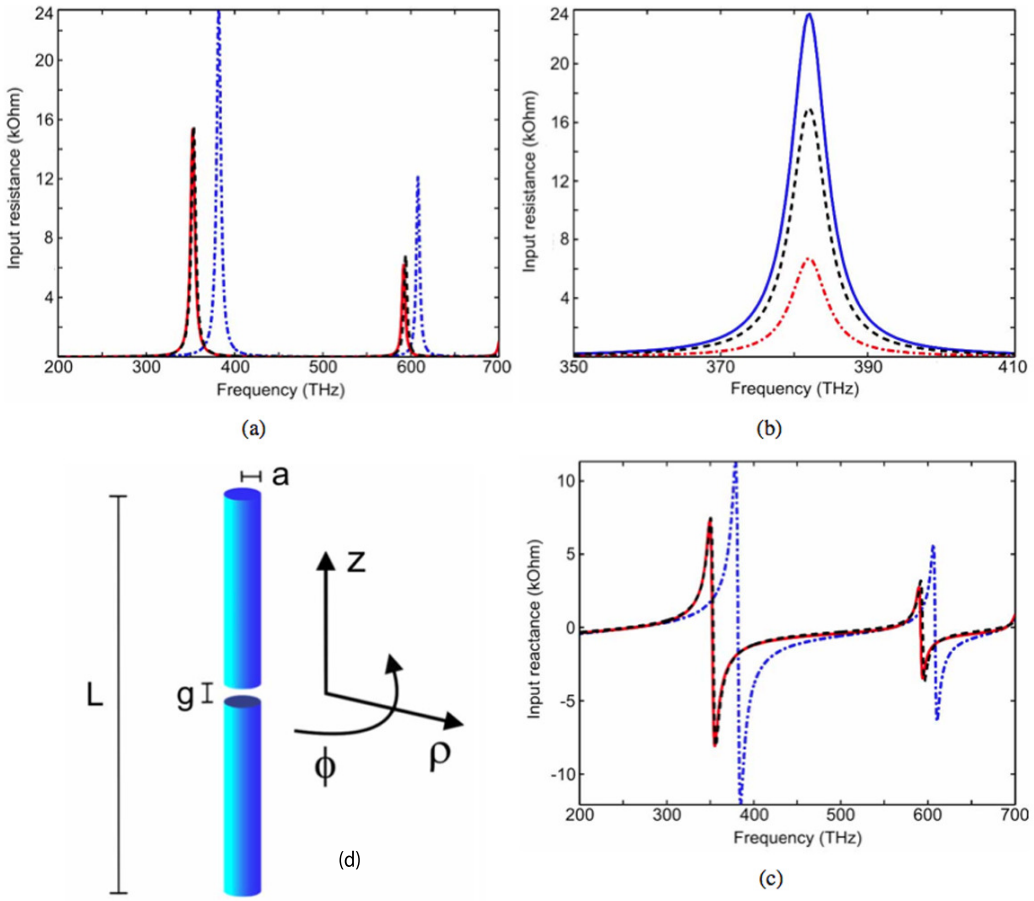

Figure 7.3: The Locatelli dipole (d) and impedance curves (a), (b), and (c). From Locatelli et al. [2009] Figs. 1 and 3.

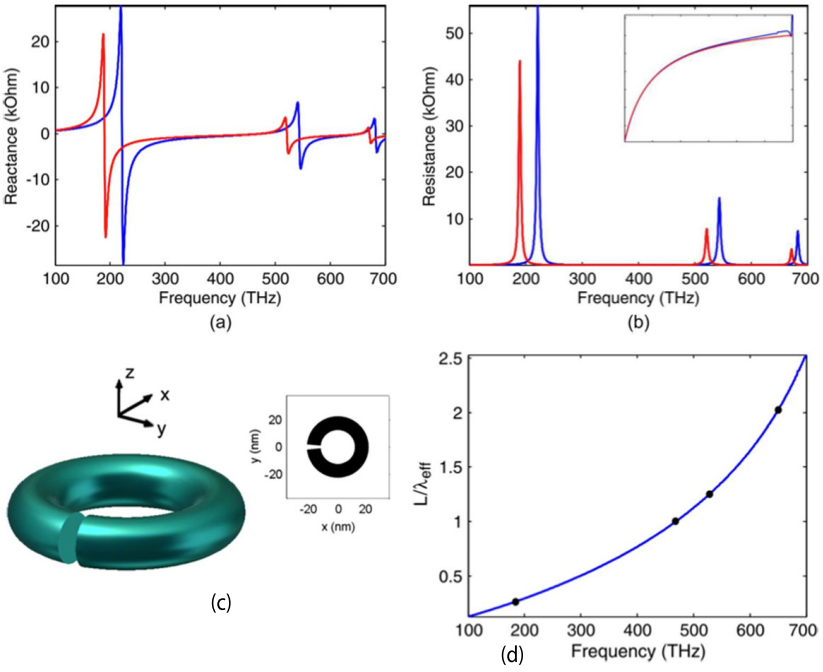

Figure 7.4: The Locatelli ring (c) and impedance curves (a) and (b). Identified wavelength scaling, approaching resonance saturation (d). From Locatelli [2011] Figs. 1, 2, and 3. $2\pi b = 110$ nm. $\omega_0 = 472$ THz (635 nm).

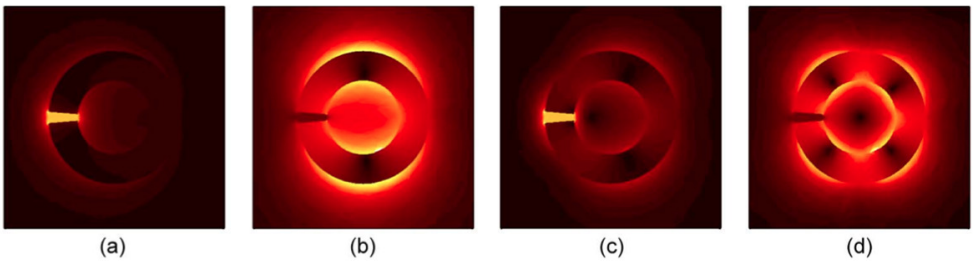

Figure 7.5: The Locatelli ring current distribution at the integer $((b)$ and $(c))$ and half-integer $((a)$ and $(c))$ resonances. From Locatelli [2011] Fig. 7. These rings have gaps; it is clear that the $\vec{E}$ field is substantially enhanced within the gap at the anti-resonance.

Part III

New Work

Chapter 8

RLC Circuit Theory for Perfectly Conducting Circular Rings (1 MHz to 100 GHz)

8.1 Introduction

Previous chapters indicate that no general analytical study of loop antennas and rings, developed from standard antenna theory, exists that is at once applicable to the Radio Frequency (RF), Micro-wave (MW), TeraHertz (THz), Infra-red (IR), and Optical (OR) regions. Nor is there any *RLC* circuit theory model, rigorously developed from the analytical model. This thesis seeks to fill that gap.

This chapter is the first step on that journey. It reaches back to the original Storer/Wu model of loop antennas, described in Chapter 5, and with a minor transformation of variables produces a fully rigorous *RLC* circuit model for perfectly conducting metal loops, applicable in the RF and MW region. From that, the impedance found by Storer/Wu is recovered. But more importantly, the functions $R = R(\omega)$, $L = L(\omega)$, and $C = C(\omega)$ for every mode are found, and the full *RLC* representation of the loop is calculated. All of the original Storer/Wu results are retained, but the *RLC* model gives new information on the inductive and capacitive behaviour of the loop for each mode and for the entire loop at any frequency. The circuit model also permits the calculation of the bandwidth and Q of each mode.

The contents of this chapter were published in McKinley et al. [2012]. The chapter following this one extends the analytical model to lossy metals and therefore to frequencies above the MW.

8.2 Derivation of the RLC Circuit Model for the Ring

Chapter 5 presents a derivation of the current distribution on a loop (shown in Fig. 8.1) excited by a delta-function voltage generator at angle $\phi = 0$ on the periphery.

The equation governing the physics is Eqn. 5.7:

$$\frac{V_0}{b}\delta(\phi) = \frac{1}{b}\frac{\partial \Phi}{\partial \phi} + i\omega A_\phi \tag{8.1}$$

where V_0 is the driving voltage, Φ is the scalar potential and A is the vector potential. The solution for the current distribution is Eqn. 5.22, reproduced there:

$$I(\phi) = \sum_{m=-\infty}^{\infty} I_m e^{im\phi} = \frac{V_0}{i\pi b_x}\left[\frac{1}{a_0} + \sum_{m=1}^{\infty}\frac{2\cos(m\phi)}{a_m}\right] \tag{8.2}$$

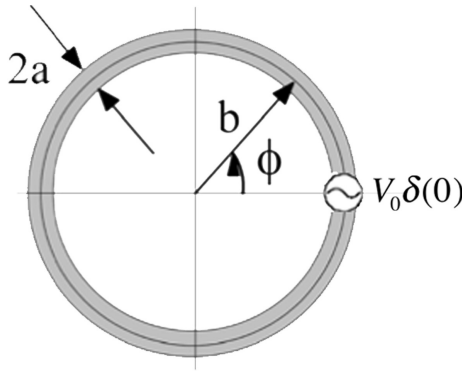

Figure 8.1: The geometry of the loop for purposes of the derivation. b is the ring radius. a is the wire radius. The size of the loop is given effectively by $\Omega = 2\ln(2\pi b/a)$.

The coefficients a_0 and a_m determine the behaviour and their functional dependence can be found in Eqns 5.20 and 5.33.

The first step is to transform variables: $Z_0 \equiv i\pi b_x a_0$ and $Z_m \equiv i\pi b_x a_m/2$. This leads to:

$$I(\phi) = \sum_{m=-\infty}^{\infty} I_m e^{im\phi} = V_0\left[\frac{1}{Z_0} + \sum_{m=1}^{\infty}\frac{\cos(m\phi)}{Z_m}\right] \tag{8.3}$$

and

$$Y = \frac{1}{Z} = \left[\frac{1}{Z_0} + \sum_{m=1}^{\infty}\frac{1}{Z_m}\right]$$

This admittance suggests that the ring can be modelled as a parallel system of impedances as viewed from the gap.

A plot of Z_m for several modes, m, show forms consistent with series resonances (see Fig. 4.3). As an example, Fig. 8.2 shows the impedances Z_1 and Z_2. The modal impedance therefore has the form

$$Z_m = R_m + j\left(\omega L_m - \frac{1}{\omega C_m}\right) = R_m\left(1 + iQ_m\left(\frac{\omega}{\omega_m} - \frac{\omega_m}{\omega}\right)\right) \tag{8.4}$$

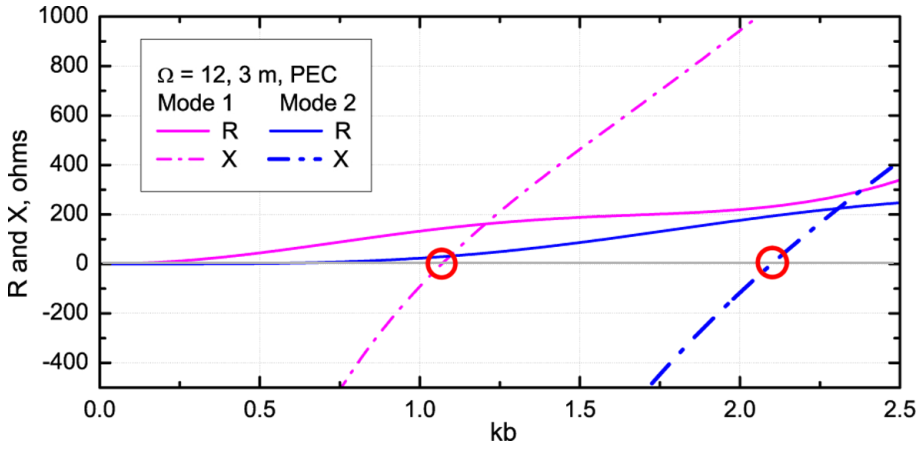

Figure 8.2: The impedances for mode 1 and mode 2 of a thin $\Omega = 12$ ($b/a = 64.2$). Note that the resonances (marked in red) occur where the imaginary parts pass through 0. At those points the real parts are positive and do not vary much. Locally, these resonances have the same form as series resonant circuits (see the discussion in Section 4.3.1).

where $Q_m = \sqrt{L_m/C_m}/R_m$.

Substituting Eqn. 5.20 and Eqn. 5.33,

$$\begin{aligned} R_m &\equiv b_x \left[k_b r_m - m^2/(k_b g_m)\right] \\ L_m &\equiv \mu_o b l_{\mu m} \\ C_m &\equiv \epsilon_o b l_{\epsilon m}/m^2 \end{aligned} \tag{8.5}$$

where r_m, g_m, $l_{\mu m}$ and $l_{\epsilon m}$ are unit-less and $k_b = 2\pi b/\lambda$, the wavenumber times the radius of the loop. μ_0 and ϵ_0 are the permeability and permittivity of free space, such that the balanced reactance of free space is $b_x \equiv \sqrt{\mu_0/\epsilon_0}$.

These unit-less functions in detail are:

$$r_m = \begin{cases} \frac{\pi}{8}\int_0^{2k_b}\left(J_{2(m+1)}(x) + J_{2(m-1)}(x)\right)dx & \text{if } m > 0, \\ \frac{\pi}{2}\int_0^{2k_b} J_2(x)dx & \text{if } m = 0. \end{cases} \tag{8.6}$$

$$g_m = \begin{cases} 1/\left[\frac{\pi}{4}\int_0^{2k_b} J_{2m}(x)dx\right] & \text{if } m > 0, \\ \infty & \text{if } m = 0. \end{cases}$$

$$l_{\mu m} = \begin{cases} \frac{1}{2}\ln\left(\frac{8b}{a}\right) - \frac{1}{2}\sum_{k=0}^{m}\frac{1}{2k+1} - \frac{1}{2}\sum_{k=0}^{m-2}\frac{1}{2k+1} \\ \quad -\frac{\pi}{8}\int_0^{2k_b}\left[\Omega_{2(m+1)}(x) + \Omega_{2(m-1)}(x)\right]dx & \text{if } m > 0, \\ \ln\left(\frac{8b}{a}\right) - 2 - \frac{\pi}{2}\int_0^{2k_b}\left[\Omega_2(x)\right]dx & \text{if } m = 0. \end{cases}$$

$$l_{\epsilon m} = \begin{cases} 1/\left[ln\left(\frac{8b}{a}\right) - 2\sum_{k=0}^{m-1}\frac{1}{2k+1} - \frac{\pi}{2}\int_0^{2k_b}\left[\Omega_{2m}(x)\right]dx\right] & \text{if } m > 0 \\ \infty & \text{if } m = 0. \end{cases}$$

Compare $l_{\mu 0}$, mode = 0, here with l_μ in Eqn. 5.5. They are the same for $k_b = 0$.

Equations 8.4 through 8.6 apply to perfectly conducting loops at all frequencies and circumferences, but practically speaking, real metallic materials are not perfectly conducting. Real metals are very lossy at high frequencies and this loss modifies these functions, the focus of the next chapter, Chapter 9.

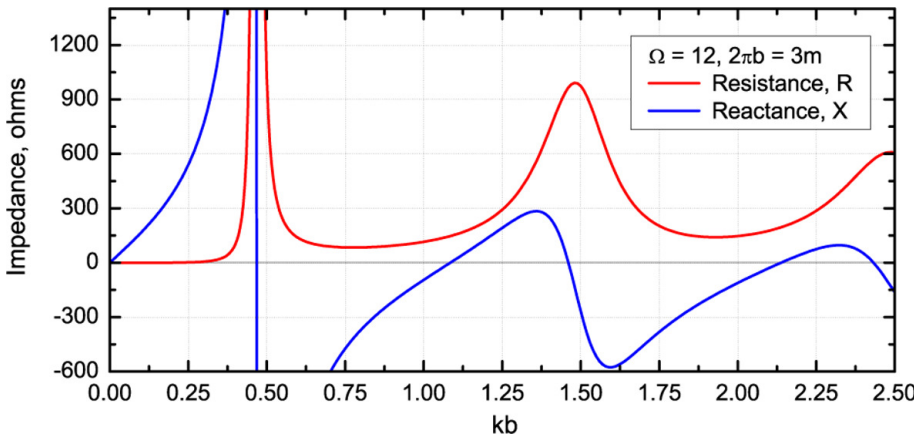

Figure 8.3: The impedance of an $\Omega = 12$ loop, showing resistive and reactive parts, using Eqns. 8.3 through 8.6. This is the same as in the Storer/Wu derivation, Fig. 5.5.

8.3 The Total Impedance, The Zero-Crossing Resonances, and The Modal Resonances.

A plot of Eqn. 8.3 using the modal impedances is given in Fig. 8.3. Note that the zero-crossings of the imaginary part match those in the Storer/Wu derivation, Fig. 5.5, as they should, because Eqn. 8.6 is not something new, it represents only a simple reorganisation of the terms.

The elements R_m, L_m, and C_m in Equations 8.5 are plotted for $0 < k_b < 2.5$ in Fig. 8.4 for modes 0, 1 and 2. Evidently these elements are not constant over frequency, as they would be in typical *RLC* circuit theory. This fact has four very interesting effects:

- Firstly, it prevents the loop from behaving like a circuit with constant values of R, L, and C. Fig. 8.5 show the natural resonances for mode 2 ($m = 2$) for an extremely thin loop, as shown in part (a) of the figure, and for a thick loop, as shown in part (b) of the figure. The modal resonances of the thin loop have traveling waves with wavelengths that fit the circumference exactly. This produces a very narrow bandwidth and therefore a high Q, because only a few wavelengths can participate in the resonance. In this case alone, can constant values be found for the series R, L, and C of each mode. Thick loops, on the other hand, present a wide choice of path length due to wire thickness, thereby broadening the resonance, and lowering the Q value.

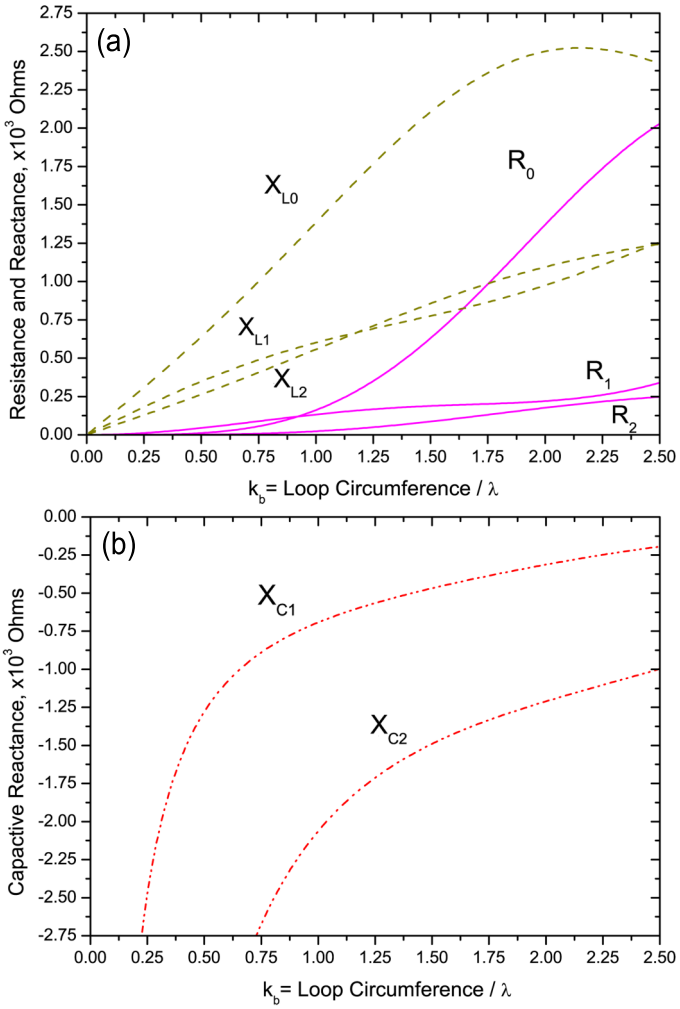

Figure 8.4: An $\Omega = 10$ ($b/a = 24$) loop. (a) The modal resistances and inductive reactances; (b) the modal capacitive reactances, for $m = 0$, 1, and 2. There is no zero mode capacitance. These results apply to perfectly conducting closed loops.

- Secondly, two principal discrepancies appear in Fig. 8.5: a shift in the resonance away from $k_{bm} = m$ and a shift upward in the reactance (a phase shift). These shifts are explained by the fact that R, L and C are functions of k_b. Specifying these functions (Eqn. 8.5) is the first key result of this thesis. We thus obtain an RLC model of the circular loop, in which the modes are treated as series RLC circuits with varying values, in parallel with each other and with a zero order mode, as illustrated in Fig. 8.6.

- Thirdly, the individual modal resonances, $m = \{1, 2, 3, ...\}$, do not occur at the zero-crossing resonances, because the modal resonances are broad enough, especially for thicker rings, that they affect each other and when added, move the total zero-crossing resonances. The sum of the effects causes the specific

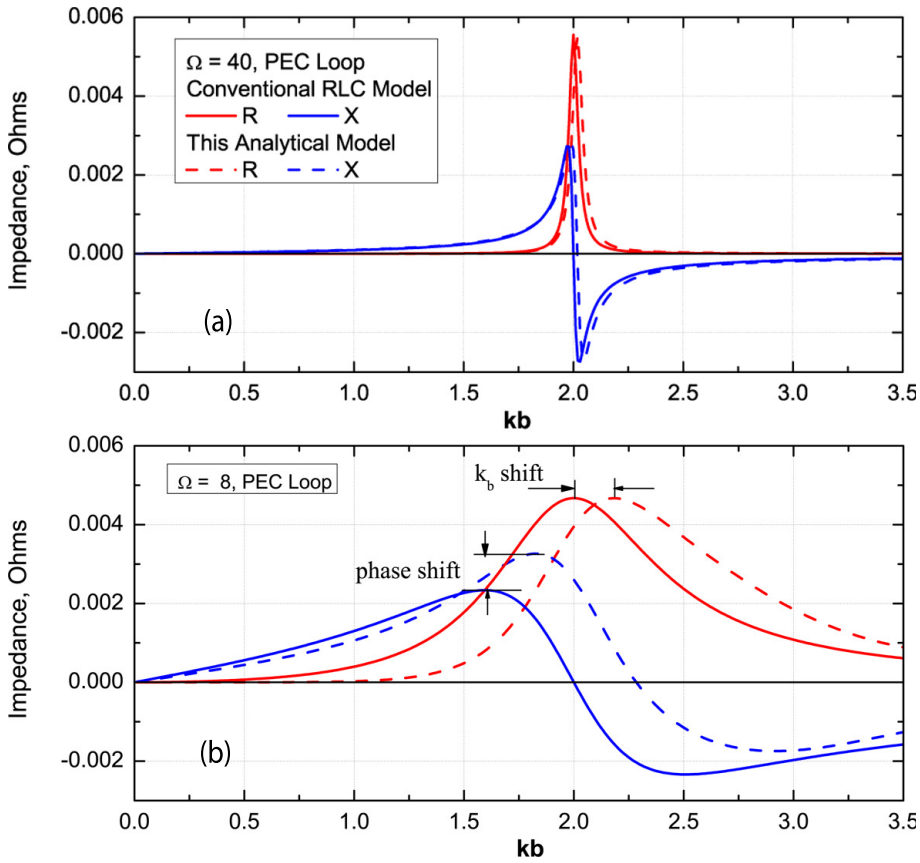

Figure 8.5: Mode 2 admittances for two differently sized loops. This analytical model is compared with a conventional series RLC circuit model, given by Eqn. 4.22 using constant values. In (a), an extremely thin loop compared with $R = 360$ ohms, $X_b = 14400$ ohms. In (b), a thicker loop compared with $R = 428$ ohms, $X_b = 1198$ ohms.

zero-crossing resonances to differ from the individual modal resonances a small bit. To see this compare the zero-crossing resonances given in Table 5.1 with the mode resonance given in Fig. 8.7. For example, the zero-crossings are $k_b = 1.09$ and 2.14, while the modal resonances are $k_b = 1.07$ and 2.10.

- And lastly, the varying RLC elements makes it difficult to assign a quality factor to the modal resonant circuit, using Eqn. 4.20, because it would vary unless one selects the L_m and C_m at some value of k_b. Since Q has no utilitarian value except at a resonance, how is resonance calculated? If the resonance function

$$\omega_m(k_b) = \frac{1}{\sqrt{L_m(k_b)C_m(k_b)}} \tag{8.7}$$

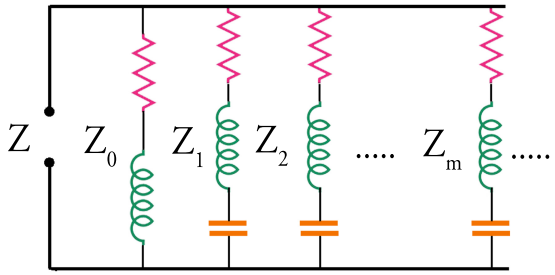

Figure 8.6: The proper *RLC* model of a circular Loop antenna looking in from the source.

is transformed to k-space, using $\omega = k_b(c/b)$.

$$k_{bm}(k_b) = \frac{m}{\sqrt{l_{\mu m}(k_b) l_{\epsilon m}(k_b)}} \tag{8.8}$$

and the right side plotted, the result is a set of rolling curves over k_b, as shown in Fig. 8.7 for the first four modes. When the variable k_b crosses these curves, the ring resonates, hence the intersection of the line $y = k_b$ with the function k_{b1} gives the resonance of the first mode, and so forth with increasing m.

This method of solving equations by plotting will be used again in Chapter 10 (see from Fig. 10.5 on), where the rolling curves will fluctuate much more. It is important therefore, to understand how the resonances must be given by the intersection of the red line with the rolling blue curves, and to be able to spot these intersections easily easily.

These resonances, with associated values of the unit-less functions, are given in Table 8.1. When referring to a value that occurs at a modal resonance, a tilde above the symbol will be used henceforth; for example, $\tilde{R}_2$ refers to the resistance of the loop at the modal resonance, $\tilde{k}_{b2}$. The Resistances $\tilde{R}_0$ and $\tilde{R}_m$ are, in fact, radiation resistances for these modes since there is no loss.

With these values Eqn. 8.5 can be calculated for each mode of a given loop, with radius b. It is important to note that the inductance and capacitance depend directly on the loop radius, but the resistance does not. This implies that there is no heat loss and therefore this resistance must be radiation resistance.

8.3.1 The Total R, L and C of the Loop at Any k_b

As was pointed out in Section 4.3, a system with many resonances will have a number of inductors and capacitors, some in series, some in parallel, but when the analysis is complete, each of the resonances will consist of some mathematical combination of

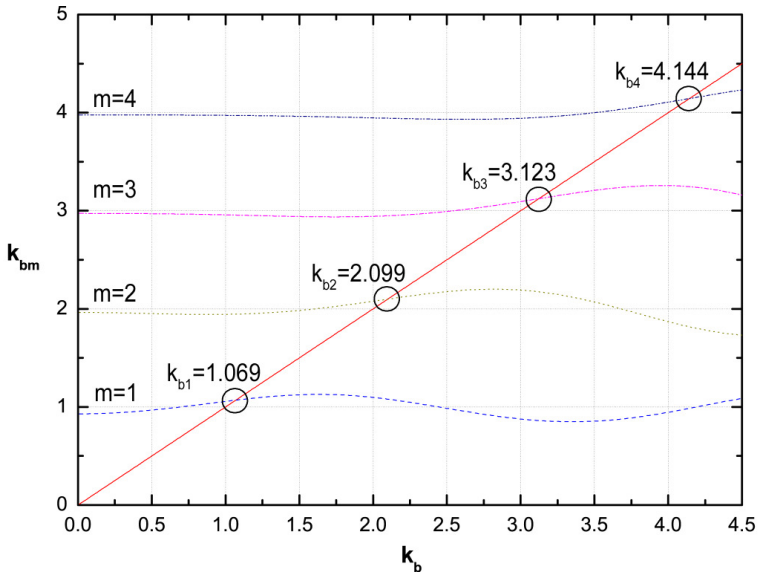

Figure 8.7: The resonance functions, $\tilde{k}_{bm}$, for the first four modes on a size $\Omega = 12$ Loop.

the inductors to produce one inductance, and of some mathematical combination of the capacitors to produce one capacitance. The same is true of the resistors. Therefore, the complicated infinity of series resonant circuits in parallel, illustrated by Fig. 8.6 can be reduced to a single R, L, and C in series. Remembering that the impedance is complex:

$$
\begin{aligned}
Z^* = \frac{Z^* Z}{Z} &= |Z|^2 \left[\frac{1}{Z_0} + \sum_1^\infty \frac{1}{Z_m} \right] = |Z|^2 \left[\frac{Z_0^*}{Z_0^* Z_0} + \sum_1^\infty \frac{Z_m^*}{Z_m^* Z_m} \right] \\
&= |Z|^2 \left[\frac{R_0 - iX_0}{|Z_0|^2} + \sum_1^\infty \frac{R_m - iX_m}{|Z_m|^2} \right] \\
&= |Z|^2 \left[\left(\frac{R_0}{|Z_0|^2} + \sum_1^\infty \frac{R_m}{|Z_m|^2} \right) - i \left(\frac{X_0}{|Z_0|^2} + \sum_1^\infty \frac{X_m}{|Z_m|^2} \right) \right] \\
&= R_T - iX_T
\end{aligned}
\tag{8.9}
$$

Equation 8.9 gives the total resistance and reactance of the loop, taking into account all of the modal impedances. It is, of course, identical to $(1/Y)^*$ where Y is given in Eqn. 8.3. In a similar fashion, the reactance can be expanded to give the total inductance and capacitance of the loop. Remembering that the capacitance has no zero mode:

$$
\begin{aligned}
X &= |Z|^2 \left[\frac{X_0}{|Z_0|^2} + \sum_1^\infty \frac{X_m}{|Z_m|^2} \right] \\
X_L = \omega L_T &= |Z|^2 \left[\frac{\omega L_0}{|Z_0|^2} + \sum_1^\infty \frac{\omega L_m}{|Z_m|^2} \right]
\end{aligned}
\tag{8.10}
$$

Table 8.1: Key RLC circuit values at the modal resonances for various sized, perfectly conducting rings.

Ω	m	$\tilde{k}_{bm}$	$\tilde{r_0}$	$\tilde{R}_0$	$\tilde{l}_0$	$\tilde{X}_{L0}$	$\tilde{r}_m$	$\tilde{g}_m$	$\tilde{R}_m$	$\tilde{l}_{\mu m}$	$\tilde{l}_{\epsilon m}$	$\tilde{b}_{xm}$	$\tilde{Q}_m$
12	1	1.069	.5075	204	4.70	1895	.5776	3.9408	143.3	2.06	.425	829	5.8
	2	2.099	1.922	1521	4.19	3312	.4976	3.5865	193.4	1.93	.471	1526	7.9
	3	3.123	1.876	2209	2.75	3234	.4619	3.4439	228.3	1.84	.502	2163	9.5
	4	4.144	1.131	1767	2.79	4361	.4414	3.3565	255.9	1.77	.527	2759	10.8
Ω	m	$\tilde{k}_{bm}$	$\tilde{r_0}$	$\tilde{R}_0$	$\tilde{l}_0$	$\tilde{X}_{L0}$	$\tilde{r}_m$	$\tilde{g}_m$	$\tilde{R}_m$	$\tilde{l}_{\mu m}$	$\tilde{l}_{\epsilon m}$	$\tilde{b}_{xm}$	$\tilde{Q}_m$
10	1	1.096	.540	223	3.712	1533	.5813	3.701	147	1.544	.539	638	4.3
	2	2.147	1.967	1592	3.118	2523	.5112	3.304	201	1.417	.612	1147	5.7
	3	3.190	1.815	2183	1.694	2038	.4821	3.125	240	1.327	.666	1596	6.7
	4	4.230	1.128	1799	1.845	2943	.4674	3.004	271	1.258	.711	2007	7.4
Ω	m	$\tilde{k}_{bm}$	$\tilde{r_0}$	$\tilde{R}_0$	$\tilde{l}_0$	$\tilde{X}_{L0}$	$\tilde{r}_m$	$\tilde{g}_m$	$\tilde{R}_m$	$\tilde{l}_{\mu m}$	$\tilde{l}_{\epsilon m}$	$\tilde{b}_{xm}$	$\tilde{Q}_m$
8	1	1.162	.625	273	2.732	1196	.5881	3.202	156	1.011	.732	443	2.8
	2	2.285	2.070	1783	1.911	1644	.5455	2.657	222	.881	.870	758	3.4
	3	3.420	1.591	2050	.5803	748	.5448	2.316	274	.786	.979	1013	3.7
	4	4.580	1.237	2134	1.035	1786	.5630	2.027	322	.708	1.077	1222	3.8

$$X_C = \frac{1}{\omega C_T} = |Z|^2 \sum_1^\infty \frac{1/(\omega C_m)}{|Z_m|^2}$$

Reducing, we have for L_T and C_T:

$$L_T = \mu_0 b l_\mu = |Z|^2 \left[\frac{L_0}{|Z_0|^2} + \sum_1^\infty \frac{L_m}{|Z_m|^2} \right] \tag{8.11}$$

$$\frac{1}{C_T} = \frac{1}{\epsilon_0 b l_\epsilon} = |Z|^2 \sum_1^\infty \frac{1/C_m}{|Z_m|^2}$$

These are functions of k_b. Fig. 8.8 (a) shows R_T and X_T for an $\Omega = 12$ loop. Notice that R_T does match the Re(Z) in Fig. 5.5. Fig. 8.8 (b) shows the inductive reactance, X_L, and capacitive reactance, X_C. Fig. 8.8 (c) shows the unit-less functions, l_μ and l_ϵ. It is worthwhile pointing out that at $k_b = 0$, the function $l_\mu = 4.24$, as for small loops, given in Section 5.2.

8.4 Conclusion

In this chapter, an *RLC* circuit model was derived from the Storer/Wu model of Chapter 5 for perfectly conducting circular rings of modest size. As with the Storer/Wu model, the analytical model does not apply as well to thick rings where $\Omega < 8$ as it does to thin loops. The model is applicable from very low frequencies to about 200 or 300 GHz for gold, since loss affects the results above that frequency. The model provides calculations for the current distribution, the complex impedance, the resistance, inductance and capacitance for all modes as a function of frequency, and the total resistance, reactance, inductance and capacitance of the ring at any frequency.

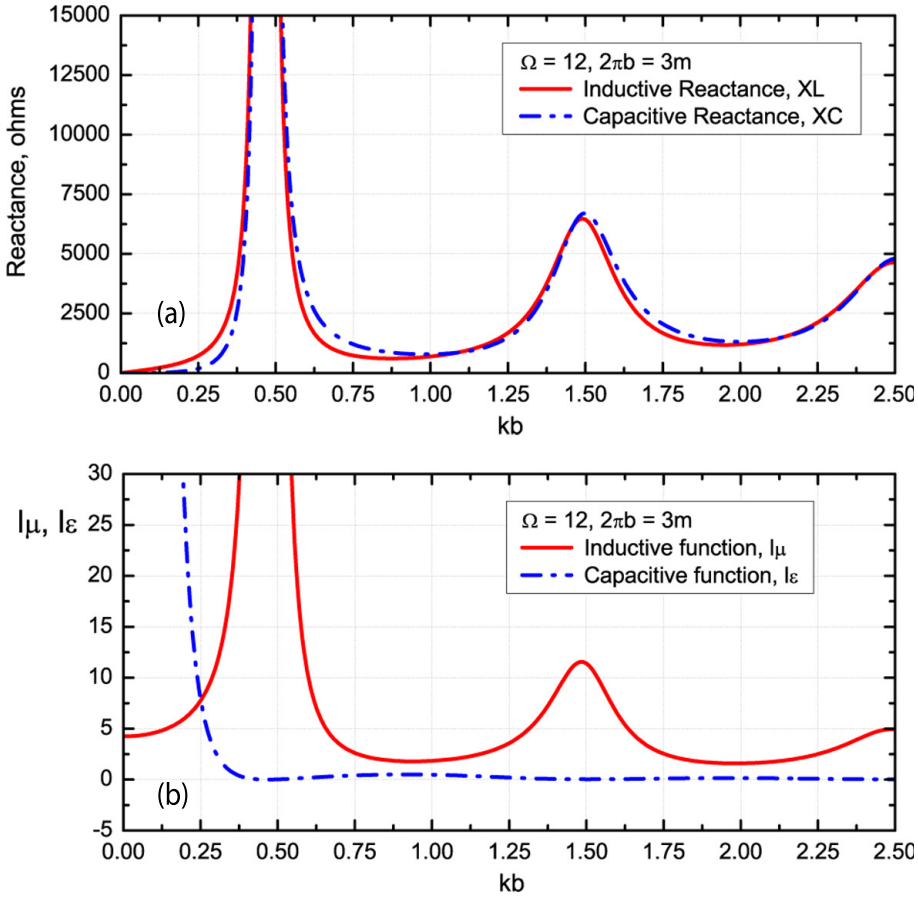

Figure 8.8: An $\Omega = 12$, PEC Loop. (a) Inductive and capacitive reactances; and (b) the unit-less functions l_μ and l_ϵ. The total reactance of the loop is $X_L - X_C$.

Chapter 9

RLC Circuit Theory for Lossy Metallic Circular Rings (3 mm to 400 nm)

9.1 Introduction

In the previous chapter, the Storer/Wu equations of Section 5.3 were rearranged using a transformation of variables to yield greater insight into the behaviour of perfectly conducting loops. The transformation produced an *RLC* circuit model. In this chapter, the analytical model will be extended to higher frequencies by accounting for material characteristics from which the ring is constructed. The method used will be one suggested by Locatelli et al. [2009] and described in Prior Work, Section 7.6. The *RLC* circuit model will be extended to the optical region, resulting in a clearer understanding of wavelength scaling and resonance saturation (noted in Section 7.5), the effect of the index of refraction of the material on current distribution and on input impedance, and of the radiation efficiency and Q of the ring in these short wavelength regions.

The contents of this chapter were published in McKinley et al. [2013].

9.2 Derivation of the Current

The essential addition to the model of Section 8.2 is a term called the "surface impedance", which describes the effect of the losses and of phase shifts between the incident driving voltage and the current around the ring. The reason for the loss is given in the discussion of kinetic inductance in Section 7.3. The problem arises from the inertia of electrons. Since electrons have mass, they have an inherent hesitation to accelerate and decelerate that all massive bodies do. This phenomenon doesn't warrant any attention at low frequencies because electron mass is so small that the reluctance is almost nil. But at THz and optical frequencies, when the incident $\vec{E}$ field alternates on the order of 10^{12} to 10^{15} times per second, the electrons simply can't keep up. First they go out of phase with the $\vec{E}$ field and second, they lose kinetic energy to radiation (since electrons radiate when they accelerate and decelerate).

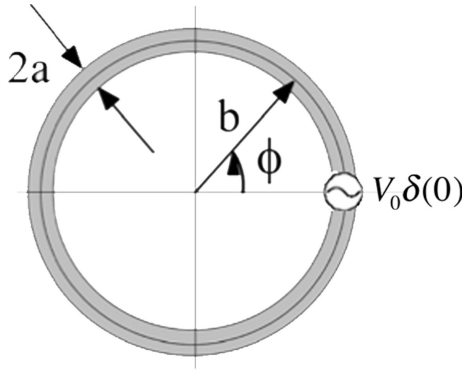

Figure 9.1: A reproduction of Fig. 5.1. The geometry of the ring for purposes of the derivation. b is the ring radius. a is the wire radius. The size of the loop is given effectively by $\Omega = 2\ln(2\pi b/a)$

There are also effects due to electron transitions across the band gaps between the outer valence shells and the conduction band. For example, at room temperature, most of the electrons in the outer shell are within the conduction band, and this is what gives metal its conduction properties at low frequency. But if the energy of an incident wave is large enough (at optical frequencies) it corresponds to the energy of the gap between the next inward shell and the conduction band, giving these electrons enough energy to jump the gap. For gold, these begin around 2.5 eV (600 THZ or 500 nm) and continue through 7+ eV.

The imposed electric field across the gap, E_ϕ given in Eqn. 5.6, causes a current in the ring which induces a voltage drop across the characteristic impedance of the material, z_s, in ohms/m. This adds to the left side of Eqn. 5.7 an additional term

$$\frac{V_0}{b}\delta(\phi) - I_\phi(\phi)z_s = \frac{1}{b}\frac{\partial\Phi}{\partial\phi} + i\omega A_\phi \tag{9.1}$$

In a perfectly conducting wire, the current moves everywhere to create an electric field which exactly cancels any imposed electric field. Therefore the driving field, E_ϕ, appears only in the gap. As a result, a boundary condition for the solution of Eqn. 9.1 is that the total electric field, given by the sum of the imposed field and the reactive field, is zero on the surface of the wire; represented by $z_s = 0$.

In an imperfectly conducting wire, this is not the case; the surface current produces an electric field through the wire, across the wire impedance, $E_s = I_\phi z_s$. The propagation vector has a primary component in the tangential direction, but also a component in the axial and toroidal directions which grow larger as the incident wavelength of the source shortens while approaching the IR. This raises several difficulties in the solution of Eqn. 9.1. An assumption that the wire is thin, $a^2 \ll b^2$, forces both to zero and allows a simpler solution. Applying the solution to thicker rings, therefore, will be less accurate than applying to thinner rings. Moreover, applying the solution in the IR and OR will also be less accurate. These are all effects

of using the thin-wire approximation.

From hereon, the derivation follows Section 5.3.2 precisely and the result for the current is:

$$\begin{aligned} I(\phi) &= \sum_{-\infty}^{\infty} \left[\frac{V_0}{i2\pi b_x a_m/2 + 2\pi b z_s} \right] e^{-im\phi} \\ &= V_0 \left[\frac{1}{Z_0 + 2\pi b z_s} + \sum_{m=1}^{\infty} \frac{\cos(m\phi)}{Z_m + 2\pi b(z_s/2)} \right] \\ &= V_0 \left[\frac{1}{Z'_0} + \sum_{m=1}^{\infty} \frac{\cos(m\phi)}{Z'_m} \right] \end{aligned} \tag{9.2}$$

where

$$\begin{aligned} Z'_0 &= Z_0 + 2\pi b z_s \\ Z'_m &= Z_m + 2\pi b(z_s/2). \end{aligned} \tag{9.3}$$

Compare this with Eqn. 5.22.

9.2.1 The Surface and Characteristic Wire Impedance

The input impedance at the driving source becomes

$$Z = \frac{V_0}{I(\phi = 0)} = 1/\left[\frac{1}{Z'_0} + \sum_{m=1}^{\infty} \frac{1}{Z'_m} \right] \tag{9.4}$$

The functional character of z_s remains to be determined. The impedance, z_s, is required to go to zero at low frequencies and to play a significant role in the mode summation at optical frequencies.

A cylindrical wire, made of an imperfectly conducting material, propagates an electromagnetic field inside that can be described well using Bessel functions of the first kind. The field external to the wire uses Hankel functions. Derivations are shown in Stratton [1941] and Hanson [2006]. Novotny [2007a] uses the same approach to derive a theory of wavelength scaling in dipoles. Stratton and Hanson give the surface impedance of a cylindrical wire as

$$z_s = \frac{\gamma}{2\pi a \sigma} \frac{J_0(\gamma a)}{J_1(\gamma a)} \equiv \frac{1}{2\pi a} Z_s \tag{9.5}$$

in ohms/m. γ is the transverse propagation constant in the wire, the same as k in Eqn. 5.10, $\gamma = k = \beta + i\alpha/2$, except that α, the damping coefficient, is no longer 0. a is the radius of the wire, so γa expresses the total phase shift and damping over the radius of the wire. $J_0(\gamma a)$ and $J_1(\gamma a)$ are the zero and first order Bessel functions of the First Kind. Under these assumptions, the conductivity is directly related to the

index of refraction, $\eta = n - i\kappa$:

$$\begin{aligned} \gamma &= \frac{\omega}{c}\eta \quad \text{and} \quad \sigma = i\omega\epsilon_0(\eta^2 - 1) \\ \frac{\gamma}{\sigma} &= -ib_x\frac{\eta}{\eta^2 - 1} \\ Z_s &= -ib_x\left(\frac{\eta}{\eta^2 - 1}\right)\frac{J_0(\gamma a)}{J_1(\gamma a)} \end{aligned} \tag{9.6}$$

where b_x is the characteristic impedance of free-space, $\sqrt{\mu_0/\epsilon_0}$. This surface impedance applies to any material for which the complex index of refraction is known. No assumptions have been made limiting the material, hence it can be a noble metal, an alloy, a semi-conductor, or an insulator. The effects of the extra term on the current and impedance differ from material to material, but this term accurately handles these differences. In this thesis, only metals will be considered.

9.2.2 Modeling the Index of Refraction

The conductivity of any material is, in general, complex and can vary dramatically over the full range of frequencies from DC to the visible. The magnitude of the conductivity of gold, in particular, begins at 4.5×10^7 siemens per meter at DC, then falls off by a factor of 30 between $\lambda = 1500$ μm in the MW and 2 μm in the infrared, where the first measured values of the index of refraction by Johnson and Christy [1972] occur. The imaginary part dominates the real from 400 μm until the onset of the inter-band and intra-band transitions in the middle of the visible region (about 600 nm), where the real part again dominates and gold picks up its yellowish color. The conductivity at low and high frequencies is shown in Fig. 9.2.

This decrease in conductivity is due to Drude behavior and to inter-band transitions. These transitions are rapid changes in the conductivity due to the freeing up of electrons from ties to the valence bands. Electron transitions occur between the outer valence bands and the conduction band when incident light matches the band gap. Drude's model doesn't include the transitions, but does provide a reasonable representation of the conductivity to the onset of the transition. Since the conductivity is directly related to the index (see Eqn. 9.6 above), it is possible to develop a Drude-like model for the index itself. However, the Drude model must be extended to include the critical points of the transitions. Several models appear in the literature that do that. Etchegoin et al. [2006, 2007] and Vial and Laroche [2007] are recent examples. The transitions appear in the models as a summation of Lorentzian resonances where the critical energy band transitions occur. The model used by Etchegoin's group was given in terms of the permittivity, $\epsilon(\omega)$ where $\epsilon = \epsilon_0\epsilon_r$ and $\epsilon_r = \eta^2 - 1$.

$$\begin{aligned} \epsilon_r(\omega) = \epsilon_\infty &- \frac{\omega_p^2}{\omega\left(\omega - i\Gamma\right)} \\ &+ \sum_m f_m\left[e^{i\phi_m}\left(\omega_m - \omega - i\Gamma_m\right)^{\mu_m} + e^{i\phi_m}\left(\omega_m + \omega + i\Gamma_m\right)^{\mu_m}\right] \end{aligned} \tag{9.7}$$

where ω_p is the metal's plasma frequency; f_m are related to the quantum probabilities of transition; ω_m are the critical Lorentzian points; and Γ_m are the Lorentz broadening (damping frequency) terms for the transitions. It uses an "infinity term", as do many of these models, to handle the low frequency end, but a simple extension ensures that both the inter-band transitions and the DC conductivity of the metal are satisfied in the same function. Writing in terms of the index:

$$\eta^2 = 1 - \frac{f_0\omega_p^2}{\omega}\left(\frac{1}{(\omega - j2\Gamma_0)} + \frac{\alpha}{(\omega - j2\beta\Gamma_0)}\right) + \sum_{m=1}^{\infty}\frac{f_m\omega_p^2}{2\omega_m}\left[\frac{e^{i\pi/\gamma_m}}{\omega_m - \omega + i\Gamma_m} + \frac{e^{-i\pi/\gamma_m}}{\omega_m + \omega - i\Gamma_m}\right] \tag{9.8}$$

Using Eqn. 9.8, the DC value of the conductivity is:

$$\sigma_0 = \frac{f_0\omega_p^2\epsilon_0}{2\Gamma_0}\left[1 + \frac{\alpha}{\beta}\right] \tag{9.9}$$

The index is shown in Fig. 9.3 for gold in the optical region, using diamonds to indicate the data measured by Johnson and Christy [1972] and using a solid line to indicate the fit. Note that the original Johnson and Christy data assumes a $\exp(-i\omega t)$ dependence, and therefore their original data is the complex conjugate of that given by the functional fit of Fig. 9.3. Table 9.1 gives the fitted parameter values for the noble metals gold, silver, and copper.

Figure 9.4 shows the real and imaginary parts of the wire impedance of a thin gold ring ($\Omega = 12$) given by Eqn. 9.6 for three different circumference lengths in the NIR and OR. The principal reason for the sudden increases in the curves is the effect of the transition bands on the Bessel function ratio, $J_0(\gamma a)/J_1(\gamma a)$. The figure shows that the degree to which a given ring is affected by the transitions depends on its circumference and the driving wavelength. Different sized rings respond to the same driving wavelength differently. For example, a 600 nm circumference ring will be affected by the transitions when the driving wavelength reaches the length of the circumference, at 600 nm. But a 350 nm ring will be affected when the driving wavelength reaches double its circumference, at 700 nm. In any case, resonance saturation puts all of the modal resonances of such rings outside transition effects. Section 9.4.1 will show that at optical circumferences these rings resonate in the region $k_b \leq .2$, shown by the insets.

9.2.3 The Driving Point Impedance and Admittance.

Figures 5.5, 9.5 and 9.6 show the input impedances for three gold nano-rings with different circumference lengths, one in the GHz region, one in the NIR and one in the OR, as given by Eqn. 9.4 and by numerical simulation using CST"s Microwave Studio^{TM}(MWS). The match between the analytical model and numerical simulation is remarkably close for all three rings and supports substantially the correctness of

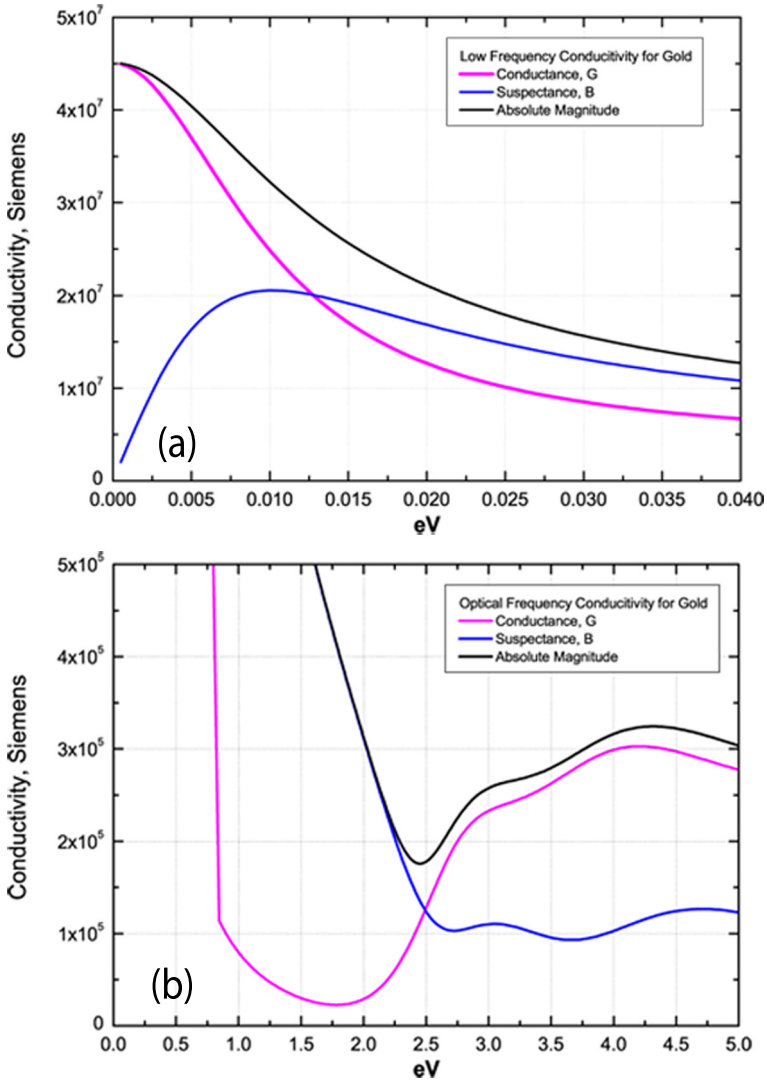

Figure 9.2: Gold's conductivity showing the Drude effects at (a) low frequency and the inter band transitions in (b) the optical region.

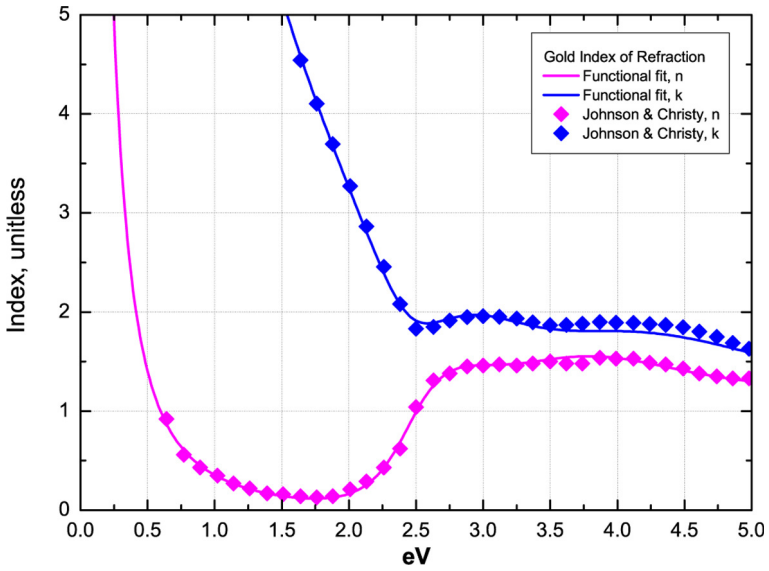

Figure 9.3: Gold's index of refraction, as given by Johnson and Christy [1972] and by the function Eqn. 9.8.

Table 9.1: Parameter fits for Eqn. 9.8 for gold, silver and copper

	$\sigma_0 \times 10^6$ $(\mho/m)$	α	β	f_0	Γ_0 (eV)	f_1	ω_1 (eV)	γ_1	Γ_1
Au	45	1.540	13.180	0.37	0.005	0.20	2.62	4.00	0.60
Ag	63	0.100	0.350	0.94	0.010	0.14	4.32	4.62	0.34
Cu	60	0.035	0.005	1.00	0.064	0.23	2.30	3.53	0.52

	f_2	ω_2 (eV)	γ_2	Γ_2 (eV)	f_3	ω_3 (eV)	γ_3	Γ_3 (eV)	ω_p (eV)
Au	0.35	3.70	4.00	1.10	0.60	7.00	4.00	2.20	9.0
Ag	0.45	5.50	12.32	1.40	0.40	7.53	4.00	2.10	9.0
Cu	0.22	3.14	2.56	0.95	0.32	4.87	2.70	1.10	8.4

model.

An examination of Figs. 5.5, 9.5 and 9.6 show that the extra optical term in Eqn. 9.3 causes the input impedance function to compress; all resonances migrate toward wavelengths longer than the circumference. Three points are important: (1) the shape of the functions are essentially the same; (2) the zero crossings migrate; and (3) the magnitude of the impedance increases with shorter circumferences. The first point means that all rings respond similarly to incident energy. The second means that the ZC resonances move toward smaller values of k_b as the circumference decreases; the ZC resonances must therefore eventually saturate. The third means that smaller rings carry smaller current magnitudes and lag the driving field.

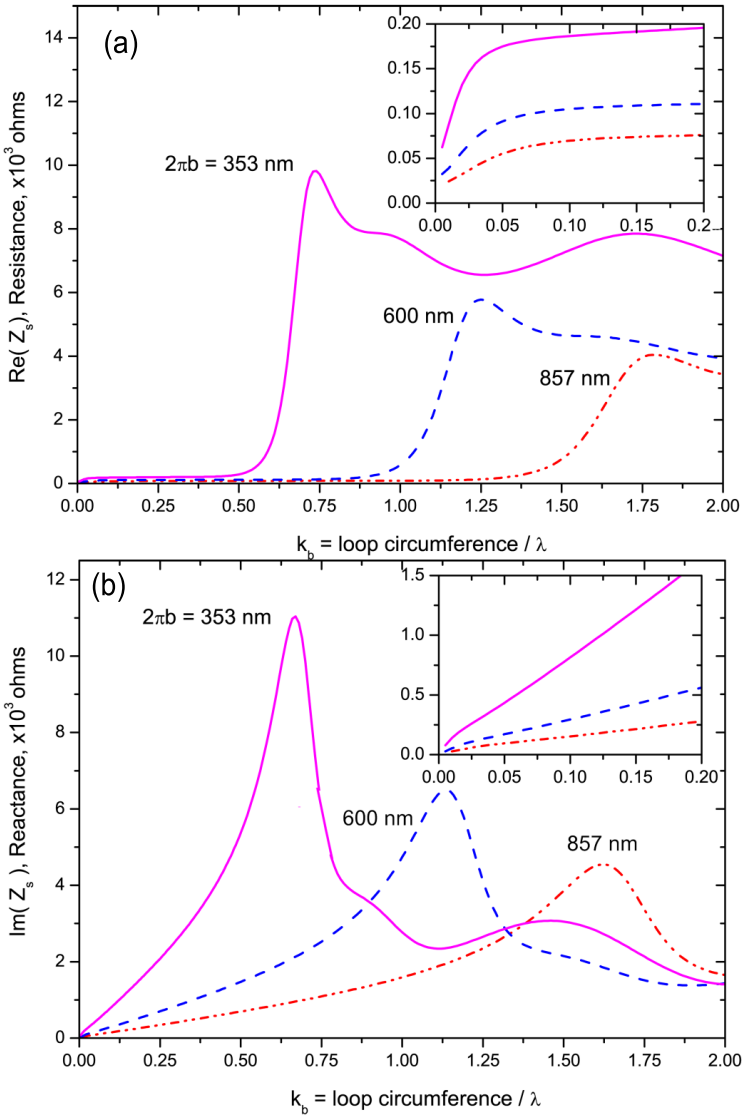

Figure 9.4: An $\Omega = 12$ gold loop in the optical region. The characteristic wire impedance, Z_s for three circumferences, from Eqn. 9.6; (a) resistance and (b) reactance. The inset shows the region where closed loops resonate: $.05 < k_b < .2$. Thicker loops show smaller values.

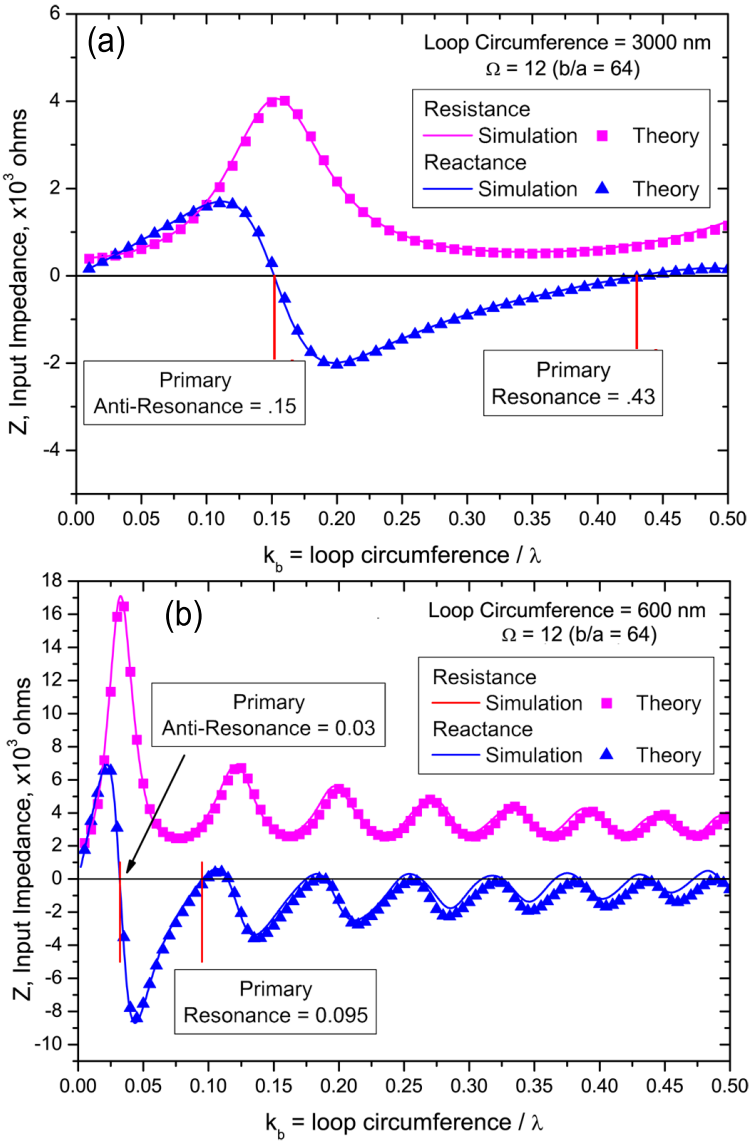

Figure 9.5: The impedance for two circular thin rings, calculated from Eqn. 5.23 compared with numerical simulations. (a) $2\pi b = 3000$ nm and (b) $2\pi b = 600$ nm.

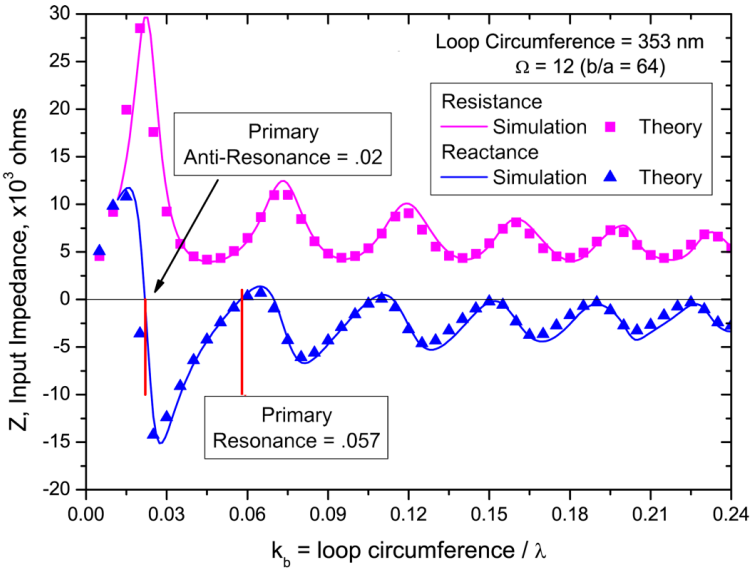

Figure 9.6: The impedance of a circular thin ring of circumference $2\pi b = 353$ nm. The first ZC resonance is at $353/.057 = 6192$ nm.

In Fig. 9.5 (b) notice that although the ring circumference matches a wavelength in the mid-visible region, the ring's first ZC resonance is at $600/.095 = 6316$ nm, well outside the OR. In Fig. 9.6 the ring circumference matches a wavelength in the UV region, the ring's first ZC resonance is at $353/.057 = 6192$ nm, not too far from the first resonance of the previous ring, which is 70% longer in circumference.

9.3 The RLC Model for Lossy Metals and Dielectrics.

An exact RLC model for the perfectly conducting closed ring was presented in Section 8.2. That model may be applied to rings in the region $0 < k_b < 2.5$. The goal now is to produce an exact RLC model for the optical rings. This is difficult in the model's present form, because the Bessel functions in Eqn. 9.6 cannot be reframed to show R, L, C elements. However, by assuming $\gamma a \ll 1$ (that is, by again asserting the thin-wire approximation), the Bessel functions can be approximated to first order in γa (Stegun and Abramowitz [1964]). This will be the only approximation for the following RLC model:

$$\frac{J_0(\gamma a)}{J_1(\gamma a)} \approx \frac{1-(\gamma a)^2/4}{(\gamma a)/2} \tag{9.10}$$

Substituting into Eqn. 9.6, the optical term, $2\pi b \times z_s = \frac{b}{a} Z_s$, can be approximated as:

$$\frac{b}{a} Z_s = -ib_x \left(\frac{b}{a}\right) \left(\frac{\eta}{\eta^2 - 1}\right) \frac{J_0(\gamma a)}{J_1(\gamma a)} \tag{9.11}$$

$$
\begin{aligned}
&= \frac{b_x}{|\eta^2-1|^2} \times \left[\left(\frac{k_b}{2} + \frac{2(b/a)^2}{k_b} \right) \mathrm{Im}(\eta^2) + i\frac{k_b}{2} \left(|\eta^2|^2 - \mathrm{Re}(\eta^2) \right) \right] \\
&+ i\frac{b_x}{|\eta^2-1|^2} \left[\frac{2(b/a)^2}{k_b} \left(1 - \mathrm{Re}(\eta^2) \right) \right] \\
&= b_x \left[\left(k_b r_s - \frac{1}{k_b g_s} \right) + i \left(k_b l_{\mu s} - \frac{1}{k_b l_{\epsilon s}} \right) \right]
\end{aligned}
$$

Using Eqn. 5.23 and the definitions,

$$
\begin{aligned}
R'_m &\equiv b_x \left[k_b(r_m + r_{sm}) - \frac{1}{k_b} \left(\frac{m^2}{g_m} + \frac{1}{g_{sm}} \right) \right] \\
L'_m &\equiv \mu_o b (l_{\mu m} + l_{\mu sm}) \\
C'_m &\equiv \epsilon_o b \frac{1}{(m^2/l_{\epsilon m} + 1/l_{\epsilon sm})}
\end{aligned}
\tag{9.12}
$$

the modal input impedance in Eqn. 5.23 becomes:

$$
\begin{aligned}
Z'_m &= R'_m + j \left(\omega L'_m - \frac{1}{\omega C'_m} \right) \\
&= b_x \left(k_b(r_m + r_{sm}) - \frac{1}{k_b} \left(\frac{m^2}{g_m} + \frac{1}{g_{sm}} \right) \right) \\
&+ i b_x \left(k_b(l_{\mu m} + l_{\mu sm}) - \frac{1}{k_b} \left(\frac{m^2}{l_{\epsilon m}} + \frac{1}{l_{\epsilon_s m}} \right) \right)
\end{aligned}
\tag{9.13}
$$

where

$$
r_{sm} = \begin{cases} \mathrm{Im}(\eta^2)/(4|\eta^2-1|^2) & \text{if } m > 0 \\ \mathrm{Im}(\eta^2)/(2|\eta^2-1|^2) & \text{if } m = 0 \end{cases}
$$

$$
g_{sm} = \begin{cases} -|\eta^2-1|^2/((b/a)^2 \mathrm{Im}(\eta^2)) & \text{if } m > 0 \\ -|\eta^2-1|^2/(2(b/a)^2 \mathrm{Im}(\eta^2)) & \text{if } m = 0 \end{cases}
$$

$$
l_{\mu sm} = \begin{cases} (|\eta^2|^2 - \mathrm{Re}(\eta^2))/(4|\eta^2-1|^2) & \text{if } m > 0 \\ (|\eta^2|^2 - \mathrm{Re}(\eta^2))/(2|\eta^2-1|^2) & \text{if } m = 0 \end{cases}
$$

$$
l_{\epsilon sm} = \begin{cases} -|\eta^2-1|^2/((b/a)^2(1-\mathrm{Re}(\eta^2))) & \text{if } m > 0 \\ -|\eta^2-1|^2/(2(b/a)^2(1-\mathrm{Re}(\eta^2))) & \text{if } m = 0 \end{cases}
$$

Since the index of refraction is wavelength dependent, it is not sufficient to specify only a value for k_b in order to calculate the modal RLC elements. One must specify a circumference as well. Fig 9.7 compares the reactance of Eqn. 5.23 using the exact Z_s term, Eqn. 9.5, and using the approximate Z_s term, Eqn. 9.13, for various circumferences of a thin ring, $\Omega = 12$ ($b/a = 64$). For circumferences larger than 20-30 μm, the approximate reactance in Eqn. 9.13 is a poor fit with the exact result

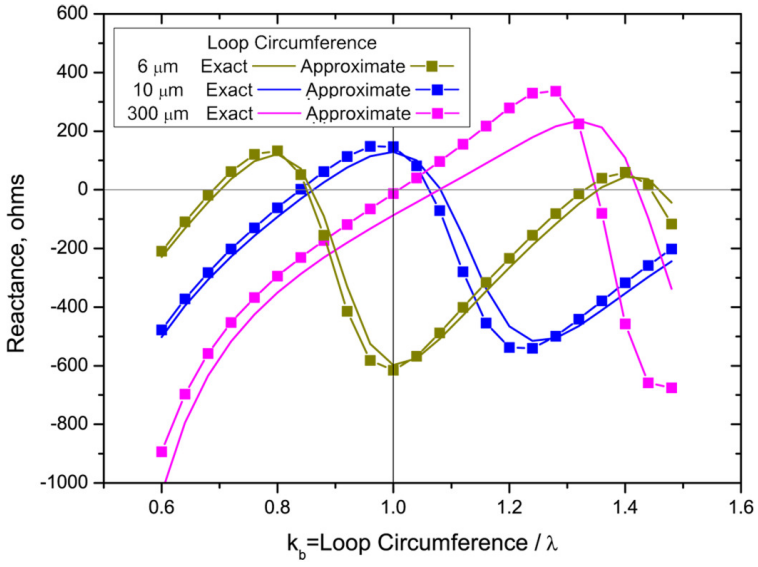

Figure 9.7: The reactance for three thin gold rings ($\Omega = 12; b/a = 64$), comparing the effect of the exact optical term Eqn. 9.5 with the approximate Eqn. 9.11. The smaller the ring, the more exact the optical term approximation becomes.

given by Eqn. 9.5. This is due to that $\gamma a \ll 1$ approximation, made so that the Bessels could be reduced to first order. But for 6 μm and shorter, the agreement is very good. Therefore, any calculations with the approximation Eqn. 9.10 can be applied to rings with circumferences shorter than about 10 μm.

9.4 The Effects of Material Characteristics on Ring Response

9.4.1 Resonance Saturation of Rings in the Optical Region

Several authors have noticed that as dipoles and rings are made shorter, they tend to resonate at wavelengths longer than their lengths, or circumferences, would suggest Okamoto et al. [2012], Khurgin and Sun [2011], Novotny [2007a], Soukoulis et al. [2007], Klein et al. [2006]. Also see Sections 7.5 and 7.6. Indeed, they eventually reach a minimum wavelength below which they will not resonate. The model given above yields an accurate functional curve for this behavior in rings. The reason is the extra optical term in Eqn. 9.3.

Using the approximation Eqn. 9.13, an equivalent expression to Eqn. 8.7, which gives the modal resonances in the OR, is:

$$k_{bmr} = \frac{2\pi b}{\lambda_{mr}} = \sqrt{\frac{m^2 + l_{\epsilon m}/l_{\epsilon sm}}{l_{\epsilon m} l_{\mu m} + l_{\epsilon m} l_{\mu sm}}}. \tag{9.14}$$

Since this assumes the small γa approximation, it applies only to rings with circumferences less than 10 μm. $l_{\mu m}$ and $l_{\epsilon m}$ are the low frequency, unit-less, functions

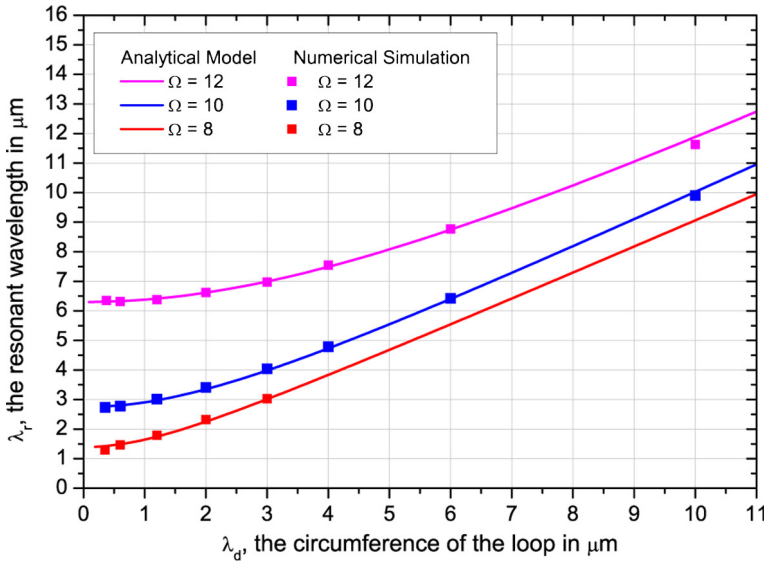

Figure 9.8: The first modal resonance (m=1) as a function of the circumference for four gold rings of various thicknesses, given by Eqn. 9.14. All rings show cutoffs in the near infrared, except the thickest.

related to the ring inductance and capacitance, respectively, found in Eqn. 8.6. $l_{\mu sm}$ and $l_{\epsilon sm}$ are the high frequency additions coming from the new optical term. Figure 9.8 shows a plot of Eqn. 9.14 for rings of various thicknesses. The model is less accurate for thick rings, because of the thin-wire approximation. Even so, the analytic model matches numerical simulations down to thicknesses of $\Omega = 8$ ($b/a = 8.7$). We see immediately a resonance saturation for each ring. The cutoff for the thinnest ring is about 6.2 μm, below which closed, gold nano-rings will have no first harmonic (m=1) resonance. The analytical model predicts a cutoff for a thick $\Omega = 6$ ring of about 600 nm, but the simulations put it at about 1.0 μm. This is because the thin-wire approximation makes theoretical results for thicker rings less accurate.

Resonance saturation occurs for hexagons and squares as well. Figure 9.9 shows ZC resonances for simulated circular, hexagonal and square rings, compared with the ZC resonances identified from numerical input impedance plots of circular rings using Eqn. 5.23. The radius of the wire, a, for these rings is taken to be the radius of a circumscribing circle through the middle of the wire at the corners. The circle circumscribing the hexagon or square itself has radius b. We conclude that the shape of the ring is not an important parameter for saturation.

9.4.2 Radiation Efficiency of the Ring

The distribution of current on a circular ring in the OR is given by Eqn. 9.2 and by Eqn. 9.4 with $V_0 = 1$. It is composed of a zero-order DC current and cosine terms associated with each mode. Figure 9.10 shows the current magnitude at $\phi = 0$ for a 600 nm circumference gold ring as a function of k_b. The first ZC resonance occurs at

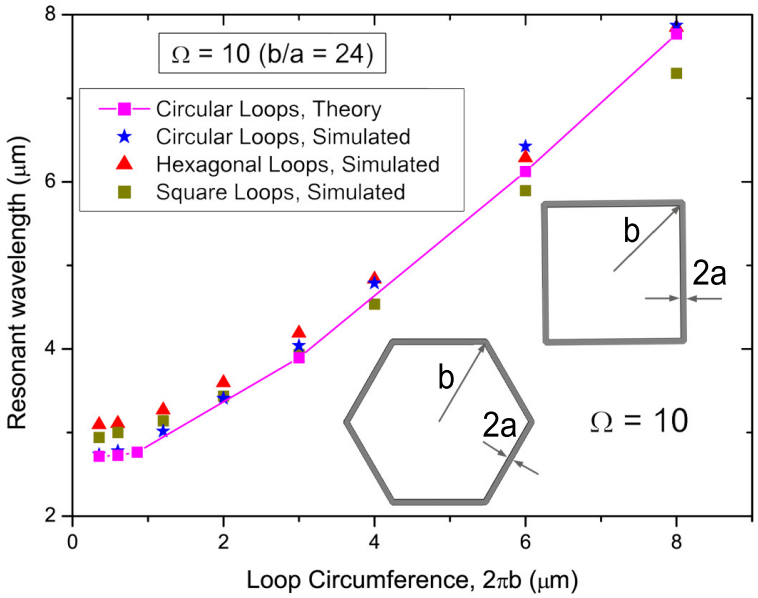

Figure 9.9: The first ZC resonances of simulated gold circular, hexagonal and square nano-rings of size $\Omega = 10$ $(b/a = 24)$ compared with ZC resonances measured from plots using Eqn. 5.23. The line joins the points calculated from Eqn. 5.23 as a guide to the eye.

$k_b \approx .1$, but the current peak occurs at $k_b \approx .09$. This slight discrepancy occurs for all rings, even at long wavelengths, as Table 9.2 shows. Interestingly, the table also shows that the current peaks occur at the ***modal*** resonances. This is important because rings radiate best where the current is high, consequently one should design to the modal resonances, not the ZC resonances. Since the modal resonances for thicker rings overlap more than in thin rings, their current peaks are not as pronounced and their current peaks are smaller and broader.

The high current in the very low k_b region in Fig. 9.10 is due to the zero-order term in Eqn. 9.2. The peak and half power points can be directly measured from the curve, which allows a calculation of the ring's modal quality factor. Q is calculated using $k_{br}/(k_{bu} - k_{bl})$, where 'u' and 'l' refer to the upper and lower half power points respectively. Table 9.3 shows these peak current magnitudes and Q as a function of the circumference of the ring, taken from such calculations.

The radiation efficiency of the ring is the power radiated divided by power input. This leads to

$$\epsilon_{rad} = \frac{R_{rad}}{R_{rad} + R_{loss}} \tag{9.15}$$

The radiation resistance is normally taken at the ZC resonance, since reactance goes to zero. However, since the current peak and the resonance are slightly different, and since one would match the generator to a ring at the current peak, the radiation resistance is that at the k_b position of the peak, R_{res}, calculated by Eqn. 9.4 . Since

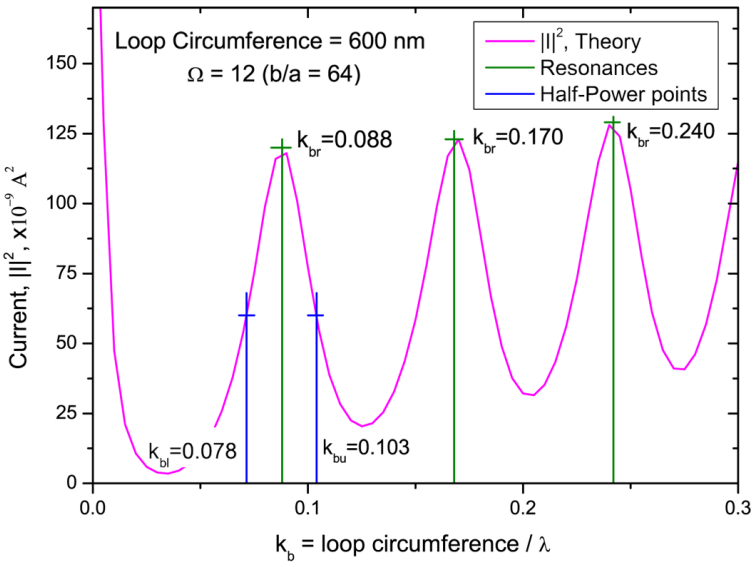

Figure 9.10: The squared modulus of the current as a function of k_b for a gold ring of circumference 600 nm. The first, second and third harmonic peaks are marked. The upper and lower half-power points of the first peak are also marked.

Table 9.2: Zero-crossing Resonances from Eqn. 5.23, Modal Resonances from Eqn. 9.14 and Squared Current Peaks from Eqn. 5.22 at $\phi = 0$ for thin gold closed rings. This table shows that the current peaks occur at the modal resonances rather than at the ZCs.

$\Omega = 12$	Resonance #1			Resonance #2		
$2\pi b$	ZC	m=1	$\|I\|^2$ Peak	ZC	m=2	$\|I\|^2$ Peak
μm	k_b	k_b	k_b	k_b	k_b	k_b
≥ 3000	1.09	1.07	1.04	2.15	2.10	2.15
10.00	0.86	0.81	0.80	1.70	1.59	1.60
8.00	0.80	0.75	0.73	1.56	1.47	1.47
6.00	0.70	0.66	0.64	1.35	1.28	1.28
3.00	0.43	0.41	0.40	0.83	0.79	0.78
0.86	0.14	0.13	0.13	0.26	0.24	0.24
0.60	0.10	0.09	0.09	0.18	0.17	0.17
0.35	0.06	0.05	0.05	0.11	0.10	0.10

there is additional loss in the optical region, the radiation resistance is

$$R_{rad} = R_{res} - R_{loss} \tag{9.16}$$

(Locatelli et al. [2009]). The radiation efficiency, then, is

$$\epsilon_{rad} = \frac{R_{res} - R_{loss}}{R_{res}} \tag{9.17}$$

We follow Hanson [2006] in deriving R_{loss} from the ohmic power loss:

$$P_{ohmic} = \frac{1}{2} R_{loss} \left| I_{in} \right|^2 = \frac{\mathrm{Re}(z_s)}{2} \int_0^{2\pi} \left| I_\phi \right|^2 b d(\phi) \tag{9.18}$$

and therefore

$$R_{loss} = \frac{1}{2\pi} \frac{b}{a} \frac{\mathrm{Re}(Z_s)}{\left| I_{in} \right|^2} \int_0^{2\pi} \left| I(\phi) \right|^2 d(\phi)$$

Table 9.3 gives a comparison of various measures for the rings of Table 9.2 at the first modal resonance for two thicknesses of wire. The thicker ring shows higher currents throughout the range, lower losses due to the thicker wire size, higher radiation efficiencies, and higher Q.

Table 9.3: Absolute square modulus of the current peak, the radiation resistance, ohmic loss, radiation efficiency and quality factor of gold closed rings with varying circumferences, and sized $\Omega = 10$ and 12. All measures given for the first modal resonance of the ring. Note that the currents are calculated using $V_0 = 1.0$ in Eqn. 5.23.

	$\Omega = 10$				
$2\pi b$	$\left\|I\right\|^2_{Pk}$	R_{rad}	R_{loss}	ϵ	Q
μm	$10^{-6} A^2$	ohms	ohms		
≥ 3000	56.2	115	1	1.00	3.7
10.00	47.7	134	22	0.86	3.8
8.00	48.5	136	27	0.83	3.9
6.00	43.0	131	38	0.77	4.0
3.00	34.5	86	92	0.48	4.6
0.86	8.7	4	324	0.01	5.9
0.60	4.5	1	450	0.00	5.8
0.35	1.6	0	782	0.00	5.6
	$\Omega = 12$				
≥ 3000	5.20	128	0	1.00	5.0
10.00	1.54	81	150	0.35	3.5
8.00	1.19	76	193	0.28	3.3
6.00	0.82	59	262	0.19	3.2
3.00	0.27	32	537	0.06	3.0
0.86	0.24	10	1849	0.01	2.8
0.60	0.12	31	2563	0.01	2.7
0.35	0.04	21	4509	0.00	2.6

9.5 General Conclusions on the Effects of Surface Impedance

In general, closed rings follow the analytic model for perfectly conducting rings (low frequencies) with, however, an extra term prominent in each mode (see Eqn. 9.3) that represents the lossy part of the material. The extra term accounts for material dispersion at frequencies higher than the MW region, where electrons can no longer oscillate in phase with the incident energy. This slowing leads to wavelength scaling and resonant saturation. The index of refraction completely accounts for these influences and appears prominently in this extra term. Careful modeling of the index is important, because the OR introduces inter-band and intra-band transitions that affect conductivity. We therefore use an extended Drude model to compute the index.

For gold, the extra term begins to influence the input impedance and current calculation at ring circumferences shorter than 3 mm, but dominates by 10 μm. The low frequency input impedance model leads to an RLC circuit representation of the ring, where element values are not constants, but rather functions of the circumference of the ring compared with driving wavelength, ie., functions of $k_b = 2\pi b/\lambda$. As the driving wavelength reaches the THz regime, wavelength scaling sets in, and these RLC values also become functions of the index of refraction, which is inherently a function of wavelength.

The modal harmonic resonances are important, because the current peaks occur there, rather than at the zero-crossing resonances of the ring. All modal harmonic resonances saturate; the first mode (m=1) saturates in the NIR for all rings thinner than $\Omega = 8$. The “roll-off" away from the linear slope toward saturation is rather abrupt, so that a rather large number of ring circumferences will give resonances at roughly the same wavelength (see Fig. 9.8).

The quality factor (Q) of thin gold ring antennas begins around 5 in the low frequencies and reduces as Drude behavior sets in, until it saturates at about 2.5. Interestingly, the Q of thick gold rings increases from about 3.7 at long wavelengths to 5.5 at saturation. The radiation efficiency decreases dramatically for both thick and thin rings as the driving wavelength shortens, due to increased losses. These data imply that the performance of OR rings is substantially poorer than their performance at RF.

Chapter 10

The Theory of a Single Impedance or Gap in the Periphery of Circular Rings

10.1 Introduction

The analytical model of Storer/Wu, expanded in Chapter 8 to a fully detailed *RLC* circuit theory in the RF and MW regions and then extended further in Chapter 9 to the THz, IR and OR, is extended further in this chapter to include gaps. Iizuka's method of placing lumped impedances evenly around a loop, given in Section 5.4, will provide results when the impedances are capacitive reactances. The effects of a capacitor placed in the periphery of a loop is examined in detail, and compared with the results of numerical simulations, in which rings with a single gap are illuminated by a plane wave across the frequency spectrum.

The governing equation for one impedance in Iizuka's model leads to an understanding of how a single gap affects the current distribution, the impedance, and ultimately the resonances of the closed loop. The extra capacitive reactance leads to a very high Q resonance in the sub-wavelength region, which will be identified here with the mode 0 inductance of the loop and the extra capacitance. It therefore will be called a "zero-order resonance". Varying the capacitor value changes the position of the resonance, effectively tuning the antenna.

The results of the comparisons with the numerical simulations are three-fold:

(1) A single gap gives rise to a zero-order, high Q resonance, similar to the resonances given by a single capacitor. Indeed, there is a capacitor value that yields maximum Q.

(2) Across the spectrum, a single gap has the same reactive behaviour as a capacitor, and gap width can be correlated with capacitor value.

(3) The models used in the literature for gaps may be adequate when simple *LC* combinations are used to discover the zero-order mode resonance, but they are

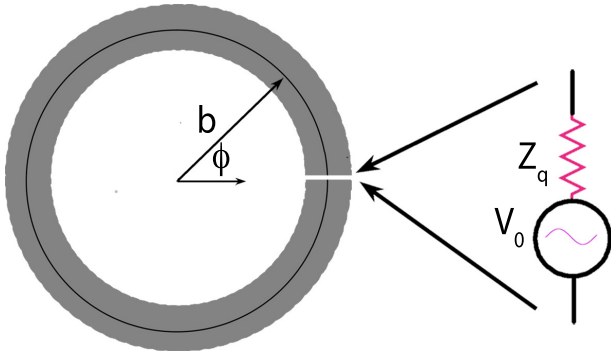

Figure 10.1: Derivation geometry for a loop with a single impedance at the source. The gap is infinitesimally small. The source and lumped Z are delta-functions at $\phi = 0$.This is a very good model for loops at RF, since no one puts gaps in RF loops.

not accurate when used with the extended Storer/Wu model for rings. Nor do they take into account the effects of wavelength scaling properly.

10.2 The Current Distribution and Impedance of a Ring with Single Impedance

The following method follows Iizuka [1965], as reviewed in Section 5.4. Place an impedance, Z_q, in series with the delta-function source. The model of the loop now appears as in Fig. 10.1. The governing equation then receives an extra term.

$$\frac{V_0\delta(\phi)}{b} - I_\phi\left[z_s + \frac{Z_q}{b}\delta(\phi)\right] = \frac{(V_0 - I_\phi Z_q)\delta(\phi)}{b} - I_\phi z_s \tag{10.1}$$
$$\frac{(V_0 - I_\phi Z_q)}{b}\delta(\phi) - I_\phi z_s = \frac{1}{b}\frac{\partial\Phi}{\partial\phi} + i\omega A_\phi$$

The derivation proceeds as in Section 9.2 except that the voltage term, V_0, may be replaced by the new term, $V_0 \to V_0 - I(0)Z_q$. As in Eqn. 9.2, the current becomes:

$$I(\phi) = \left(V_0 - I(0)Z_q\right)\left[\frac{1}{Z_0'} + \sum_{m=1}^{\infty}\frac{\cos(\phi)}{Z_m'}\right] \tag{10.2}$$
$$= \left(V_0 - I(0)Z_q\right)\frac{1}{Z_{CL}}$$

where Z_{CL} is the impedance of the closed loop without the series impedance. The input impedance is defined as the ratio of the source voltage to source current at $\phi = 0$:

$$I(0)\left(1 + \frac{Z_q}{Z_{CL}}\right) = V_0 \tag{10.3}$$

or

$$Z_{CL} + Z_q = \frac{V_0}{I(0)} = Z$$

This is an expected result since the Z_q impedance was placed in series with the voltage source and was taken as a lumped impedance; therefore it should appear in series with the closed loop antenna impedance in the result.

10.2.1 The Effects of Z_q as a Capacitive Reactance

Assume now that the impedance is a capacitor with reactance $X_q = 1/(\omega C_q)$. Taking this to k-space and using $C = \epsilon_0 b l_{\epsilon q}$ as defined in Eqn 8.5, $X_q = b_x/(k_b l_{\epsilon q})$, where b_x is the characteristic impedance of free space. Substituting into Eqn. 10.3:

$$\begin{aligned} Z = Z_{CL} + Z_q &= R_{CL} + iX_{CL} - iX_q \\ &= R + iX_L - iX_C - iX_q \\ &= R + i(X_L - (X_C + X_q)) \end{aligned} \tag{10.4}$$

where the subscript "CL" was dropped on the R, X_L, and X_C of the closed loop. The capacitive reactances of the closed loop and of the lumped capacitor add: $X_C + X_q$.

The effect of this added capacitance on the resonances of the loop can be visualised. Fig. 10.2 (a) shows the inductive reactance of an $\Omega = 12$, $2\pi b = 3$ m, perfectly conducting loop as a red line. A resonance occurs whenever an inductive reactance equals a capacitive reactance. The absolute value of the sum, $|X_C + X_q|$, is therefore superimposed for a variety of X_q values to show the crossings. All of the k_b values where an $|X_C + X_q|$ crosses the red X_L curve, indicate a resonance of the loop, either a true resonance or an anti-resonance. Therefore, in Fig. 10.2 (a), (b), and (c), look for crossings of the red line.

The important features to notice are as follows:

(1) In (a), increasing $X_C + X_q$ eventually reaches a value for which it no longer crosses the red curve. That is, there is a capacitance which saturates the loop and there can be neither true resonances nor anti-resonances.

(2) In (b), in the "sub-wavelength" region, $k_b < 0.47$, a new true resonance appears, as marked by magenta circles, and blue-shifts as X_q increases.

(3) In (c) the mode 1 resonance of the closed loop blue-shifts, but the anti-resonance, normally at $k_b = 1.46$ is red-shifting, as given by the magenta and green circles. As X_q increases the resonances eventually disappear.

Fig. 10.2 (d) shows another view of the same phenomenon. The total loop reactance drops because the capacitive reactance, which is always negative, is becoming increasingly more negative. Eventually all of the resonances disappear and X_q dominates.

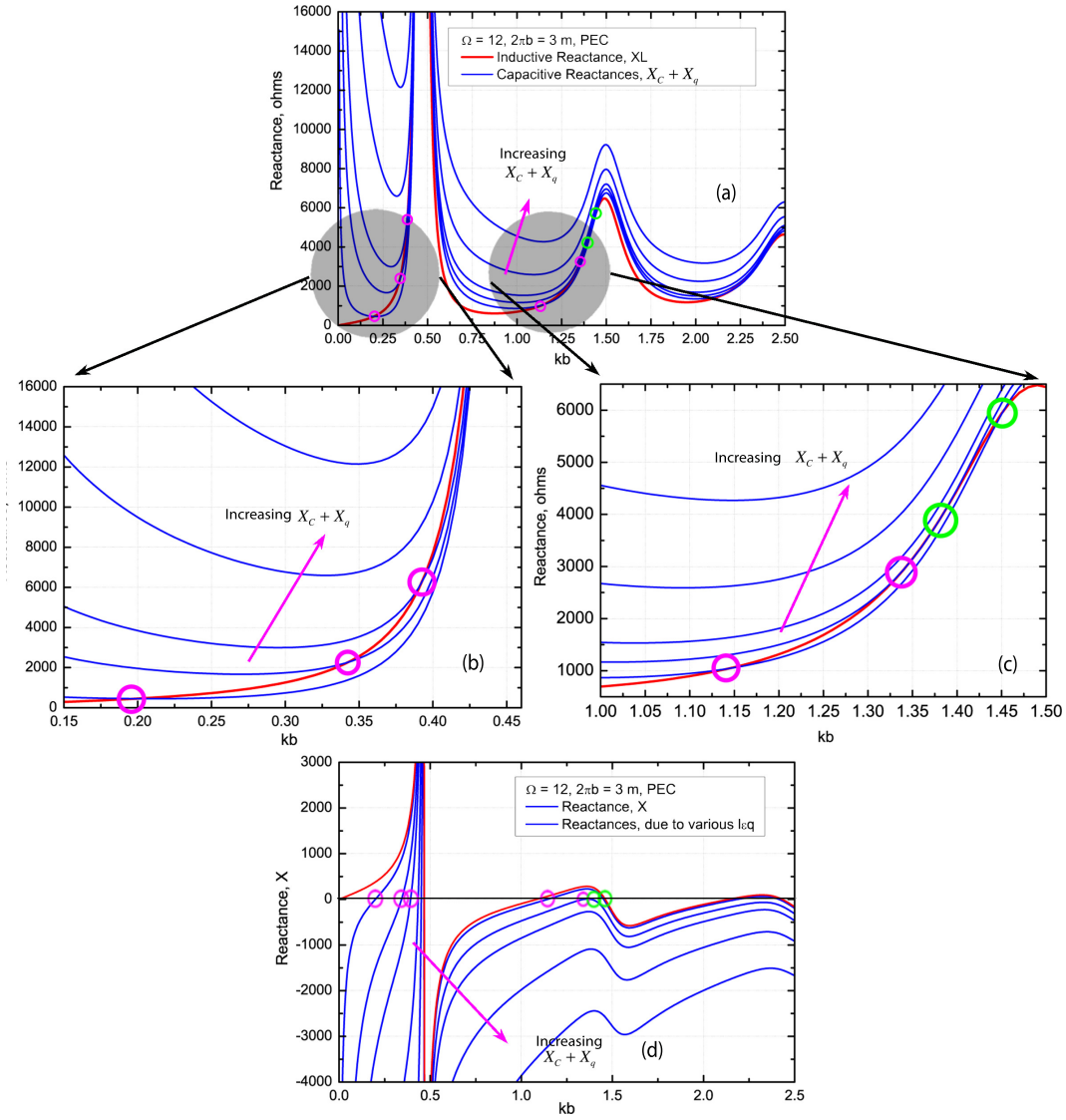

Figure 10.2: The effect of adding capacitors in series with an $\Omega = 12$, 3m, PEC closed loop, as given by Eqn. 10.4. In (a) the inductive reactance curve, X_L, is shown in red. Various capacitive reactances, X_q, are added to the closed loop capacitive reactance, X_C, shown as blue curves. Resonances occur where the blue curves cross the red curve. In (b) a new resonance arises and blue-shifts, as shown by the magenta circles. This is the sub-wavelength region. In (c) the resonances near $k_b = 1$ to 1.5, pinch-off as $X_C + X_q$ increases. The magenta circles mark resonances; the green mark anti-resonances. In (d) the total reactance for various added capacitive reactances is compared with that of the closed loop. Magenta and green circles match up with those in (b) and (c).

Recall that although capacitive reactances add because they are in series, the capacitances themselves do not. The total capacitive value is smaller than either one of the two values. This reduced value will be called C'.

$$X_C + X_q = \frac{1}{\omega C_{CL}} + \frac{1}{\omega C_q} = \frac{1}{\omega}\frac{1}{C'} \qquad (10.5)$$
$$\text{where } C' = \frac{C_{CL}C_q}{C_{CL} + C_q}$$

If the capacitive value, C_q gets very small, the capacitive reactance X_q gets very large and capacitor acts like an open circuit cutting off current to the ring. Conversely, if the capacitive value become large, the reactance becomes small and the capacitor acts like a short circuit to the current; this reverts the loop to a closed loop. Both extremes make the additional capacitor completely ineffective.

10.2.2 The Sub-wavelength, Zero-mode Resonances

The absolute value of the admittance, squared, of the same loop, as obtained from Eqn. 10.4, is shown in Fig. 10.3. The same set of capacitors as in Fig. 10.2 are applied to the loop. The sub-wavelength resonances clearly appear. To what should these be attributed? According to Eqn. 10.4, every value of capacitor, C_q, changes the total capacitance, C', of the loop and each new C' resonates with the closed loop inductance, L_{CL}.

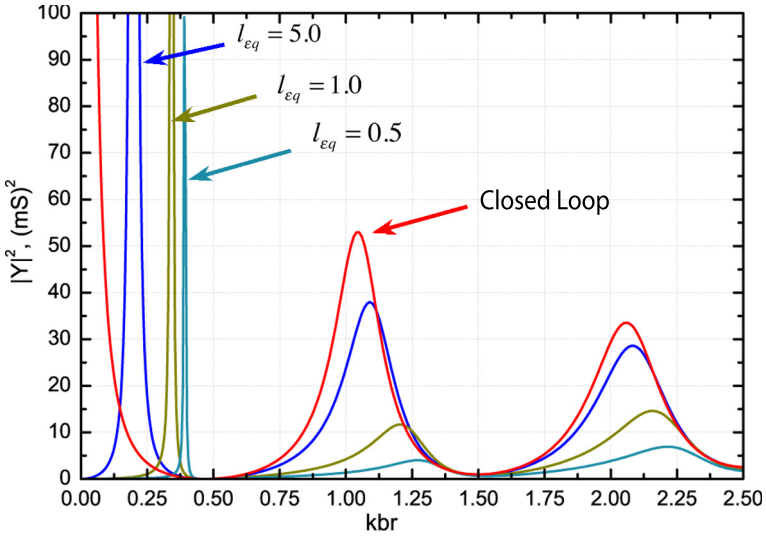

Figure 10.3: The squared modulus of the admittance, $|Y|^2$ for various capacitor values in the $\Omega = 12,3$ m loop. The sub-wavelength resonances grow weaker as the anti-resonance is approached. Note that the Q of the resonances vary.

In Section 8.3.1 it was shown that many modes add to create the total inductance and capacitance of the loop. One must sum the effect of all of them for accuracy at

any desired k_b. However, in the sub-wavelength region, all of the other modes are far enough away that they should have little impact on the inductance of the loop. A sufficiently thin loop, such as $\Omega = 12$, in fact, will have its closed loop inductance in this region determined almost entirely by mode 0. To show this, Fig. 10.4 (a) compares the inductance given by mode 0 with the total inductance of a thin closed loop. The largest difference occurs close to the anti-resonance and is about 8%. This is not the case for the loop capacitance, however. There is no mode 0 capacitance; and mode 1 is not a good approximation for the total capacitance. The same figure shows in (b) that the total loop capacitance is a combination of the lumped capacitor and the closed loop capacitor for $k_b > 0.20$. In the region $0 < k_b < 0.2$, the closed loop capacitance dominates.

This means that these sub-wavelength resonances are determined by the zero-mode inductance of the closed loop and by a combination of the closed loop capacitance and the lumped capacitor. In the region $0 < k_b < 0.2$, L_0 and C_q determine the resonance. In the region $k_b > 0.20$, L_0 and the combined capacitor, C', do. These resonances come to an end at the anti-resonance, $k_b = 0.47$.

10.2.3 Quality Factor, Q, of the Zero-Order Resonances

The resonances can be calculated using the standard approach.

$$\omega_r = \frac{1}{\sqrt{LC'}} \rightarrow k_{br} = \frac{1}{\sqrt{l_\mu l'_\epsilon}} \tag{10.6}$$

where L is the inductance of the closed loop and C' is the combined capacitance of the closed loop and the added capacitor. $C' = \epsilon_0 b l'_\epsilon$. This relation can be plotted the same way that the relation Eqn. 8.7 was plotted in Fig. 8.7. The right hand side is a function of k_b, so it will produce a rolling curve for each new value of $l_{\epsilon q}$. The resonance occurs where the straight line $y = k_b$ intersects with the rolling curve. A set of lumped capacitors, $l_{\epsilon q}$, with their rolling curves are shown in Fig. 10.5 (a) for an $\Omega = 10$ gold loop, and in Fig. 10.6 (a) for a thicker loop. These curves do not change from the RF to about 300μm, the THz regime. The intersections, indicating the zero-order resonances blue-shift with increasing $l_{\epsilon q}$. The upper limit of the intersections, which marks the anti-resonance, is clearly evident.

The quality factor for these resonances can be found using the standard approach, Eqn. 4.20:

$$Q = \frac{1}{R}\sqrt{\frac{L}{C'}}\bigg|_{k_{br}} = \frac{b_x}{R}\sqrt{\frac{l}{l'_\epsilon}}\bigg|_{k_{br}} \tag{10.7}$$

Figures 10.5 (b) and 10.6 (b) show the quality factors immediately below their corresponding resonances in (a). These factors are truly remarkable, all of them being in > 1000 with a maximum, 2063, at $k_b = 0.35$ for the thinner loop and 3300 at $k_b = .3$ for the thicker loop. To see such high Q peaks in numerical simulations requires high resolution on the independent variable, k_b, as in Fig. 10.10.

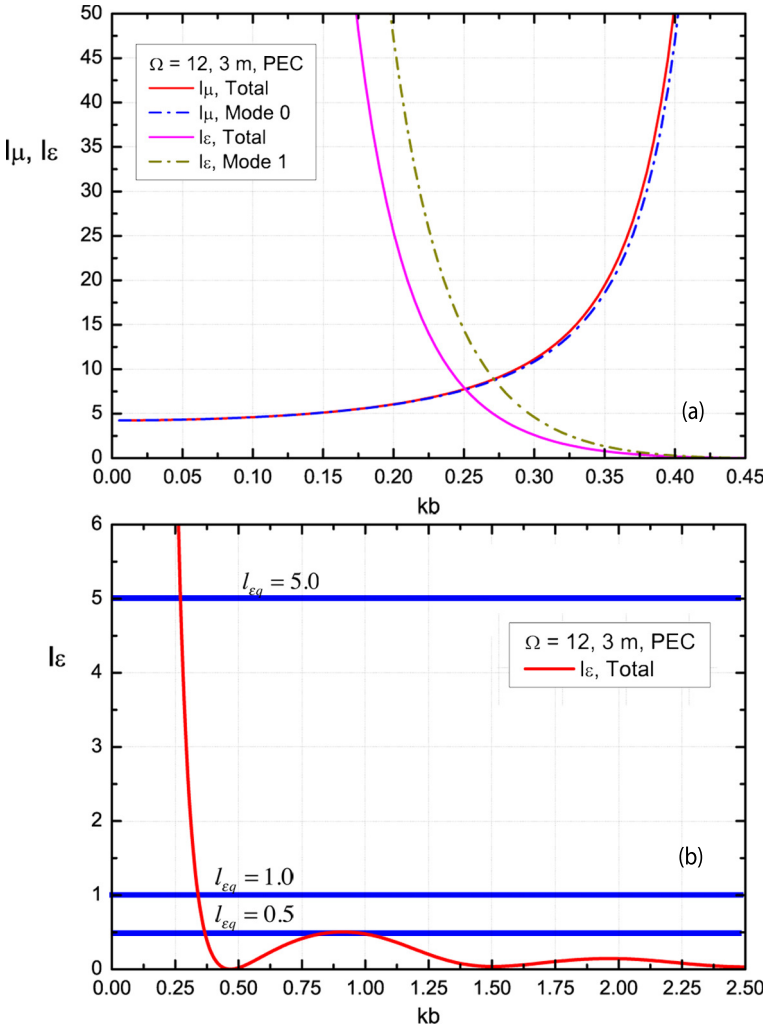

Figure 10.4: (a) The Inductance and capacitance of an $\Omega = 12$, 3m, PEC closed loop in the sub-wavelength region. In (a) a comparison of $l_{\mu 0}$ with the total inductance l_μ; at $k_b = .4$, the difference is about 8.5%. Also a comparison of $l_{\epsilon 1}$ with the total capacitance; the mode 1 capacitance does not dominate over the other modes. In (b) the total capacitance of the loop compared with several of the lumped capacitors.

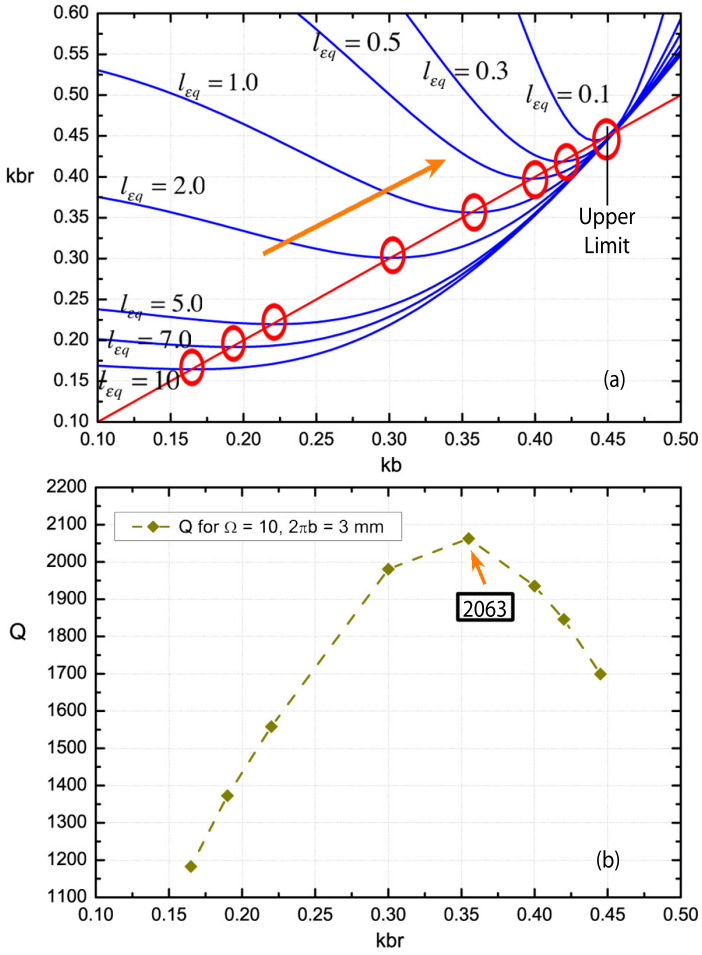

Figure 10.5: An $\Omega = 10$ gold ring with $2\pi b$ = 3 m (RF), 3 mm (MW), and 300 μm (THz). (a) The ZO resonances, using Eqn. 10.6. (b) The Q of these resonances, using Eqn. 10.7. There is a peak in the quality factor occurring about $k_b = 0.35$, given by a capacitor value $l_{eq} = 1.0$. The dashed line guides the eye.

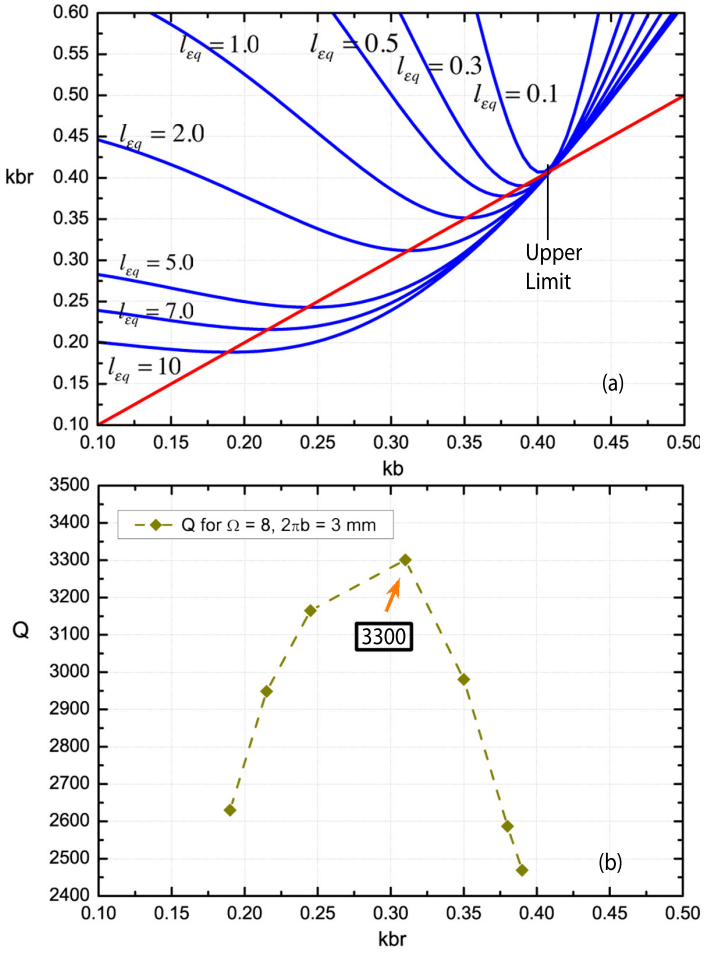

Figure 10.6: Repetition of Fig. 10.5; with a thicker ($\Omega = 8$) loop. The peak of the quality factor has red-shifted, but increased by 60% over the thinner loop.

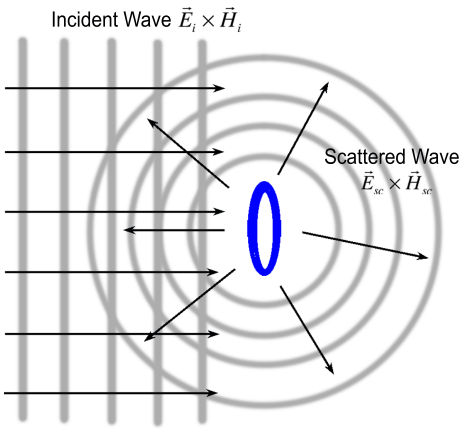

Figure 10.7: The relation between fields during scattering off a loop antenna.

10.3 The Transition from Lumped Impedance to Gap Impedance

10.3.1 The Use of the Radar Cross-section

In the case of analytical model, a gap in series with a voltage source can be modelled mathematically using the delta-function technique. But this can't be done with the numerical simulation tool, MWS, some another method must be developed to simulate a gap in series with the source.

One solution is to illuminate the loop, as discussed in Section 3.2.3, and as shown in Fig. 10.7. In the case of illumination, the single gap acts like a voltage source as long as the incident $\vec{E}$ is polarised to develop a voltage across the gap, as noted by Zhan and Chui [2014]. The latter's paper was reviewed in Section 6.5, because they had found a zero-order resonance due to the presence of the gap. Their s and p polarisations are shown in Fig. 10.8; it is the s polarisation that energises the loop, while the p does not. This has been reported by others (Katsarakis et al. [2004]; Enkrich et al. [2005]; Rockstuhl et al. [2007]). Therefore, the model should give results that are comparable to results of simulation using an illuminating plane wave under the correct polarisation. The simulation produces a radar cross-section (RCS), which should be directly comparable to a calculation of the radiated power, $|Y(0)|^2 R_{rad}$, as discussed in Section 3.2.3.

Fig 10.9 (a) shows simulated cross-sections for three $\Omega = 10$, gold rings, each with the same gap width ratio, $g/a = 0.5$, illuminated in the RF, MW, and THz regimes. They all show a zero-order resonance at $k_b \approx 0.4$. The data in the figure are normalised to the area of the loop, because the cross-sectional area diminishes as the area of the ring diminishes (a cross-sectional area is usually on the order of the area of the target object). Four points of interest are important:

(1) The zero-order resonance at $k_b = 0.4$ created by the gap in all three rings correlates with a capacitor value of $l_{eq} = 0.5$ according to Fig. 10.5.

(2) This resonance does not move as the ring moves through the different regimes.

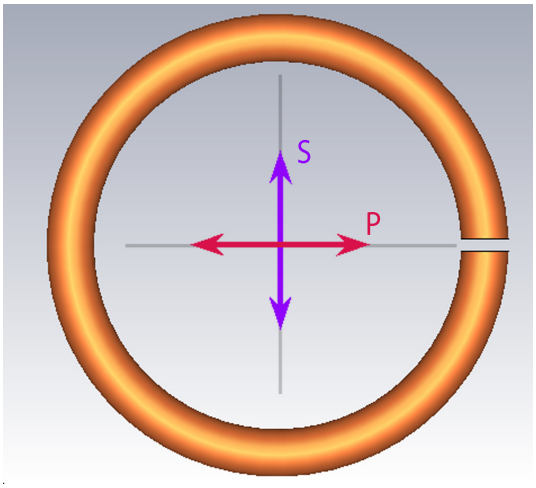

Figure 10.8: Polarisations of the plane wave as given by Zhan and Chui [2014].

Moreover, all have the same relative peak and width (and therefore same Q), compared with their first order mode.

(3) The gap blue-shifts the mode 1 resonance to about 1.4, where it stays for all three rings.

(4) The cross-sections are on the order of 5 to 8 for the mode 1 peak, but much higher for the ZO resonance.

10.3.2 The Gap as a Capacitive Reactance.

The match between the results of model, given in Fig. 10.5, and the results of simulations given in Fig. 10.9 suggests the validity of the assertion that a gap behaves like a capacitor. However, for a gap to behave truly like a capacitive reactance, it must not change its capacitance value over k_b (i.e., $C_{gap} = \mu_0 b l_{\epsilon g}$, where $l_{\epsilon g}$ is constant), and the reactance itself must respond inversely proportional to k_b (i.e., $X_{gap} = b_x / k_b l_{\epsilon g}$). Does the gap really behave this way?

Fig. 10.10 compares the theoretical RCS, $|Y|^2 R_{rad}$ (namely, Eqn. 10.4 and $l_{\epsilon q} = 0.5$) for the $\Omega = 10$, 3 mm and 300 μm rings with the corresponding simulated RCS curves. It appears that the two simulated rings follow the lumped capacitor curve across k_b, verifying the assertion, at least for $\Omega = 10$ sized loops in the MW and THz range, and strongly suggesting that the gap does behave like a capacitive reactance. If it didn't follow a $1/k_b$ functional form, some spreading or narrowing of the first mode resonance would be occurring.

The analytical model picks up a mode 2 resonance that the numerical simulation does not see. This is probably because the illuminated gap does not behave like a delta-function voltage generator. Perhaps it is a resonance that can be excited internally, by an internal generator, like the delta-function source, but cannot be

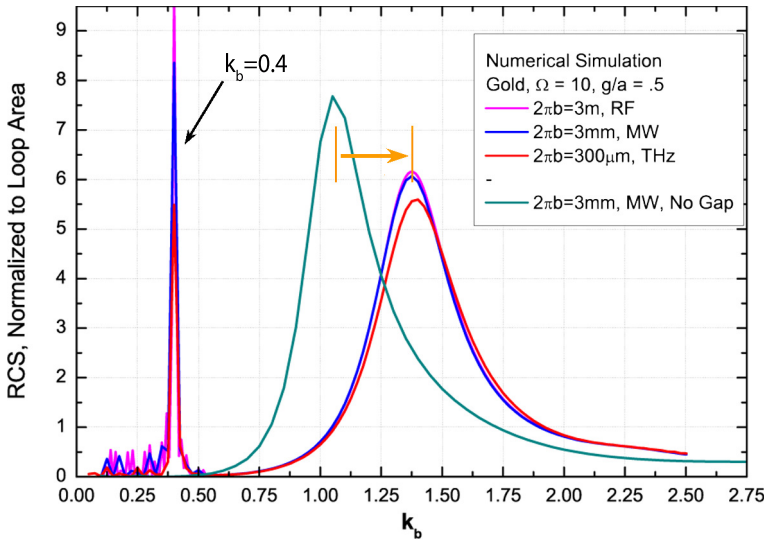

Figure 10.9: Radar cross-sections normalised to loop area from numerical simulations of three $\Omega = 10$ gold rings illuminated in the RF, MW, and THz regions. Each ring has a gap at $\phi = 0$ of width ratio $g/a = 0.5$. The gap blue-shifts the first mode resonance, but leaves the zero-order resonance at the predicted position in place.

excited externally; so called "dark modes". It could also be due to polarisation, but this is unlikely, as Figs. 10.11 and 10.12 show.

- The current distributions on the loop at the two mode peaks, one given by numerical simulation, the other by the analytical model using Eqn. 10.2 are shown in the first figure. The distributions are exactly the same for numerical simulation and analytical model. The second mode does indeed exist, the capacitor does not prevent it from occurring; the magnitudes of the currents are simply different.

- In the second figure, a numerical simulation using the P polarisation is used. The RCS shows a mode 1 resonance that sits right on top of the closed loop mode 1 resonance, and the figure does not show the zero-order resonance, indicating that the illuminated wave does not see the gap at all.

Further study of this effect remains for future work.

10.3.3 The Effects of Material Loss

In Chapter 9 the effects of loss due to characteristics of the material from which the ring is made were included in the model. The effects of these lossy characteristics can be seen when Fig. 10.5 and Fig. 10.9 are extended to the IR and OR regions. In Fig. 10.9 the scattering cross-sections were shown for low frequency gold rings, as given by numerical simulations. In Fig. 10.13, the cross-sections are shown for short wavelengths, 30 μm, 10 μm and 4 μm rings, but from calculation using the

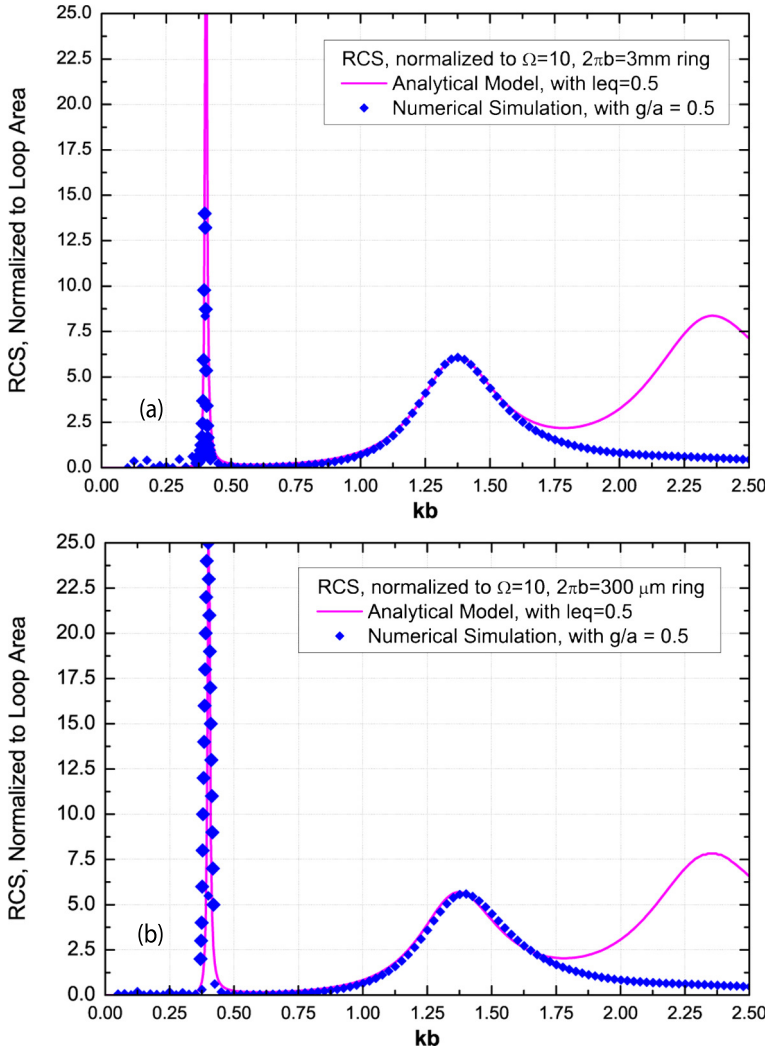

Figure 10.10: Results of the analytical model compared with numerical simulations results for two $\Omega = 10$, gold rings. (a) 3 mm (MW) and (b) 300μm (THz). In both cases the gap behaves like a lumped capacitor across the spectrum.

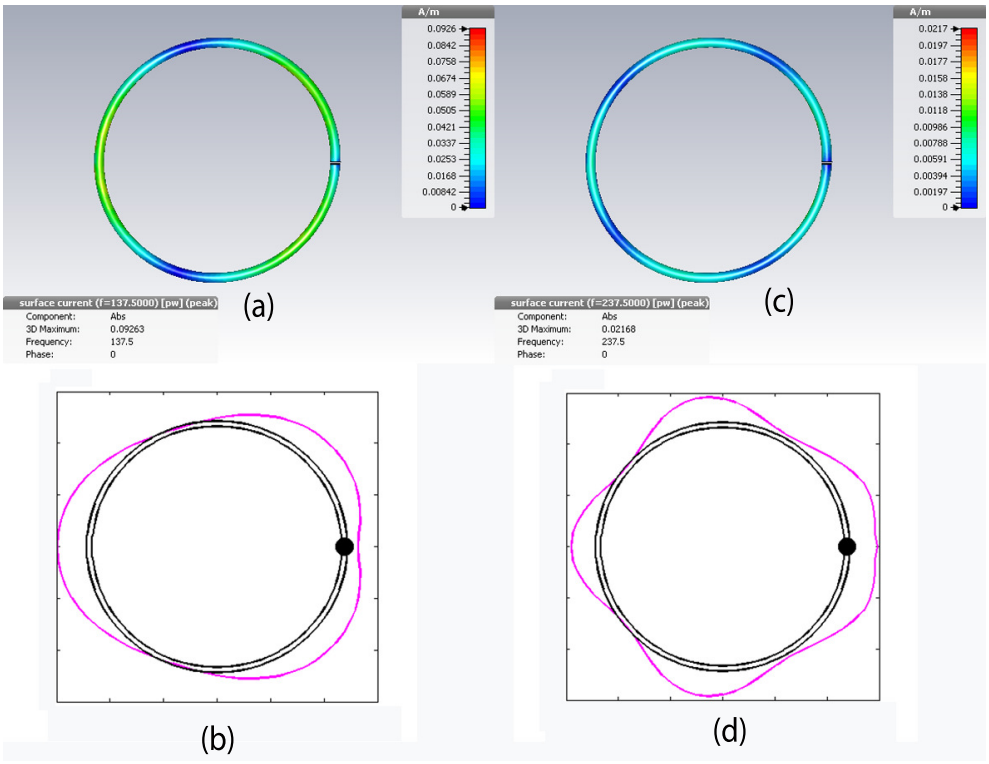

Figure 10.11: A comparison of numerical simulations of RCS for an $\Omega = 10$, 300μm loop. P-polarised plane wave does not stimulate the gap at all. The loop behaves as if it were a closed loop.

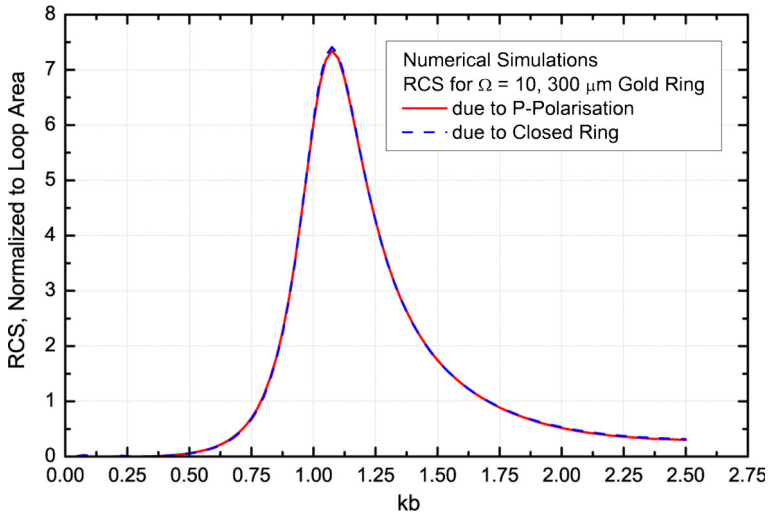

Figure 10.12: Results of the analytical model compared with numerical simulations results for two $\Omega = 10$, gold rings. (a) 3 mm (MW) and (b) 300μm (THz). In both cases the gap behaves like a lumped capacitor across the spectrum.

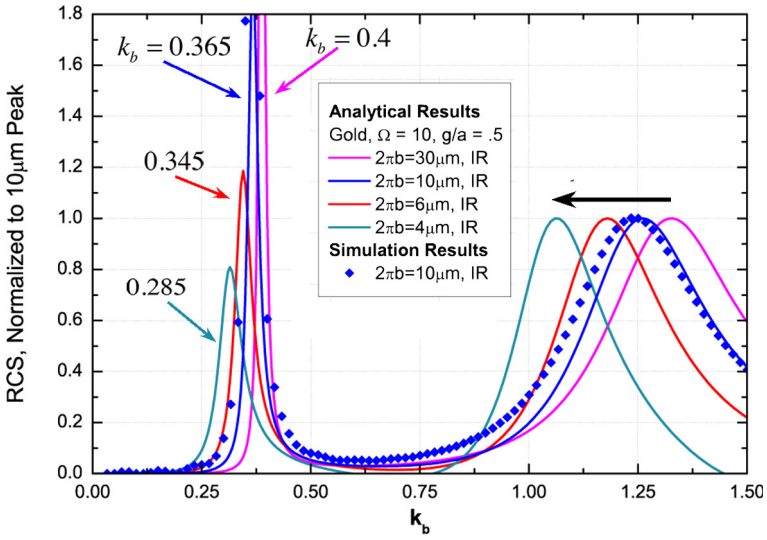

Figure 10.13: Theoretical calculations of the RCS in the infra-red region. The zero-order resonances collapse and the mode resonance red-shifts.

analytical model (Eqn. 10.6). The 30 μm curves overlap those at longer wavelengths given by the simulations in Fig. 10.9. The 10 μm and 4 μm curves red-shift due to the resonance saturation (wavelength scaling), and the height of the zero-order resonance drops quickly due to increasing loss. The Radar Cross-section, taken from a simulation of the 10 μm ring, is overlaid and the results suggest that the gap acts capacitively even at these short wavelengths, as they did at 3m and 300 mm in Fig. 10.10.

Similarly, Figs. 10.14 and 10.15 shows the high frequency effects on the zero-order resonances that were shown in Figs. 10.5 and 10.6 at low frequencies. The easiest way to see the effect is to look at the red-shift of the upper limit line from $k_b = 0.42$ at 10μm to 0.35 at 3μm. A careful look at the intersections between red and blues lines will also show the red-shift. The corresponding Q values of these resonances are also much lower due to the loss.

10.3.4 Gap Size Correlated with Capacitor Value

At every point of intersection in these four figures, a capacitor value is matched to a resonance. These are extracted and plotted in Fig. 10.16. No resonances occur at k_b values above the upper limits of the curves, because there are no intersections to the right of those values. These mark the smallest capacitors that will cause a zero-order resonance for rings of this size with one gap.

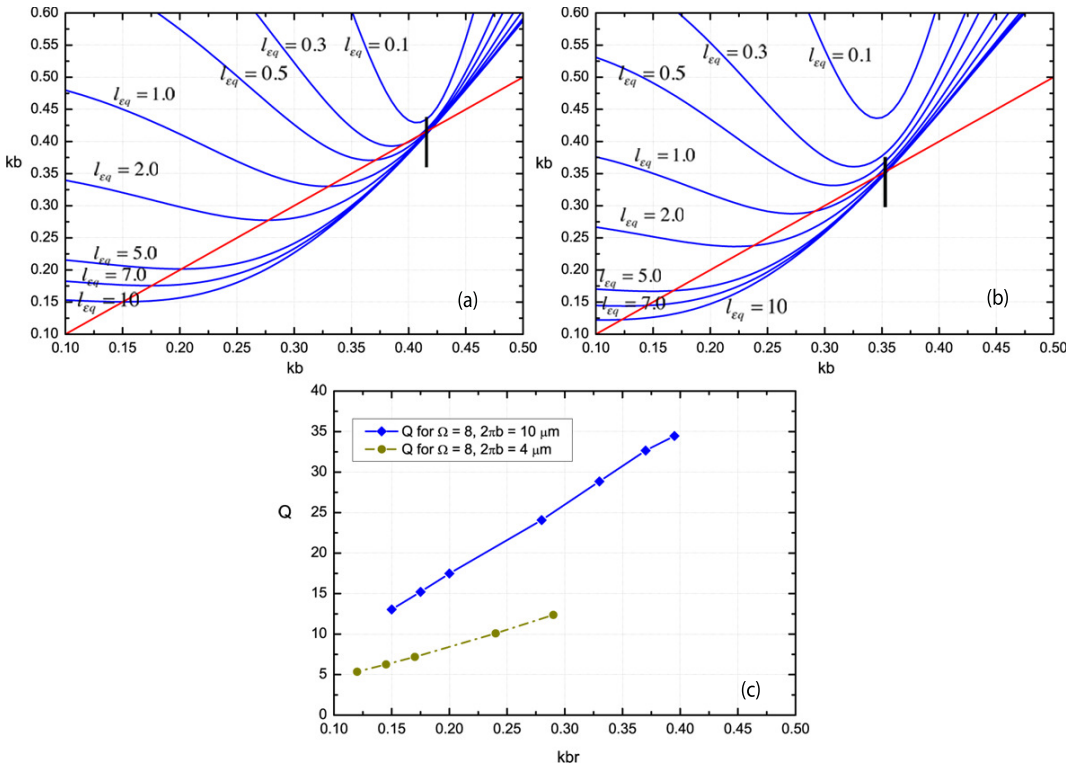

Figure 10.14: The ZO resonances and Q for an $\Omega = 10$ gold ring with $2\pi b$ = 10 μm and 4 μm in the IR. There is no peak in the quality factor for either ring.

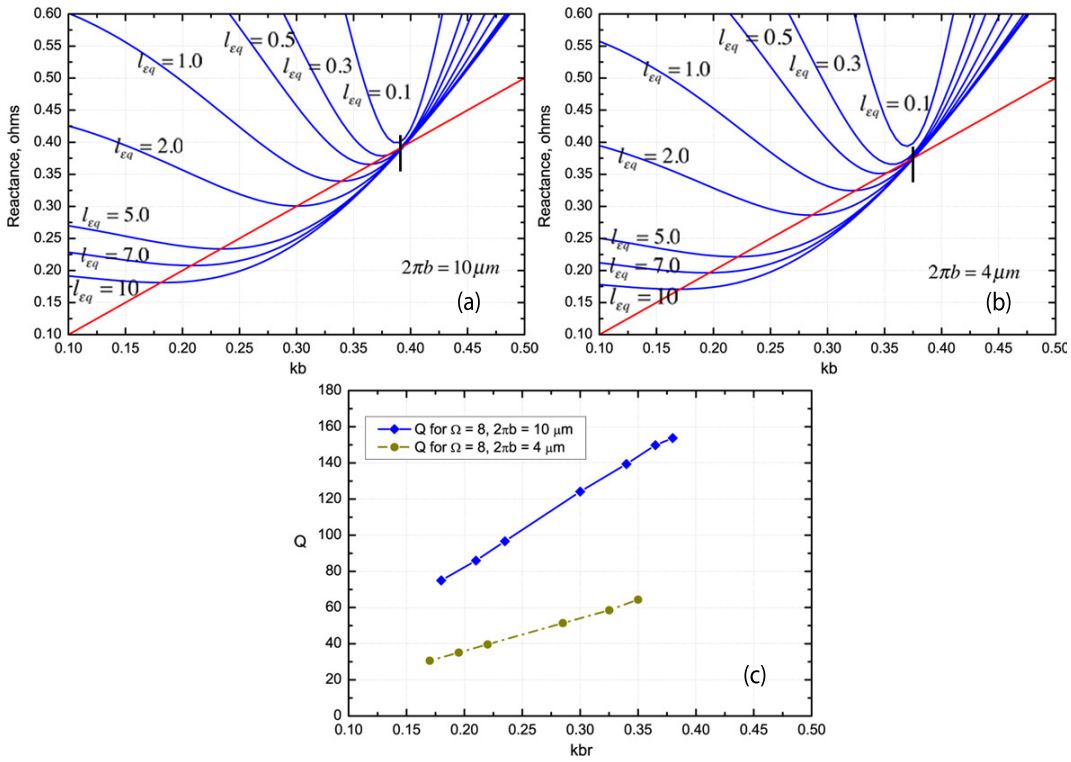

Figure 10.15: The ZO resonances and Q for an $\Omega = 8$ gold ring with $2\pi b$ = 10 μm and 3 μm in the IR. There is no peak in the quality factor for either ring.

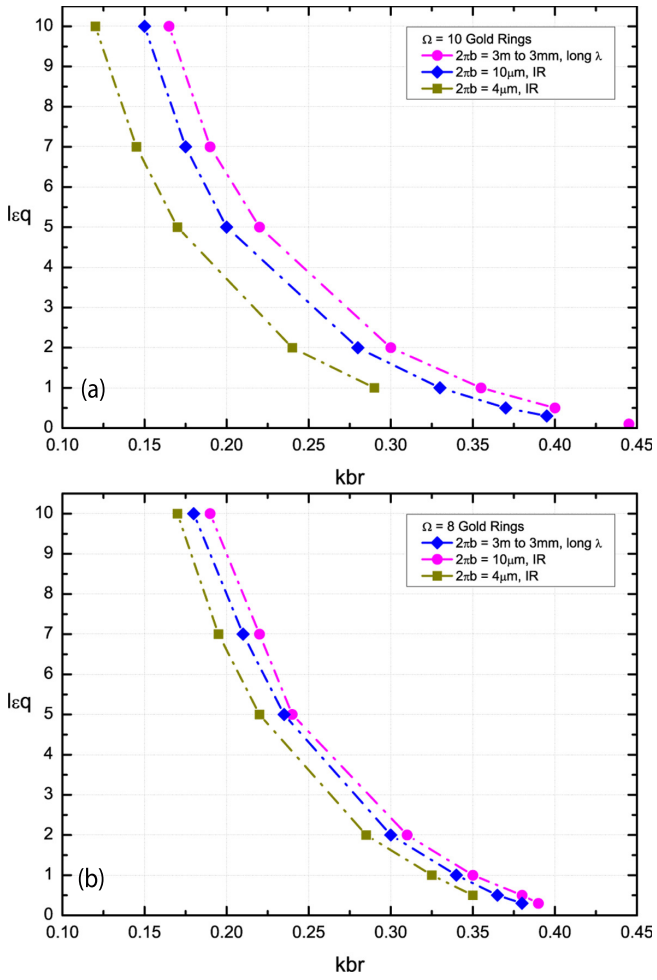

Figure 10.16: The capacitor values required to establish zero-order resonances. (a) $\Omega = 10$ and (b) $\Omega = 8$ gold rings. From the RF through MW and THz to the IR.

10.4 Models of Gap Capacitance

10.4.1 Gap Models in the Literature

Three models for gaps in dipoles and in rings have appeared in the literature.

- **The Flat-Plate Model** (Corrigan et al. [2008]), in which the gap is asserted to have the geometrical properties of a flat-plate capacitor; namely, two flat plates with square area, A, separated by a dielectric a distance, g. The capacitive value is $C_{gap} = \epsilon_0 A/g$. If this is the case, then the relation between $l_{\epsilon q}$ and the gap ratio, g/a can be derived easily if we assume a round wire:

$$C_{gap} = \epsilon b l_{\epsilon q} = \epsilon \frac{\pi a^2}{g} = \epsilon b \frac{\pi}{(b/a)(g/a)} \tag{10.8}$$

or

$$l_{\epsilon,fp} = \frac{\pi}{(b/a)(g/a)}$$

- **The Flat-Plate with Fringe Effects** (Sydoruk et al. [2009]), in which the electric field is assumed to escape the gap somewhat, thus affecting the overall capacitance of the gap. Fringe effect is usually accounted for in a round wire using $C_{fringe} = \epsilon_0(2\pi a + g)$. The total relationship becomes:

$$C_{gap} = \epsilon_0 b \left(\frac{\pi}{(b/a)(g/a)} + \frac{2\pi}{b/a} + \frac{g/a}{b/a} \right) \tag{10.9}$$

or

$$l_{\epsilon,frng} = \frac{\pi}{(b/a)(g/a)} \left(1 + 2(g/a) + \frac{(g/a)^2}{\pi} \right)$$

- **The Flat Plate with Fringe Effects and With Surface Capacitance** (Sydoruk et al. [2009]; Delgado et al. [2009]), in which the surface charge distributed around the ring affects the overall resonances of the loop. If one has a simple LC model of the loop, this added capacitance should be added to the gap capacitance in order to calculate the resonance. The gap model producing $l_{\epsilon q}$ takes this surface charge into account, so it would be appropriate to compare it with this model. The surface charge for a round wire is:

$$C_{surf} = 4a\epsilon_0 \ln\left(\frac{4b}{g}\right) = \epsilon_0 b \frac{4}{b/a} \ln\left(\frac{4(b/a)}{(g/a)}\right) \tag{10.10}$$

or

$$l_{\epsilon,surf} = l_{\epsilon,frng} + \frac{4}{b/a} \ln\left(\frac{4(b/a)}{(g/a)}\right)$$

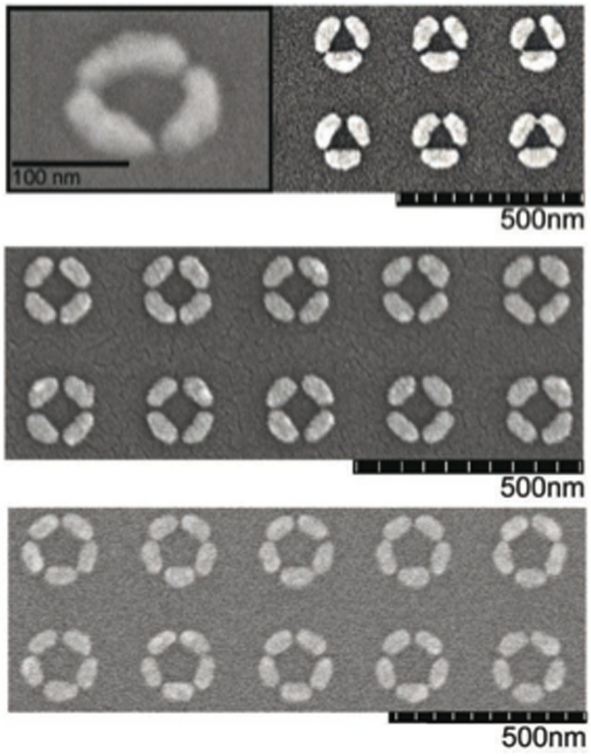

Figure 10.17: Rings with 6 nm gaps by Clark and Cooper [2011].

10.4.2 The Reduction in Total R, L, and C

The gap also reduces the total ring resistance, inductance, and capacitance due to a slight shortening of the metal forming the loop. This reduction, ρ, is related to an angular section of the ring and thus to the gap ratio g/a:

$$\rho = \frac{\Delta\phi}{2\pi} = \frac{b\Delta\phi}{2\pi b} = \frac{g/a}{2\pi(b/a)} \tag{10.11}$$

As an example of the magnitude of the reduction, consider the gap ratio, $g/a = 0.5$, that was used in the numerical RCS simulations for Figs. 10.9 to 10.13. The thicker loop ($\Omega = 8$) has a size ratio, $b/a = \exp(8/2)/(2\pi) = 8.7$. The gap reduction, ρ, in that case is 1% of the circumference. Loop antennas in the RF region will use rolled, trimmer or other type capacitor rather than a gap for tuning. However, gaps in optical rings can get much wider. The gaps in Fig. 10.17 are only 6 nm wide, but occupy a good percentage of the ring circumference, so it is important to take into account the effect of the reduction.

10.5 Practical Gaps and the Best Model

The problem of matching gap widths with capacitor values can be solved by comparing the zero-order resonances created by the gap in numerical simulations with the resonances calculated using capacitor values in the analytical model. Table 10.1 shows gap ratios used in the simulations and their corresponding resonances (as k_{Br} values). Next to it are the capacitor values that generate a match with the analytical model (as values of $l_{\epsilon q}$. These matches are shown for 10 and 300 μm.

They suggest two important points:

- The gap does not have to be too big before these resonances hit the upper limit near the anti-resonance at $k_b = .47$ in the case of 300 μm and $k_b = .43$ in the case of 10 μm. These upper limits were pointed out in the earlier figures.

- In order to find a resonance below $k_b = .30$, the gap must be made very, very small. A gap ratio of 0.2 implies a gap width of $0.2a$, where a is the radius of the wire.

Table 10.1: Zero-order resonances given by various gap widths in two sizes of nano-rings. Corresponding capacitor values, $l_{\epsilon q}$, taken from Fig. 10.16 are compared with the two models in Eqns. 10.8 and 10.9.

$\Omega = 10$

	300 μm		10 μm		All λ		
g/a	k_{br}	$l_{\epsilon q}$	k_{br}	$l_{\epsilon q}$	$l_{\epsilon,fp}$	$l_{\epsilon,frng}$	$l_{\epsilon,surf}$
0.2	0.36	1.00	0.33	1.11	0.67	0.94	1.98
0.5	0.40	0.54	0.37	0.56	0.27	0.55	1.44
1.0	0.43	0.23	0.39	0.34	0.13	0.44	1.21
1.5	0.44	0.07	0.40	0.24	0.09	0.42	1.12

$\Omega = 8$

	300 μm		10 μm		All λ		
g/a	k_{br}	$l_{\epsilon q}$	k_{br}	$l_{\epsilon q}$	$l_{\epsilon,fp}$	$l_{\epsilon,frng}$	$l_{\epsilon,surf}$
0.2	0.33	1.50	0.30	2.00	1.80	2.55	4.92
0.5	0.40	0.35	0.37	0.53	0.72	1.50	3.46
1.0	0.43	0.06	0.39	0.24	0.36	1.20	2.83
1.5	0.44	0.00	0.42	0.00	0.24	1.14	2.58

Fig. 10.18 shows what $\Omega = 8$ and 10 gaps look like. A comparison with Fig. 10.17 should make it clear that practically fabricated gaps in rings will generally place the resonance very near the upper limit. Tuning a ring by changing the gap may seem intuitively possible, but Table 10.1 suggests that it is not likely to be possible in actual

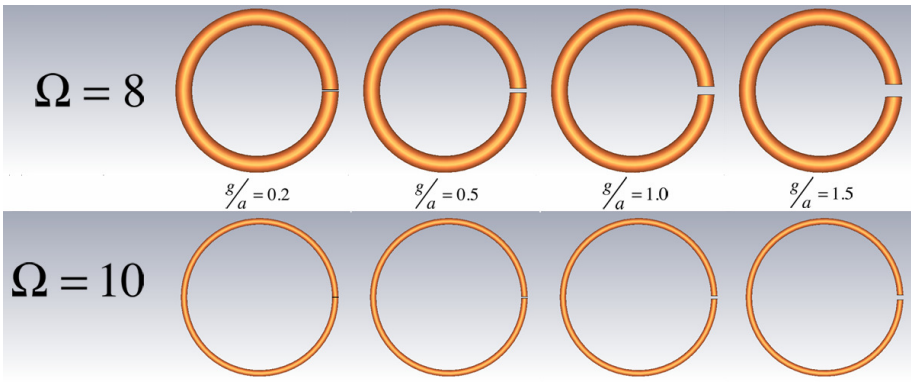

Figure 10.18: Gaps of various widths in $\Omega = 8$ and 10 sized rings.

practice. Therefore, worrying about fabricating a gap size to obtain a particular zero-order resonance for a given loop in the IR and OR is not likely a worthwhile design approach, given the limits of fabrication with methods in use today.

For example, an $\Omega = 8$ gold ring of circumference 10 μm has a radius of $b = 1.6\mu$m and a wire radius of $a = 1.6/8.7 = 183$ nm. A gap ratio of 0.2 means that the gap width itself is $0.2 \times 183 = 36.5$ nm. Given the 6 nm gaps now being fabricated, this is evidently a practical gap, and one might be able to tune the ring around the actual resonance at $10/0.33 = 30.3\mu$m (where $k_{br} = 0.33$ taken from the table).

On the other hand, suppose one wants a ring to resonate in the IR, say about 2.0 μm. The circumference of the ring needs to be $2.0 \times 0.33 = 0.66\mu$m. The radius is 105 nm with wire radius, $a = 12$ nm. The gap width is 2.4 nm for a gap ratio of 0.2 and 18 nm for a gap ratio of 1.5. While the 18 nm gap may be practical, resonance saturation has set in by 2 μm and tuning is not really possible because of the flattening of the saturation curve in that region. One can see the flattening in the $\Omega = 8$ red curve of Fig. 9.8.

Table 10.1 also shows that none of the gap models proposed in the literature includes effects due to wavelength scaling, and second, that the capacitive values they produce do not correlate well with gap values from the numerical simulations and analytical model using Section 10.3.4, though the fringe model does pretty well with the smallest gaps.

10.6 Comparison with the Literature

In Section 6.5 a review of the paper Zhan and Chui [2014] showed a resonance in the sub-wavelength region at $kb = .47$. This is an $\Omega = 12.88$ loop; no diameter or gap width is given. The presence of the resonance and its position agrees with the results of this chapter. Thin loops of this size have their anti-resonance at $k_b = 0.47$ and a reasonable gap, as has been shown, will push the resonance toward that upper limit. Hence, in analysing such a resonance, there is possibility of confusion as to the source of the resonance. It is due to the gap resonating with the mode 0 inductance

of the loop; it is not due to the anti-resonance.

10.7 Conclusion

The addition of a single capacitive impedance in the periphery of a loop, whether at low or high frequency, generates a unexpectedly high-Q resonance in the sub-wavelength region. The Qs are remarkably high, in the several thousands, and there is a peak in the Q curve around $k_b = 0.35$. The resonance itself is expected because the closed loop acts inductive in this region. Indeed the inductance of the loop in this region is dominated by the mode 0 inductance of the loop and it is this inductance, together with the capacitance of the closed loop and the additional capacitance that creates the resonance; hence the name for these resonances: "zero-order resonances".

Rolled or trimmer capacitors can be used to effect the resonance and tuning at low frequency (RF and MW); but gaps need to be used for higher frequencies (THz and IR). Matching the resonances given by numerical simulation with calculations of resonances using the analytical model leads to a correspondence between gap width in a high frequency ring and a capacitive value. Up to about 10μm for $\Omega = 10$ loops and 6μm for $\Omega = 8$ rings, varying gap width may allow for tuning, but for shorter wavelengths, gap tuning is probably ineffectual given current fabrication methods.

Chapter 11

Design Examples and Problems

11.1 Introduction

This chapter presents some general considerations when designing loops and rings for particular regions of the spectrum. One of the very useful results of this thesis is a body of MATLAB code that can provide much information about a loop without the long wait time of a numerical simulation tool like MWS. The code is described in Appendix B. Understanding the principle issues with regard to loops and rings, which are delineated in the Conclusions will also provide the basis for quick "back of the envelope" calculations that will suggest whether a particular size loop or ring will give the desired characteristics.

11.2 General Design Considerations

When designing loop antennas at low frequency for the RF and MW regions, or rings at short wavelengths for the THZ, IR and OR, the following approach makes the best use of the results of this thesis:

- Determine first the design frequency and rough bandwidth of operation. These will determine whether losses will play a significant role in the behaviour of the loop.
- Then if the region of interest is the RF or MW, use the general results of Chapter 8; if THZ, IR or OR, use the results of Chapter 9.
- If a very narrow bandwidth is required, consider using a capacitor (if low frequency) or a gap (if short wavelength) in the periphery of the loop, perhaps near the source. The advantage is an extremely high Q factor; Qs on the order of several thousand are possible. Large loop antennas at low frequency will also be tuneable using the capacitor. Tuning won't be possible in the IR or OR, but may work in the THZ region.
- The actual size of the loop is determined by the design wavelength, λ_d. The first resonance in a closed loop will occur near that frequency, and the circumference of the loop will be about $2\pi b = \lambda_d$. However, the very high Q, zero-order

resonances using capacitors are readily attainable for perfectly conducting metals and can vary between $0.2 < k_b < 0.47$. If the loop meets those specs, then design the loop for the highest Q resonance, at about 0.35. This means that the size of the loop will be $2\pi b = 0.35\lambda_d$, considerably shorter in circumference than the wavelength.

- If the design wavelength is in the THZ or IR down to about 4 μm, use the smallest gap possible in the periphery. Expect the resonance to be near $\lambda_d/.4$, unless λ_d is in the saturation region (<10-30 μm), then remember resonance saturation.
- If the design wavelength is in the OR, there is unfortunately no noble metal that will allow a closed ring resonance below about 3 or 4 μm, due to resonance saturation. Use of multiple gaps may be a help, but this work was not studied in the thesis and remains as future work.

11.3 Estimate the Q of a Closed Loop Antenna for the 20-meter Amateur Band.

The answer to this is found in the material of Section 5.3 and Chapter 8.

- The 20 meter band is low frequency, so the material may be considered perfectly conducting.
- All PEC loops have their resonances at the same place in k_b space.
- The best resonance to use is the fundamental mode resonance, which, according to Table 8.1, occurs at $k_b = 1.069$. That same table gives the Q of the loop as 5.8.

Double checking using values from the table: the Q is

$$Q_m = \frac{\sqrt{L_m/C_M}}{R_M} = b_x \frac{\sqrt{l_{\mu m}/l_{\epsilon m}}}{R_m} = 377\left(\frac{2.06/0.425}{143.3}\right) = \boxed{5.8} \tag{11.1}$$

11.4 Design a Loop Antenna with a Single Capacitor for the 2-meter Amateur Band.

The answer to this is in Section 5.3 and Chapters 8 and 10.

- The two-meter band occupies the frequencies 144 MHz to 148 MHz (λ = 2.03 to 2.08 m) in Australia.
- The single capacitor will cause a zero-order resonance. Fig. 10.5 shows the resonances for an $\Omega = 10$, gold loop, but we want to use perfectly conducting material and perhaps make the loop thinner. We could run the MATLAB code for $\Omega = 12$, PEC. Instead, let's estimate using data in this thesis. The 10 loop

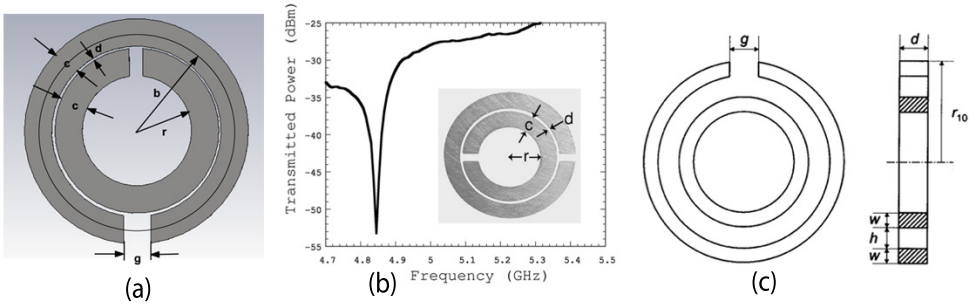

Figure 11.1: Three rings reviewed in Chapter 6. (a) The Pendry ring: c=1.0 mm; d=0.1 mm; r=2.0 mm; width = 1.0 mm. (b) The Smith Ring: $c = 0.8$ mm; $d = 0.2$ mm; $r = 1.5$ mm. (c) The Shamonin Ring: $r_{10} = 9$ mm; $w = 0.5$ mm; $h = 1.0$ mm; $d = 2.5$ mm.

is not much different from a 12, and this is low frequency, so gold operating at 300 μm is almost perfectly conducting. The figure says that the highest Q occurs at $k_b = .35$.

- Designing for a resonance in the mid-band at 2.06 m, the circumference should therefore be: 2.06 × 0.35 = 0.72 m.

- The best capacitor value from the figure is $l_{\epsilon q} = 1.0$, which means that a capacitor is needed with the value

$$C_q = \epsilon_0 b l_{\epsilon q} = 8.85 \times 10^{-}12 \times \frac{0.72}{2\pi} \times 1.0 = 1pf \tag{11.2}$$

- Setting the circumference to 0.72m, the ends of the bands are at $k_b = 0.346$ and 0.355, which means that the capacitor of 1.0 will keep a high Q throughout the band.

- Much more useful is a capacitor that varies over a range, allowing a tuning of the loop over the 2 meter band. An appropriately sized capacitor might be a trimmer capacitor of appropriate voltage rating, which doesn't vary much from 1 pf, perhaps something like .8 to 1.2 pf.

11.5 Approximate the Resonances of the Pendry, Smith and Shamonin Split Ring-Resonators, Reviewed in Chapter 6.

The rings are shown in Fig. 11.1.

It is sufficient to convert to the standard variables used in the thesis and calculate the resonance of the outer ring. The radius of the outside ring in the Pendry configuration is $b = r + d + 1.5c = 3.6$ mm.

- The design wavelength, therefore, is $\lambda_d = 2\pi b = 22.62$ mm. This corresponds to $\boxed{13.26GHz}$. This is very close to the 13.47 GHz reported by the group for their resonance.

- One will remember that theirs was a 3 dimensional structure, where the capacitance they calculated was between the rings, not from the gap. The capacitance of the gap therefore is not needed, which means that the ring is being used at its fundamental resonance, and not at its zero-order resonance.

The ring given in Smith et al. [2000] has a radius $b = r + d + 1.5c = 2.9$ mm or circumference $2\pi b = 18.22$ mm. This corresponds to 16.46 GHz.

- They give a resonance at 4.845 GHz, which would mean a $k_b = 4.85/16.46 = 0.3$. This would correspond to a gap ratio about 0.2, much too small for the gap shown. The model of Chapter 10 applies to round wires rather than these flat disks, but these results do suggest that the ring is sub-wavelength and has found a zero-order resonance.

The Shamonin outer ring has a radius $b = r_{10} - 0.5w = 8.75$ mm. Therefore, $2\pi b = 55$ mm, or 5.45 GHz. In this case, the authors calculated the capacitance of the gap and reported a calculated resonance as 2.72 GHz. This means that they are using the zero-order resonance, where 0.45 is the upper limit of the zero-order resonances.

- The wire is rectangular with square area $dw = 2.5(.5) = 1.25$ (mm)^2. The equivalent round wire radius is $a = \sqrt{1.25/\pi} = .40$ mm. Hence $g/a = 1/0.40 = 2.5$, a good sized gap, leading the resonance to appear at the upper limit, $k_b = 0.45$.

- The resonance will be $5.45 \times 0.45 = \boxed{2.45GHz}$. This is a bit shy of their reported 2.72 but closer than in the Smith case, possibly because the Shamonin ring is so thin and less "disky".

11.6 Design a High Q, Single Gap, Copper Ring for 300 GHz.

The high Q will come from the zero-order resonance, which we want to be 300 GHz. Perhaps an $\Omega = 10$ ring will do with a lumped capacitor of about $l_{eq} = 1.5$.

- The desired resonance, 300 GHz, corresponds to 1 mm wavelength.

- Since 1 mm is > 300 μm, we can use the resonances in Fig. 10.5, neglecting the fact that it is for gold not copper, and find that k_{br} for $l_{eq} = 1.5$ is ≈ 0.32.

- The circumference of the loop should be $1 \times 0.32 = 0.32$ mm, or radius $b = 0.32/2\pi = 51\mu$m.

- The capacitor value to use is $C = \epsilon_0 \times 51\mu m \times 1.5 = 0.68 \times 10^{-15}$ F. This is much too small for a physical capacitor, so we should provide it with a gap.

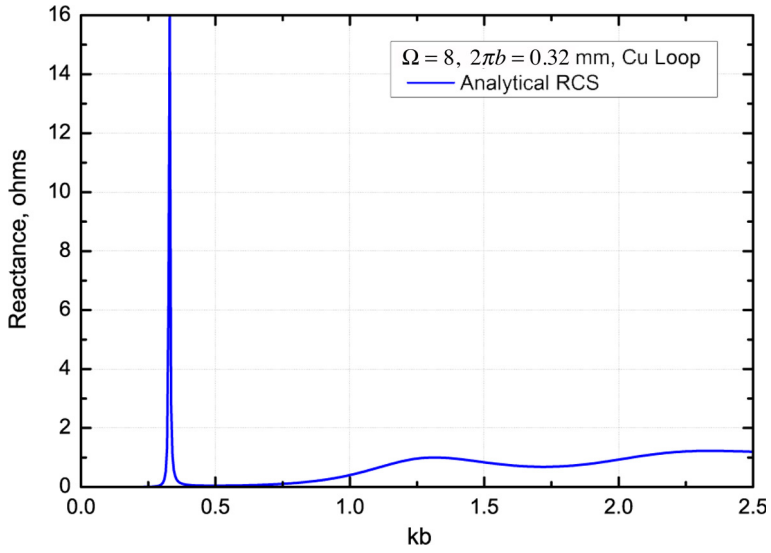

Figure 11.2: Prob #5: An $\Omega = 8$ copper ring for 300 GHZ (1 mm). The zero-order resonance is exceptionally high with Q = 1456.

- To do so, we should probably use an $\Omega = 8$ wire or thicker. Table 10.1 suggests that an $l_{eq} = 1.5$ corresponds to a gap size of $g/a = 0.2$. Can we make this?
- For an $\Omega = 8$ ring with $b = 51\mu$m, the wire size is $a = 51/8.7 = 5.9\mu$m. Therefore the gap width should be $g = 5.9 \times 0.2 = 1.18\mu$m. That may be doable.

To check on these results, we run the MATLAB code, using:

```
[kbList, RCS, ACS] = CalculateRCS('z', [0;0;1.5], [1], 'omega', 8, 'circum',
.32, 'units', 'mm', 'material', 'Cu' )
```

Fig. 11.2 shows the resulting Radar Cross-section. The zero-order resonance is at $k_b = 0.33$, which is equivalent to a wavelength of $\lambda_d = .32/.33 = .970$ mm. This is 309 GHz, as needed.

The quality factor, Q, can be calculated using the following MATLAB code:

```
[Q, Qcl, R, lu, le] = CalculateZOQ( [.33], [0;0;1.5], 'omega', 8, 'circum',
.32, 'units', 'mm', 'material', 'Cu' )
```

The result is Q = 1456, quite a high Q.

11.7 Estimate the Q of a Square, Silver Ring for Use at 1 THz, a zero-order resonance.

Squares are not much different than circular rings and in Fig. 9.9 it was shown that wavelength scaling and resonant saturation applies to them in about the same way that it does to a circular loop. We assume a round wire formed in the shape of a square and regard it as equivalent to the circle passing through the corners. Gaps at

1 THz will all be so large that they force the resonance to the upper limit, around $k_{br} = 0.4$.

- The corresponding wavelength for 1 THz is 300 μm.
- The design wavelength is therefore $\lambda_d = 300 \times 0.4 = 120\mu$m.
- The radius therefore is $b = 120/2\pi = 19.1\mu$m.
- And the gap ratio will be on the large side, say , 1.5 or more.

To check this we, run MATLAB code:

```
[kbList, RCSProb6, ACSProb6] = CalculateRCS('z', [0;0;1.5], [1], 'omega',
8, 'circum', 120, 'units', 'um', 'material', 'Ag' )
```

The resulting resonance is at $k_{br} = 0.395$, which is very close to 0.40, as predicted.

11.8 What is the shortest resonant wavelength that can be expected from a gold ring?

The answer to that for the closed loop is given in Fig. 9.8. It is about 1 μm for an $\Omega = 8$ ring. Adding multiple capacitors doesn't help bring a good resonance beyond $k_b = 1.0$, so some other way of reaching the optical region is necessary.

Chapter 12

Conclusions

12.1 Introduction

The general realisation on which this thesis is based, is that no general analytical study of loop antennas and rings, developed from standard antenna theory, exists that is at once applicable to the Radio Frequency (RF), Micro-wave (MW), TeraHertz (THz), Infra-red (IR), and Optical (OR) regions. Nor is there any *RLC* circuit theory model, rigorously developed from the results of that study. This thesis was intended to fill that gap.

This goal has been achieved.

I will outline the results of the study, draw some general conclusions and then suggest future work that would be based on the material of this thesis.

12.2 Principal Technical Results

The following are the most important technical results of this study:

- An analytical set of mathematical functions has been derived from Maxwell's equations that give the current distribution on closed and single gapped loops at all frequency regimes from the RF through OR, constructed of any metal for which the index of refraction is known.
- The analytical functions indicate that loops will resonate at many modes, determined in the main by their circumference and whether they have an impedance or gap in the periphery. Generally, the strength of the modes die out as the modal number increases, but not rapidly, so that some rings have good Q factor at many harmonic frequency bands. This also means that such a loop will radiate at these harmonics, if the source is noisy enough to contain frequencies within those bands.
- A detailed *RLC* circuit model has been derived from these functions, accurate at all frequency bands, from which the total R, L and C of the loop at any frequency or wavelength, and the R, L and C of any modal resonance, can be calculated. The circuit elements are functions of frequency; that is, $R = R(\omega)$, $L = L(\omega)$, and $C = C(\omega)$.

- The circuit model suggests that the loop is properly represented by an infinite set of series resonant circuits all in parallel with each other. Each series resonant circuit represents one harmonic mode. A mode 0 circuit exists consisting of a series resistor and inductor.

- The input impedance of the circuit model can be calculated as a function of wavelength for closed loops and single gap loops.

- From the circuit model, the radiation resistance, resistive loss, radiation efficiency, radar cross-section, and quality factor (Q) can be calculated.

- The analytical functions predict wavelength scaling and resonance saturation accurately. For example, they predict accurately the resonances of a lossy metallic ring at all wavelengths into the OR.

- While loops designed for the RF and MW region act nearly like perfect conductors, no matter what metal they are made from, they begin to lose this characteristic as their design frequency increases into the THZ region. By the time the IR has been reached, the rings have acquired so much resistive and reactive loss that they have very weak currents, so that even though their Q factors may be reasonable (3 to 8), they are not effective radiators or receivers. The intra and inter-band transitions may add electrons to increase the conductivity, yet the electrons can not respond rapidly at these high frequencies to the incident wave, and hence do not improve ring response.

- A single impedance in an RF or MW loop, or a gap in a THZ or OR ring, will introduce a zero-order resonance in the sub-wavelength region with an extremely high Q factor on the order of several thousand. The resonance is tuneable in a thin, large loop at the RF, MW, THZ or far IR, but given today's fabrication methods, is not likely to be tuneable in a nano-scale loop in the near IR or OR.

- Gap width and capacitance value of the gap are closely related. However, none of the simple models suggested in the literature, such as the flat-plate capacitance model, generates the correct relationship, at least for gaps in rings.

12.3 General Conclusions

Until the end of the 20th century, loops were thought as magnetic dipoles, useful perhaps as magnetic sensors, but for not much more. They were certainly not considered useful in RF communications. There were several good reasons for this:

(1) A loop that was large enough to radiate well had to be on the order of a wavelength. In the RF region this is several meters in circumference, well too large to be comfortably portable, a bit unsightly as a TV or radio antenna on a house.

(2) It was difficult to get a very high Q with a loop, so the modal resonances were broad. Noisy sources also tended to transmit on the harmonics, as much as on the fundamental.

(3) Radiation efficiency was poor compared to the dipole and to many other antenna configurations.

In general all of these points were verified by this study. Closed loops do not have particularly useful characteristics for communications. What they do have, however, is the basis for a surprising effect when a capacitor is placed in the periphery. That capacitor interacts with the mode 0 inductance of the closed loop, and combines with the capacitance of the closed loop to generate a very high Q resonance. Moreover, the use of the capacitor reduces the size of the required loop by half.

The gap also opens up interesting phenomena at frequencies higher than the RF. The smaller gap make communication loops easier to build in the MW and THz regions and drives a high-Q resonance around which design can proceed. Since the loops are small, arrays are easier to build, which may lead to high-gain directional arrays and capacitive tuning of the resonance.

Gapped loops may also be useable in the far IR, since fabrication methods have reached a point that nano-scaled rings with nano-scaled gaps can be made to order. The effects are less pronounced as the IR is approached, due to material losses. It may be, though, that a material will be found that provides good conductivity in this region, and loops here could be used for communications or to enhance as yet unknown optical effects.

12.4 Future Work

Other avenues of research are opening for rings.

- One of the key areas is the use of band-gap materials (Schuller et al. [2007]; West et al. [2010]; Filonov et al. [2012]; Liu et al. [2013]), such as dielectrics, semiconductors and semiconductor alloys take the place of the noble metals. These include, among many others, silicon, germanium, tellurium, silicon-carbide, titanium-dioxide, graphene and perovskite. The goal here is to find useable resonances in the optical region. In fact, both metals and semi-conductors are so lossy that both would be useless in the optical region, except that electrons in the outer bands of these semi-conductors are suddenly released to the conduction band when incident energy reaches their band gaps (see the discussion on the interband transitions in Section 9.2.2). These band transitions produce available electrons in semi-conductors on the order of 10 times those in metals. But the effects still cannot overcome the high absorption characteristics. Electrons in the conduction bands simply can not follow the rapidly changing $\vec{E}$ field of an incident optical wave. Simply increasing the number of electrons available may not be enough to counter these absorption problems.

- Another area of further research focuses on toroidal currents in rings. These are the currents that are set to zero during the initial derivation of the differential equations describing currents in the ring. It is an approximation called the "thin-loop" approximation. But these currents, if controlled, could produce a constrained magnetic flux within the closed ring; they may be associated with modes that can not be excited externally, sometimes called "dark" modes. Such toroidal currents are the objects of some interest in the optical region, since they could provide a way of storing energy at these very high frequencies. Dielectric materials would be used to support such currents using the inter-band transitions. Unfortunately, it is likely that absorption characteristics will rapidly dampen these currents.

- One promising area for research are gapped rings that focus on that zero-order resonance. Unfortunately, the ring must be very small in diameter if the zero-mode resonance is to appear in the optical region. To gain the optical frequencies, multiply gapped rings may be the answer, in which each segment of the ring acts like an inductor, and together with one of the gaps creates its own little LC circuit. The circumference will not then produce as strong a limit to the resonances, with the result that the loop may actually have resonances that show in the optical region.

- Multiple impedances, particularly multiple capacitances or gaps, around the loop would change the current phasing as well as the position and Q of the resonances. Manipulation of the capacitance could allow a certain degree of beam control. Marrying this with very high Q resonances would be an interesting project.

- It would very interesting to fabricate 3D structures of loops at MW or THZ region for the purposes of beam control, as is suggested by Ahmadi and Mosallaei [2010]. My father also had visions of such a thing when he drew Fig. 12.1 in 1968.

- Nested loops and rings might be beneficial for nano-scaled rings, as suggested by Memarzadeh and Mosallaei [2011]. Fig. 12.2 shows a conception of nested loops in my father's personal papers as well.

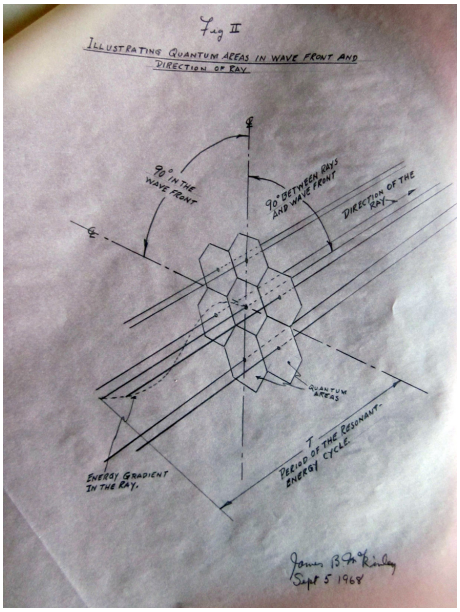

Figure 12.1: A vision of phased rays in 3D. Found in personal papers, McKinley II [1968b]

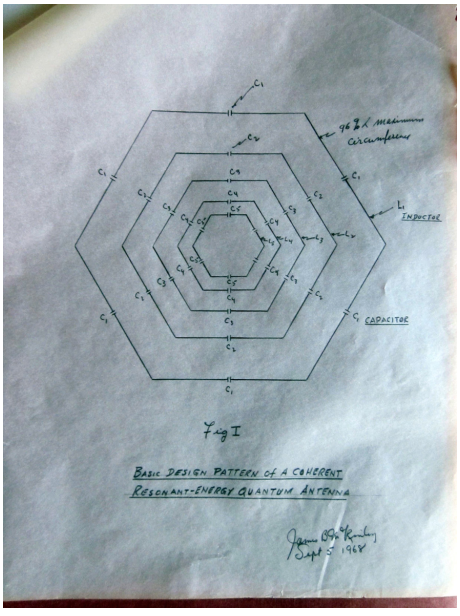

Figure 12.2: A vision of nested loops in 3D. Found in personal papers, McKinley II [1968a]

Part IV

Appendices

Appendix A

Simulating the Physics of 3D Ring Structures

A.1 Introduction

Three tools were used principally in simulating loops and rings.

(1) An industry standard numerical simulation tool, *Microwave Studio* (MWS), developed by the German company, CST[1]. It is used widely around the world to examine the effects of electromagnetic fields on structures.

(2) The Graphing Calculator by PacificTech[2] is a fast responding, rapid prototyping tool yielding plots of mathematical formula and functions.

(3) MATLAB, by Mathworks[3] is a fully develop programming environment for mathematical needs. Appendix B is devoted to the code built for the thesis.

A.2 Microwave Studio (MWS)

A.2.1 Capabilities

MWS has been used for many years in the RF and MW regions, and has recently moved into the THZ and optical regions. It has become a general purpose electromagnetic simulator, using classical principles, based on a Finite Integration Technique, furnishing results either in time domain or frequency domain.

The FIT method splits the domain of calculation into many small elemental grid cells, called the "mesh"; it discretises Maxwell's equation along the boundary of those cells and over the area enclosed by those boundaries. FIT can be applied to hexagonal grids and tetrahedral grids. On Cartesian (flat) grids, the FIT formulation can be written in Time Domain to reproduce standard Finite Difference Time Domain (FDTD) methods, but the latter are limited to staircase approximations of boundaries,

[1]Computer Simulation Technology AG, Microwave Studio. 2012. Darmstadt, Germany. www.cst.com

[2]Pacific Tech. Berkeley, CA. 2012. www.pacifict.com

[3]Natick, MA, USA; www.Mathworks.com

whereas MWS applies what is called the *Perfect Boundary Approximation* (PBA) that maintains all the advantages of Cartesian grids, but allows accurate modelling of curved structures.

Two solvers are used to generate the results of the thesis: the Transient (or Time Domain Solver) and the Frequency Domain Solver. Both yield the same results, given the same 3 dimensional structure; however, the meshing is critical in both cases, and results will not be similar unless the mesh is fine enough in both cases to accurately capture field behaviour in the same way. A period of trial and error on new models is required to be sure that both are yielding the same results.

The Time Domain solver simulates a structure's behaviour over a wide frequency range in a single computational run, and it therefore produces results more quickly, however, experience seems to indicate that it requires a much large number of mesh cells to produce accurate results.

The Frequency Domain solver requires considerably more time for a run than does the time domain solver. Technical support at CST suggests that one run a structure quickly in the Time Domain, playing with the meshing until satisfied, then run in Frequency Domain to be sure that the results are similar. They claim the FD solver is more accurate and can be trusted. All results for Closed Loops in the thesis were run with the FD solver. The TD Solver was used for loops with gaps once the meshing was tested against the FD solver results.

MWS handles material characteristics in several ways. In the simplest case the permittivity and permeability of a material can be specified using scalars, or alternatively, by specifying the material's electric and magnetic conductivity. Loss is specified by giving the material's "tangent delta". For materials with more complex response, one of 11 different dielectric and magnetic dispersion functions can be assigned to the material with coefficients set by the user. Alternatively, a list of measured dispersion data over frequency can be assigned to the material. This last method is used in the thesis for the noble metals. gold, silver and copper with data taken from Johnson and Christy [1972].

A.2.2 Port Sources

Rings in the analytical model are energised using a delta-function voltage source across and infinitesimal gap. There is no such voltage source in MWS, but it can be approximated by using a "discrete power port" across a finite gap. Figure A.1 shows the port across the gap and its equivalent electrical circuit. The port has two pins which are connected to either side of the gap and the overall length must be much shorter than the wavelength of interest. The connecting wires are perfectly conducting, and in the first version of CST used, must be tied to perfectly conducting metal. The requirement was relaxed in the current version being used. It was not a problem for the loop antennas run in Chapter 8, which focused on perfectly conducting loops, but became an issue for the next Chapter 9, when the loops were made of real metals. The problem was solved by embedding little PEC balls within the metal of the loop and connecting the port to exposed portions of the ball (see Fig. **??**).

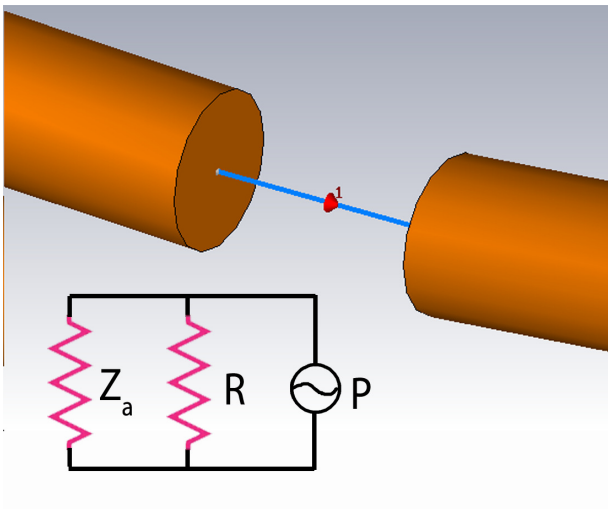

Figure A.1: MWS representation of (a) the discrete power port for the driven ring, and of (b) the equivalent circuit representation of the port, as given in MWS documentation.

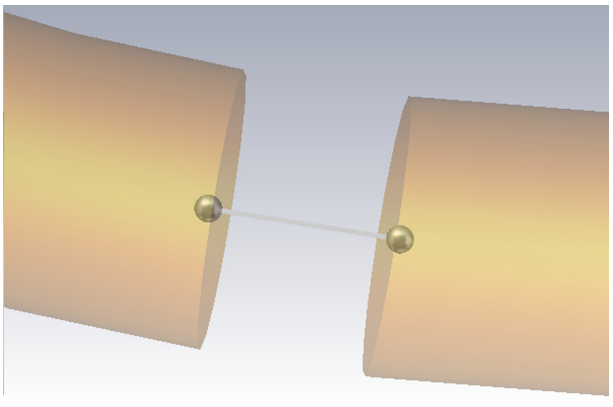

Figure A.2: PEC balls were used in the beginning of the study to overcome a problem with the port simulation.

The size of the gap now introduces some capacitance, which was found in Chapter 10 to produce an additional resonance. At the time of the earlier studies on closed loops and rings the gap width was handled by trial and error, looking for changes in the impedance resonances. Gaps widths used were $g = .03b$ initially and $.05b$ finally. These map into $g/a = 1.9$ and 3 respectively for $\Omega = 10$ rings and $g/a = .7$ and 1.2 respectively for $\Omega = 8$ rings. Comparing with Table. 10.1, the 1.9 and 3 gaps were too wide to cause problems with the $\Omega = 10$ loops, but this is not true for the .7 and 1.2 gaps. Fortunately, some post-processing was added to remove the effect of the gap assuming that they acted as flat-plate capacitors, following the literature (see Section 10.4.1). Interestingly, the zero-order resonances were never seen, suggesting that the gap capacitances really did not have much affect at all on the simulation results, no matter what their size. This would be because the gap is not in series with the source, but in parallel. Subtracting out the effect of a small parallel capacitor was helpful, but may not have been necessary.

Port power is kept at magnitude 1 watt by the simulator; the port resistor can be set by the user. Standard power matching theory says that the greatest power will be transferred when the port impedance matches the antenna impedance. Consequently, the best choice for the port resistance is the real part of the antenna impedance at resonance where the imaginary part of the load goes to 0. The process, then, is to run the simulation with an arbitrary port resistance, find the first resonance and see if the real part of Z_a has the same value. If not, adjust the port-resistance and run again, repeating until they are the same. This gives maximum power flow to the ring and a common basis for comparing the current and Q of different sized rings.

MWS calculates the S-matrix (scattered power). Squaring the S_{11} element of the matrix gives the reflection coefficient, and resonance occurs when this term goes to 0. It is a way of finding all of the principle resonances that is a bit different from finding the imaginary zero-crossings of the impedance. Figure A.3 compares $|S_{11}|^2$ with the imaginary part of the ring input impedance for an $\Omega = 12, 2$ μm loop. This is a particularly illuminating way of telling the differences between the resonances and the anti-resonances.

A.2.3 Boundary Conditions

One way to substantially speed up simulation time is to set boundary conditions that account for symmetries. This was done for all of the closed loop simulations, but not for the simulations which included gaps. In the former, the loop or ring sits in free space in the XY plane with the port gap at $(0, -b, 0)$. Two symmetry planes are set: the YZ plane has the tangential component of $\vec{E} = 0$ (i.e., $\vec{E}_t = 0$) and the XY plane $\vec{H}_t = 0$. The design frequency is defined: $f_d = c/(2\pi b)$, where c is the speed of light. The frequency range is set: $< .1f_d$ to $2.5f_d$. The horizontal axis measure, k_b, is calculated in post-processing by dividing this range by f_d. Post-processing calculates the real and imaginary parts of the impedance, Z, and the reflected power, S_{11}^2. R_p is at first arbitrary, but is iteratively replaced until S_{11}^2 reaches minimum. At this value, R_p equals $Re(Z)$ and maximum power flows from the port into the antenna. If the

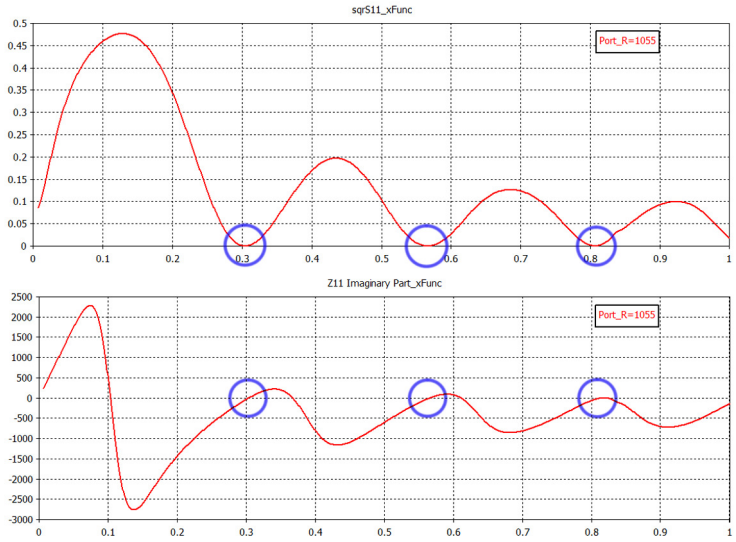

Figure A.3: MWS calculations for an $\Omega = 12$, 2 μm ring. (a) The reflection coefficient, which when it goes to 0, indicates maximum power transferred to the ring and radiated. That occurs at a resonance. The peaks correspond to the anti-resonances and indicate that the loop is reflecting power maximally. (b) The imaginary part of the impedance, which indicates resonances when the imaginary part crosses 0. True resonances occur when the reflected power and the zero-crossings coincide, as shown.

antenna resonates, the minimum occurs very close to $Im(Z) = 0$.

A.2.4 Illuminating sources

Illumination by plane wave is the alternative method for energising the ring when it contains a gap, since a gap cannot be placed in series with a discrete port. The illuminating Electric field magnitude can be set, always to 1 for normalisation purposes for this thesis. Figure A.4 shows an $\Omega = 10$ ring illuminated by a polarised plane wave and the domain of calculation. Boundaries are opened, so that they do not reflect, in such a way the total $\vec{E}$ can be collected at every far-field point. Subtracting the incident known $\vec{E}$ gives the scattered field and hence the scattered power. The absorption cross-section is the difference between the incident and scattered cross-section.

MWS provides a far-field monitor to collect scattered power at some given wavelength. Adding many such monitors yields a full spectrum collection of power and hence the radar cross-section (RCS), used in Chaptercha:Gaps. Surface current monitors are also available at user selected frequencies, allowing a comparison of the current distribution on the simulated ring with the theoretically calculated current distribution.

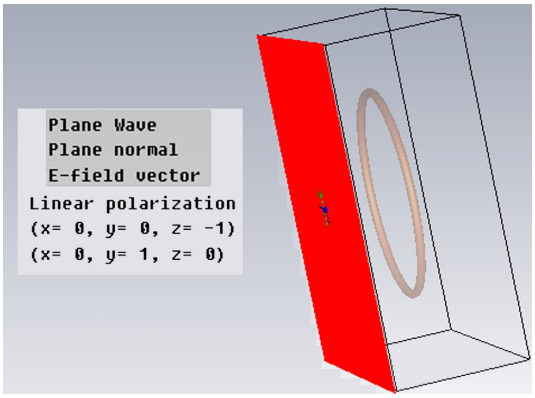

Figure A.4: A sample of an illuminated ring. This one is for an $\Omega = 10$ loop.

A.3 PacificTech's Graphing Calculator

Most of the calculations that were finally done in MATLAB were accomplished first on a tool developed by the company PacificTech, called "The Graphing Calculator". I consider it a rapid prototyping engine that provides very rapid turn-around for plotting functions and data. Some of its benefits:

- Functions written in mathematical format in the programming region of the tool are immediately displayed in the plotting region in 2D, 3D or 4D, whichever is appropriate.
- Writing a number of functions superimposes them in the plotting region; function display can be turned on and off discriminately by function.
- Substituting functions as variables in functions is allowed as long as the outcome is not circular.
- A coefficient can be attached to slider, so that its effect on the shape of the graph can be quickly determined. This feature is particularly useful if one needs to fit data to a function, as was done in Section 9.2.2.
- The tool handles scalars, vectors, and matrices, and draws them as needed in 3D or 4D space.
- Variables can be any length and contain most alphanumeric symbols.
- Animation of a parameter is available and a movie can be extracted from the results.
- It will solve algebraic equations when the user moves the variables within the equation.
- It will take the full or partial derivative of a function and evaluate simple integrals

- It handles summations to any limit, positive and negative.
- It handles data tables. In fact, data copied in Excel is readily pasted into the tables.
- A column in tables can be specified as a forum columns so that its members are the results of calculations on other columns in the same table.
- Copied graphs are transparent, so they can be copied back into the tool for comparison with another graph later on. This is particularly useful if one wants to see minor differences between to plots taken some time apart.

Appendix B

Computation Code in MATLAB format.

B.1 Introduction

MATLAB is a general purpose, numerical calculating tool that uses the matrix as its basic form of numerical variable. This allows for two types of processing: normal matrix methods and element by element computations. This capability allows Matlab to handle very large data sets in numerical computations very easily. The resolution of dependent and independent variables used by a function is clearly exposed within the matrix representing these variables.

This appendix explains the code used to generate the results of the thesis, enough that a user should be able to generate the same results without very much effort. The code itself is available on the attached CD.

B.2 Organization of the Program

The main code is divided into two directories. "Primary Control Code" provides the top level files needed to perform most tasks.

B.2.1 Directory "Primary Control Code"

In general, LoopDescriptor.m holds the default descriptive information about the loop being worked on. The parameter 'varargin', which appears as one input parameter in all of the primary functions overrides these defaults. It works the same for every function in which it appears. Any of the files will explain how to form the parameter and what characteristics of the loop can be overridden. If you prefer not to override using 'varargin', you can simply change the defaults in LoopDescriptor.m. That is often the fastest and easiest way to do it, but you have to remember to check that the current values are the ones you want. For transparency and clarity, a list of current loop characteristics appears first thing whenever a function is invoked.

- *CalculateLoopImpedance.m*: This calculates the input impedance and admittance of the loop over a variable called 'kb', which equals the wavenumber of the

driving wavelength (namely 2 pi / wavelength) times the radius of the loop 'b'.

- *CalculateLoopCurrent.m*: This calculates the current at any place on the loop and will plot the current distribution against the angle 'phi' in two different ways: with 'phi' on the horizontal axis (using phiPlotType = 'XY'), or with 'phi' around a circular loop (using phiPlotType = 'rPhi'). The driven source is at phi = 0 on the right hand side, center, of the drawn loop.

- *CalculateRCS.m*: This calculates the function $|I(0)|^2 R_{rad}$ against 'kb'. $|I(0)|$ is the absolute value of the input current at 'kb'; 'R_{rad}' is the radiation resistance at 'kb'. For PEC materials the $real(Z)$ is the radiation resistance, since there is no loss in the material. $|I(0)|^2 * R_{rad}$ is a function that is proportional to the RCS; the magnitude is not the same as the actual RCS, but the resonances it produces are the same as the RCS resonances given by the illumination of an incident wave.

- *CalculateEVList.m*: This calculates a list of electron volt values corresponding to a given loop circumference and list of kb values. The circumference must be in meters; for example 300e-6 for 300 um. The kbs are calculated on the basis of that circumference as kb = 1.0.

- *CalculateRefractiveIndex.m*: This calculates a list of refractive indices given an eVList and a material.

- *CalculateZOQ.m*: This calculates the zero-order resonances for a given list of kb's. The kbr's refer to the zero-order resonances. Any other kb will give a meaningless Q. The calculation requires a list of Z3Loops. See the file description for what a z3Loop is.

- *PlotModalResonance.m*: This plots the modal resonance functions and shows the intersection line that defines the actual modal resonances of the given loop.

- *PlotZOResonances.m*: This function plots the zero order resonance for a single lumped capacitor in series with the voltage source at phi=0. It produces results just like those of the function PlotModalResonances.m but for one capacitor.

B.2.2 Directory "Ancillary code"

This directory contains functions that you may want to use; feel free to explore. The directory "Internal Private" contains classes and functions used internally and are not expected to be useful to anyone except those expanding the code.

Each of the other directories contains code to help the primary functions in the Primary Code Directory do their work. Hopefully, all of these files are self-explanatory.

B.2.3 Use

Put the top level directory into the MATLAB path. Open one of the main function files. Copy the call to the command line, add the appropriate parameters, and run. Have fun.

If you want to adjust the code, feel free. If you want to contact me about the code, feel free to do so at arni.mckinley@gmail.com

Appendix C

The Design of a 1968 Closed Circuit Resonant Loop (CCRL).

In the 1960's my father began designing loop antennas with one capacitor. A typical design appears in his personal papers. I recall that he went straight to the single capacitor rather than begin with the closed loop, prompted, I am sure by his interest in resonance and, what was to him the obvious choice of mating a capacitor to an inductive loop. Fig. C.1 shows one of his earliest design in 1964, which he tested using a light build across the small coil to discover the standing wave on the loop.

On the right hand side, one can see clearly that he found the best circumference near the half wavelength.

The resonant frequency and characteristic impedance of the matching tank circuit at the coupling end of Fig. C.1 is

$$f_o = \frac{1}{2\pi\sqrt{L'C}} = \frac{1}{2\pi\sqrt{.57\mu H \times 227pF}} = 14 \text{ MHz} \tag{C.1}$$
$$b_x = \sqrt{\frac{L'}{C}} = \sqrt{\frac{.57\mu H}{227pF}} = 50.1 \text{ ohms}$$

Evidently the design of the loop is for the 20 meter band (14 MHz) with a coupling to a 50 ohm coax cable.

On the loop side of the coupling is an inductor and two capacitors. He found that the capacitors added in value, which implies that they are in parallel, as they would be, roughly, in the sub-wavelength region. The resonance and characteristic impedance of this combination is

$$f_o = \frac{1}{2\pi\sqrt{LC}} = \frac{1}{2\pi\sqrt{1.29\mu H \times 100pF}} = 14 \text{ MHz} \tag{C.2}$$
$$b_x = \sqrt{\frac{L}{C}} = \sqrt{\frac{1.29\mu H}{100pF}} = 114 \text{ ohms}$$

The circumference of the loop including the 89 cm of the inductive/capacitive coupling section is 689 cm. This corresponds to 43.5 MHz. This would be what I

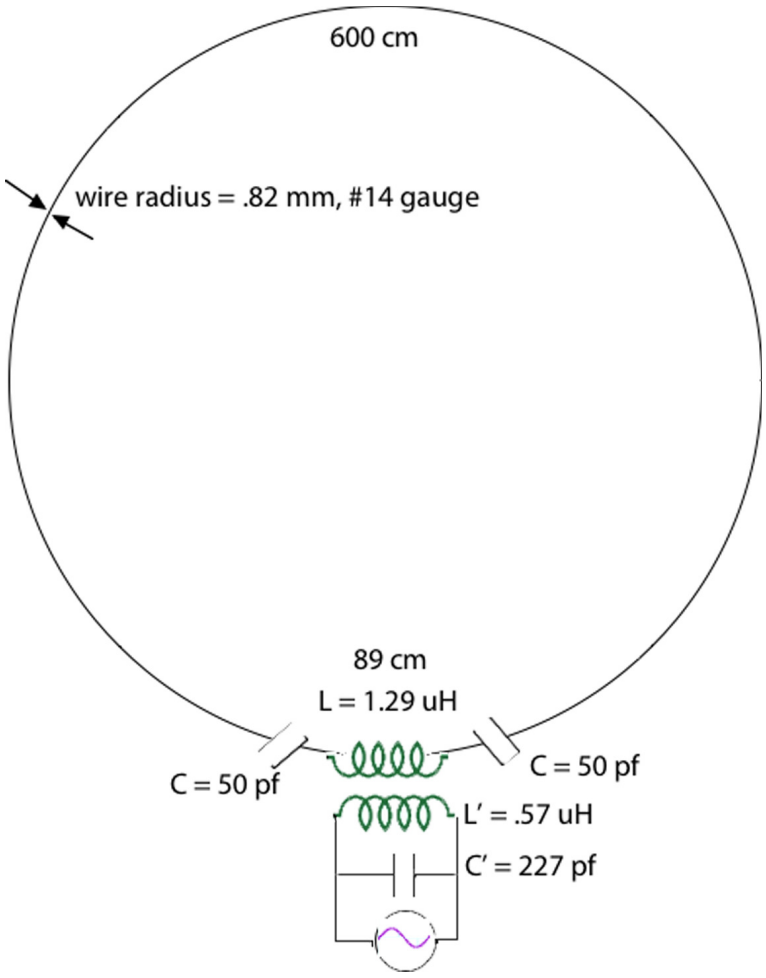

Figure C.1: The design for a single capacitor loop for the 20 meter band from the late 1960s (McKinley II [1964]).

call in the text the design wavelength and design frequency. The k_b value of the resonance is

$$k_b = \frac{14.0}{43.5} = 0.32 \tag{C.3}$$

This is definitely sub-wavelength. He had captured the zero-order resonance very close to the optimal Q (see Fig. 10.5).

The loop is very thin. Using the given dimension $b = 689/2\pi = 110$ cm and $a = 0.82$ mm, the ratio $b/a = 1337$, or an $\Omega = 18.1$.

Bibliography

Agio, M., 2012. Optical antennas as nanoscale resonators. *Nanoscale*, 4 (2012), 692–706. doi:10.1039/C1NR11116G. http://dx.doi.org/10.1039/C1NR11116G. (cited on page 17)

Ahmadi, A. and Mosallaei, H., 2010. Plasmonic nanoloop array antenna. *Opt. Lett.*, 35 (2010), 3706–3708. (cited on pages 7, 63, and 136)

Aizpurua, J.; Hanarp, P.; Sutherland, D. S.; Kall, M.; Bryant, G. W.; and Garcia de Abajo, F. J., 2003. Optical properties of gold nanorings. *Phys. Rev. Lett.*, 90 (Feb 2003), 057401. doi:10.1103/PhysRevLett.90.057401. http://link.aps.org/doi/10.1103/PhysRevLett.90.057401. (cited on page 63)

Akyildiz, I. F.; Jornet, J. M.; and Han, C., 2014. Terahertz band: Next frontier for wireless communications. *Physical Communication*, 12, 0 (2014), 16 – 32. doi:http://dx.doi.org/10.1016/j.phycom.2014.01.006. http://www.sciencedirect.com/science/article/pii/S1874490714000238. (cited on page 10)

Alda, J.; M Rico-Garcis, J.; M. Lopez-Alonso, J.; and G., B., 2005. Optical antennas for nano-photonic applications. *Nanotechnology*, 16 (2005), S230. (cited on pages 6 and 17)

Alu, A.; Salandrino, A.; and Engheta, N., 2007. Parallel, series, and intermediate interconnections of optical nanocircuit elements. 2. nanocircuit and physical interpretation. *J. Opt. Soc. Am. B*, 24, 12 (Dec 2007), 3014–3022. doi:10.1364/JOSAB.24.003014. http://josab.osa.org/abstract.cfm?URI=josab-24-12-3014. (cited on page 64)

Aydin, K. and Ozbay, E., 2007. Capacitor-loaded split ring resonators as tunable metamaterial components. *J. Appl. Phys.*, 101 (2007), 024911. (cited on page 5)

Balanis, C., 2005. *Antenna Theory: Analysis and Design*. Wiley-Interscience, third edn. (cited on pages 12, 32, and 40)

Beck, F. J.; Mokkapati, S.; and Catchpole, K. R., 2010. Plasmonic light-trapping for si solar cells using self-assembled, ag nanoparticles. *Progress in Photovoltaics: Research and Applications*, 18, 7 (2010), 500–504. doi:10.1002/pip.1006. http://dx.doi.org/10.1002/pip.1006. (cited on page 7)

Bharadwaj, P.; Deutsch, B.; and Novotny, L., 2009. Optical antennas. *Adv. Opt. Photon.*, 1, 3 (Nov 2009), 438–483. doi:10.1364/AOP.1.000438. http://aop.osa.org/abstract.cfm?URI=aop-1-3-438. (cited on pages 7 and 17)

Cai, Y.; Li, Y.; Nordlander, P.; and Cremer, P. S., 2012. Fabrication of elliptical nanorings with highly tunable and multiple plasmonic resonances. *Nano Letters*, 12, 9 (2012), 4881–4888. doi:10.1021/nl302428z. http://pubs.acs.org/doi/abs/10.1021/nl302428z. (cited on page 63)

Catchpole, K. R.; Mokkapati, S.; Beck, F.; Wang, E.-C.; McKinley, A.; Basch, A.; and Lee, J., 2011. Plasmonics and nanophotonics for photovoltaics. *MRS BULLETIN*, 36 (JUNE 2011). (cited on page 7)

Chiam, S.-Y.; Singh, R.; Zhang, W.; and Bettio, A. A., 2010. Controlling metamaterial resonances via dielectric and aspect ratio effects. *Appl. Phys. Lett.*, 97 (2010), 191906. (cited on page 7)

Chong, T. K.; Wilson, J.; Mokkapati, S.; and Catchpole, K. R., 2012. Optimal wavelength scale diffraction gratings for light trapping in solar cells. *J. Opt. A*, 14 (2012), 024012 (9pp). (cited on page 7)

Chowdhury, D. R.; Singh, R.; Reiten, M.; Chen, H.-T.; Taylor, A. J.; O'Hara, J. F.; and Azad, A. K., 2011a. A broadband planar terahertz metamaterial with nested structure. *Opt. Express*, 19, 17 (Aug 2011), 15817–15823. doi:10.1364/OE.19.015817. http://www.opticsexpress.org/abstract.cfm?URI=oe-19-17-15817. (cited on page 63)

Chowdhury, D. R.; Singh, R.; Reiten, M.; Zhou, J.; Taylor, A. J.; and O'Hara, J. F., 2011b. Tailored resonator coupling for modifying the terahertz metamaterial response. *Opt. Express*, 19, 11 (May 2011), 10679–10685. doi:10.1364/OE.19.010679. http://www.opticsexpress.org/abstract.cfm?URI=oe-19-11-10679. (cited on pages 5, 7, and 63)

Clark, A. W. and Cooper, J. M., 2011. Nanogap ring antennae as plasmonically coupled serrs substrates. *Small*, 7, 1 (2011), 119–125. doi:10.1002/smll.201001438. http://dx.doi.org/10.1002/smll.201001438. (cited on pages xviii, 63, and 122)

Collin, R., 2003. Limitations of the thevenin and norton equivalent circuits for a receiving antenna. *Antennas and Propagation Magazine, IEEE*, 45 (2003), 119–124. (cited on page 13)

Corrigan, T. D.; Kolb, P. W.; Sushkov, A. B.; Drew, H. D.; Schmadel, D. C.; and Phaneuf, R. J., 2008. Optical plasmonic resonances in split-ring resonator structures: an improved lc model. *Opt. Express*, 16, 24 (Nov 2008), 19850–19864. doi:10.1364/OE.16.019850. http://www.opticsexpress.org/abstract.cfm?URI=oe-16-24-19850. (cited on page 121)

Delgado, V.; Sydoruk, O.; Tatartschuk, E.; MarquÃ©s, R.; Freire, M.; and Jelinek, L., 2009. Analytical circuit model for split ring resonators in the far infrared and optical frequency range. *Metamaterials*, 3, 2 (2009), 57 – 62. doi:10.1016/j.metmat.2009.03.001. http://www.sciencedirect.com/science/article/pii/S1873198809000164. (cited on pages xv, 63, 67, 68, and 121)

Dutta, C. M.; Ali, T. A.; Brandl, D. W.; Park, T.-H.; and Nordlander, P., 2008. Plasmonic properties of a metallic torus. *The Journal of Chemical Physics*, 129, 8 (2008), 084706. doi:10.1063/1.2971192. http://link.aip.org/link/?JCP/129/084706/1. (cited on page 63)

Elhawil, A.; Stiens, J.; DeTandt, C.; Ranson, W.; and Vounckx, R., 2010. An equivalent circuit model of single circular open-ring resonators. *IEEE JOURNAL OF SELECTED TOPICS IN QUANTUM ELECTRONICS*, 16, 2 (MARCH/APRIL 2010). (cited on pages 63 and 67)

Engheta, N.; Salandrino, A.; and Alù, A., 2005. Circuit elements at optical frequencies: Nanoinductors, nanocapacitors, and nanoresistors. *Physical Review Letters*, 95, 9 (08 2005), 095504. http://link.aps.org/doi/10.1103/PhysRevLett.95.095504. (cited on pages 17, 63, and 64)

Enkrich, C.; Wegener, M.; Linden, S.; Burger, S.; Zschiedrich, L.; Schmidt, F.; Zhou, J. F.; Koschny, T.; and Soukoulis, C. M., 2005. Magnetic metamaterials at telecommunication and visible frequencies. *Physical Review Letters*, 95, 20 (11 2005), 203901–. http://link.aps.org/doi/10.1103/PhysRevLett.95.203901. (cited on page 112)

Etchegoin, P. G.; Ru, E. C. L.; and Meyer, M., 2006. An analytic model for the optical properties of gold. *J. Chem. Phys.*, 125 (2006), 164705. (cited on page 88)

Etchegoin, P. G.; Ru, E. C. L.; and Meyer, M., 2007. "erratum: "an analytic model for the optical properties of gold". *J. Chem. Phys.*, 127, 18 (2007), 189901. (cited on page 88)

Fan, M.; Andradec, G. F.; and Brolo, A. G., 2011. A review on the fabrication of substrates for surface enhanced raman spectroscopy and their applications in analytical chemistry. *Analytica Chimica Acta*, 693 (2011), 7–25. (cited on page 7)

Filonov, D. S.; Krasnok, A. E.; Slobozhanyuk, A. P.; Kapitanova, P. V.; Nenasheva, E. A.; Kivshar, Y. S.; and Belov, P. A., 2012. Experimental verification of the concept of all-dielectric nanoantennas. *Applied Physics Letters*, 100, 20 (2012), 201113. doi:http://dx.doi.org/10.1063/1.4719209. http://scitation.aip.org/content/aip/journal/apl/100/20/10.1063/1.4719209. (cited on page 135)

Gardiol, F. and Fournier, Y., February 2006. Salvan: Cradle of wireless, how marconi conducted early wireless experiments in the swiss alps. *Microwave Journal*, (February 2006), 124–136. (cited on page 12)

Goldstein, H., 1980. *Classical Mechanics*. Addison-Wesley Series in Physics. Addison-Wesley Publishing, 2nd edn. (cited on page 22)

Gonzalez, F. and Boreman, G., 2005. Comparison of dipole, bowtie, spiral and log-periodic ir antennas. *Infrared Physics and Technology*, 46 (2005), 418–428. (cited on page 6)

Grover, F. W., 1981. *Inductance Calculations: Working Formulas and Tables*. Instrument Society of America, Research Triangle Park, N.C. (cited on page 56)

Hallen, E., 1938. Theoretical investigations into the transmitting and receiving qualities of antennae. *Nova Actae Regiae Soc.Sci. Upsaliensis*, Ser. IV, 11, No.4 (1938), 1 – 44. (cited on pages 31 and 34)

Halpern, A. R. and Corn, R. M., 2013. Lithographically patterned electrodeposition of gold, silver, and nickel nanoring arrays with widely tunable near-infrared plasmonic resonances. *ACS Nano*, 7, 2 (2013), 1755–1762. doi:10.1021/nn3058505. http://pubs.acs.org/doi/abs/10.1021/nn3058505. (cited on page 63)

Hammond, P. and Sykulski, J., 1994. *Engineering Electromagnetism: Physical Processes and Computation*. Oxford University Press, Oxford. (cited on page 56)

Hanson, G. W., 2006. On the applicability of the surface impedance integral equation for optical and near infrared copper dipole antennas. *IEEE Transactions on Antennas and Propagation*, 54, 12 (2006), 3677–3685. (cited on pages 68, 87, and 100)

Heine, C. and Morf, R. H., 1995. Submicrometer gratings for solar energy applications. *Appl. Opt.*, 34, 14 (May 1995), 2476–2482. doi:10.1364/AO.34.002476. http://ao.osa.org/abstract.cfm?URI=ao-34-14-2476. (cited on page 7)

Hsieh, L.-H. and Chang, K., 2002. Equivalent lumped elements g, l, c, and unloaded q's of closed- and open-loop ring resonators. *Microwave Theory and Techniques, IEEE Transactions on*, 50, 2 (Feb 2002), 453–460. doi:10.1109/22.982223. (cited on page 52)

Iizuka, K., 1965. The circular loop antenna multiloaded with positive and negative resistors. *Antennas and Propagation, IEEE Transactions on*, 13, 1 (1965), 7–20. (cited on pages 31, 45, 48, and 104)

Jackson, J. D., 1999. *Classical Electrodynamics*. Wiley, New York, 3rd edn. (cited on pages 17, 57, 58, and 64)

Johnson, P. B. and Christy, R. W., 1972. Optical constants of the noble metals. *Phys. Rev. B*, 6, 12 (1972), 4370 – 4379. (cited on pages xiii, xvi, 16, 88, 89, 91, and 142)

Kanda, M., 1984. An electromagnetic near-field sensor for simultaneous electric and magnetic-field measurements. *Electromagnetic Compatibility, IEEE Transactions on*, EMC-26, 3 (August 1984), 102–110. (cited on pages 5 and 7)

Katsarakis, N.; Koschny, T.; Kafesaki, M.; Economou, E. N.; and Soukoulis, C. M., 2004. Electric coupling to the magnetic resonance of split ring resonators. *Applied Physics Letters*, 84, 15 (2004), 2943–2945. doi:http://dx.doi.org/10.1063/1.1695439. http://scitation.aip.org/content/aip/journal/apl/84/15/10.1063/1.1695439. (cited on page 112)

Khurgin, J. B. and Sun, G., 2011. Scaling of losses with size and wavelength in nanoplasmonics and metamaterials. *Appl. Phys. Lett*, 99, 21 (2011), 211106. doi:10.1063/1.3664105. http://link.aip.org/link/?APL/99/211106/1. (cited on page 96)

King, R. W. P., 1969. *The Loop Antenna for Transmission and Reception*, vol. 7 of *Inter-University Electronic Series*, chap. 11, 458–482. McGraw-Hill, New York, 1 edn. (cited on page 40)

Klein, M. W.; Enkrich, C.; Wegener, M.; Soukoulis, C. M.; and Linden", S., 2006. Single-slit split-ring resonators at optical frequencies: limits of size scaling. *Opt. Lett.*, 31 (2006), 1259–1261. (cited on page 96)

Koh, A. L.; Fernández-Domínguez, A. I.; McComb, D. W.; Maier, S. A.; and Yang, J. K. W., 2011. High-resolution mapping of electron-beam-excited plasmon modes in lithographically defined gold nanostructures. *Nano Letters*, 11, 3 (2011), 1323–1330. doi:10.1021/nl104410t. http://pubs.acs.org/doi/abs/10.1021/nl104410t. (cited on page 64)

Koh, A. L.; McComb, D. W.; Maier, S. A.; Low, H.; and Yang, J. K. W., 2010. Sub-10 nm patterning of gold nanostructures on silicon-nitride membranes for plasmon mapping with electron energy-loss spectroscopy. *Journal of Vacuum Science Technology B: Microelectronics and Nanometer Structures*, 28, 6 (Nov 2010), C6O45–C6O49. doi:10.1116/1.3501351. (cited on pages 7 and 64)

Krasnok, A. E.; Maksymov, I. S.; Denisyuk, A. I.; Belov, P. A.; Miroshnichenko, A. E.; Simovski, C. R.; and Kivshar, Y. S., 2013. Optical nanoantennas. *Physics-Uspekhi*, 56, 6 (2013), 539. http://stacks.iop.org/1063-7869/56/i=6/a=539. (cited on page 7)

Kraus, J. D. and Carver, K. R., 1973. *Electromagnetics*. McGraw-Hill, 2nd edn. (cited on page 10)

Larsson, E. M.; Alegret, J.; Käll, M.; and Sutherland, D. S., 2007. Sensing characteristics of nir localized surface plasmon resonances in gold nanorings for application as ultrasensitive biosensors. *Nano Letters*, 7, 5 (2007), 1256–1263. doi:10.1021/nl0701612. http://pubs.acs.org/doi/abs/10.1021/nl0701612. (cited on pages 7 and 64)

Lin, C. and Povinelli, M. L., 2009. Optical absorption enhancement in silicon nanowire arrays with a large lattice constant for photovoltaic applications. *Opt. Express*, 17, 22 (Oct 2009), 19371–19381. doi:10.1364/OE.17.019371. http://www.opticsexpress.org/abstract.cfm?URI=oe-17-22-19371. (cited on page 7)

Linden, S.; Enkrich, C.; Wegener, M.; Zhou, J.; Koschny, T.; and Soukoulis, C. M., 2004. Magnetic response of metamaterials at 100 terahertz. *Science*, 306, 5700 (2004), 1351–1353. http://www.sciencemag.org/content/306/5700/1351.abstract. (cited on page 63)

Liu, W.; Miroshnichenko, A.; and Kivshar, Y., 2013. Control of light scattering by nanoparticles with optically-induced magnetic responses. *arXiv:1312.6983v1 [physics.optics]*, (2013). (cited on page 135)

Locatelli, A., 2011. Peculiar properties of loop nanoantennas. *IEEE, Photonics Journal*, 3, 5 (2011), 845–853. (cited on pages xv, 63, 69, and 71)

Locatelli, A.; Angelis, C. D.; Modotto, D.; Boscolo, S.; Sacchetto, F.; Midrio, M.; Capobianco, A.-D.; Pigozzo, F. M.; and Someda, C. G., 2009. Modeling of enhanced field confinement and scattering by optical wire antennas. *Opt. Express*, 17, 19 (2009), 16792–16800. (cited on pages xv, 67, 70, 85, and 100)

Lyshevski, S. and Lyshevski, M., 2000. Analysis, dynamics, and control of microelectromechanical systems. In *American Control Conference, 2000. Proceedings of the 2000*, vol. 5, 3091–3095 vol.5. doi:10.1109/ACC.2000.879134. (cited on page 6)

Maksymov, I. S.; Miroshnichenko, A. E.; and Kivshar, Y. S., 2012. Actively tunable bistable optical yagi-uda nanoantenna. *Opt. Express*, 20, 8 (Apr 2012), 8929–8938. doi:10.1364/OE.20.008929. http://www.opticsexpress.org/abstract.cfm?URI=oe-20-8-8929. (cited on page 7)

McKinley, A. F.; White, T. P.; and Catchpole, K. R., 2013. Theory of the circular closed loop antenna in the terahertz, infrared, and optical regions. *Journal of Applied Physics*, 114, 4 (2013), 044317. doi:http://dx.doi.org/10.1063/1.4816619. http://scitation.aip.org/content/aip/journal/jap/114/4/10.1063/1.4816619. (cited on page 85)

McKinley, A. F.; White, T. P.; Maksymov, I. S.; and Catchpole, K. R., 2012. The analytical basis for the resonances and anti-resonances of loop antennas and metamaterial ring resonators. *J. Appl. Phys.*, 112, 9 (2012), 094911. doi:10.1063/1.4764104. http://link.aip.org/link/?JAP/112/094911/1. (cited on pages 62 and 75)

McKinley II, J. B., 1964. The design of a single capacitor ccrl. Personal papers.

McKinley II, J. B., 1968a. Basic design pattern of a coherent resonant-energy quantum antenna. Personal papers. (cited on pages xviii and 137)

McKinley II, J. B., 1968b. Illustrating quantum areas in wave front and direction of ray; picture. Personal papers. (cited on pages xviii and 137)

McKinley II, J. B., 1968c. Two pictures of closed circuit resonant loop antennas (ccrl). Personal papers. (cited on pages iv and xiii)

Memarzadeh, B. and Mosallaei, H., 2011. Array of planar plasmonic scatterers functioning as light concentrator. *Opt. Lett.*, 36 (2011), 2569–2571. (cited on pages 7, 63, and 136)

Mokkapati, S.; Beck, F. J.; de Waele, R.; Polman, A.; and Catchpole, K. R., 2011. Resonant nano-antennas for light trapping in plasmonic solar cells. *Journal of Physics D: Applied Physics*, 44, 18 (2011), 185101. http://stacks.iop.org/0022-3727/44/i=18/a=185101. (cited on pages 7 and 17)

Novotny, L., 2007a. Effective wavelength scaling for optical antennas. *Phys. Rev. Lett.*, 98 (Jun 2007), 266802. doi:10.1103/PhysRevLett.98.266802. http://link.aps.org/doi/10.1103/PhysRevLett.98.266802. (cited on pages 87 and 96)

Novotny, L., 2007b. *The History of Near-field Optics*, vol. Progress in Optics, 50, chap. 5, 137– 184. Elsevier, Amsterdam, The Netherlands. (cited on page 6)

Novotny, L. and Van Hulst, N., 2011. Antennas for light. *Nature Photonics*, 5, 2 (2011), 83–90. http://www.scopus.com/inward/record.url?eid=2-s2.0-79551607809&partnerID=40&md5=915ef3512d6dec308794a6dcb2721dca. (cited on pages 7 and 17)

Okamoto, T.; Otsuka, T.; Sato, S.; Fukuta, T.; and Haraguchi, M., 2012. Dependence of lc resonance wavelength on size of silver split-ring resonator fabricated by nanosphere lithography. *Opt. Express*, 20, 21 (Oct 2012), 24059–24067. doi:10.1364/OE.20.024059. http://www.opticsexpress.org/abstract.cfm?URI=oe-20-21-24059. (cited on page 96)

Pendry, J. B., 2000. Negative refraction makes a perfect lens. *Phys. Rev. Lett.*, 85, 18 (October 2000), 3966–3969. (cited on page 49)

Pendry, J. B.; Holden, A. J.; Robbins, D. J.; and Stewart, W. J., 1999. Magnetism from conductors and enhanced nonlinear phenomena. *IEEE TRANSACTIONS ON MICROWAVE THEORY AND TECHNIQUES,*, 47, 11 (November 1999). (cited on pages xiv, 5, 7, 17, 49, 50, 52, 53, and 56)

Radkovskaya, A.; Shamonin, M.; Stevens, C. J.; Faulkner, G.; Edwards, D. J.; Shamonina, E.; and Solymar, L., 2005. Resonant frequencies of a combination of split rings: Experimental, analytical and numerical study. *Microwave and Optical Technology Letters*, 46, 5 (2005), 473–476. doi:10.1002/mop.21021. http://dx.doi.org/10.1002/mop.21021. (cited on page 5)

Rockstuhl, C.; Zentgraf, T.; Pshenay-Severin, E.; Petschulat, J.; Chipouline, A.; Kuhl, J.; Pertsch, T.; Giessen, H.; and Lederer, F., 2007. The origin of magnetic polarizability in metamaterials at optical frequencies - an electrodynamic approach. *Opt. Express*, 15, 14 (Jul 2007), 8871–8883. doi:10.1364/OE.15.008871. http://www.opticsexpress.org/abstract.cfm?URI=oe-15-14-8871. (cited on page 112)

Salandrino, A.; Alu, A.; and Engheta, N., 2007. Parallel, series, and intermediate interconnections of optical nanocircuit elements. 1. analytical solution. *J. Opt. Soc. Am. B*, 24, 12 (Dec 2007), 3007–3013. doi:10.1364/JOSAB.24.003007. http://josab.osa.org/abstract.cfm?URI=josab-24-12-3007. (cited on page 64)

Schuller, J. A.; Zia, R.; Taubner, T.; and Brongersma, M. L., 2007. Dielectric metamaterials based on electric and magnetic resonances of silicon carbide particles. *Phys. Rev. Lett.*, 99 (Sep 2007), 107401. doi:10.1103/PhysRevLett.99.107401. http://link.aps.org/doi/10.1103/PhysRevLett.99.107401. (cited on page 135)

Shamonin, M.; Shamonina, E.; Kalinin, V.; and Solymar, L., 2004. Properties of a metamaterial element: Analytical solutions and numerical simulations for a singly split double ring. *J. Appl. Phys.*, 95, 7 (2004), 3778. http://dx.doi.org/doi/10.1063/1.1652251. (cited on pages xiv, 5, 13, 49, 51, 53, 54, and 55)

Shamonin, M.; Shamonina, E.; Kalinin, V.; and Solymar, L., 2005. Resonant frequencies of a split-ring resonator: Analytical solutions and numerical simulations. *Microwave and Optical Technology Letters*, 44, 2 (2005), 133–136. doi:10.1002/mop.20567. http://dx.doi.org/10.1002/mop.20567. (cited on pages xiv, 5, 53, and 54)

Shelby, R. A.; Smith, D. R.; and Schultz, S., 2001. Experimental verification of a negative index of refraction. *Science*, 292, 5514 (2001), 77–79. doi:10.1126/science.1058847. http://www.sciencemag.org/content/292/5514/77.abstract. (cited on pages xiv, 5, 49, 50, and 51)

Silveirinha, M. G.; Alù, A.; Li, J.; and Engheta, N., 2008. Nanoinsulators and nanoconnectors for optical nanocircuits. *Journal of Applied Physics*, 103, 6 (2008), 064305. doi:http://dx.doi.org/10.1063/1.2891423. http://scitation.aip.org/content/aip/journal/jap/103/6/10.1063/1.2891423. (cited on pages xiv and 64)

Smith, D. R.; Padilla, W. J.; Vier, D. C.; Nemat-Nasser, S. C.; and Schultz, S., 2000. Composite medium with simultaneously negative permeability and permittivity. *Phys. Rev. Lett.*, 84 (May 2000), 4184–4187. doi:10.1103/PhysRevLett.84.4184. http://link.aps.org/doi/10.1103/PhysRevLett.84.4184. (cited on pages 5, 10, 49, 54, and 130)

Soukoulis, C. M.; Koschny, T.; Zhou, J.; Kafesaki, M.; and Economou, E. N., 2007. Magnetic response of split ring resonators at terahertz frequencies. *Physica Status Solidi (b)*, 244, 4 (2007), 1181–1187. doi:10.1002/pssb.200674503. http://dx.doi.org/10.1002/pssb.200674503. (cited on pages 63, 67, and 96)

Staffaroni, M.; Conway, J.; Vedantam, S.; Tang, J.; and Yablonovitch, E., 2012. Circuit analysis in metal-optics. *Photonics and Nanostructures - Fundamentals and Applications*, 10, 1 (2012), 166 – 176. doi:10.1016/j.photonics.2011.12.002. http://www.sciencedirect.com/science/article/pii/S1569441011001143. (cited on pages 17, 63, and 65)

Stegun, I. and Abramowitz, M., 1964. *Handbook of Mathematical Functions With Formulas, Graphs and Mathematical Tables*. Applied Mathematics Series, 55. US. Governent Printing Office, WDC. (cited on pages 40 and 94)

Stockman, M. I., 2006. Does nature allow negative refraction with low losses in optical region? *J. Cond. Mat.*, 14 (2006), 0611350. (cited on page 67)

Storer, J. E., 1956. Impedance of the thin wire loop. *Trans. AIEE*, 75 (November 1956), 606 – 619. (cited on pages 5 and 31)

Stratton, J. A., 1941. *Electromagnetic Theory*. McGraw-Hill Book Company, New York and London. (cited on pages 68 and 87)

Sydoruk, O.; Tatartschuk, E.; Shamonina, E.; and Solymar, L., 2009. Analytical formulation for the resonant frequency of split rings. *J. Appl. Phys.*, 105 (2009), 014903. (cited on pages 5 and 121)

Synge, E. H., 1928. A suggested model for extending microscopic resolution into the ultra-microscopic region. *Phil. Mag.*, 6 (1928), 356–362. (cited on page 6)

Tretyakov, S., 2007. On geometrical scaling of split-ring and double-bar resonators at optical frequencies. *Metamaterials*, 1, 1 (3 2007), 40–43. http://www.sciencedirect.com/science/article/pii/S1873198807000060. (cited on pages xv, 63, 67, and 68)

Veselago, V. G., 1968. Tthe electrodynamics of substances with simultaneously negative values of permittivity and permeability. *Soviet Physics Uspekhi*, 10, 4 (January-February 1968). (cited on page 49)

Vial, A. and Laroche, T., 2007. Description of dispersion properties of metals by means of the critical points model and application to the study of resonant structures using the fdtd method. *J. Phys. D: Appl. Phys.*, 40 (2007), 7152–7158. (cited on page 88)

Wang, T.; Zhang, J.; Xue, P.; Chen, H.; Ye, S.; Wang, S.; Yu, Y.; and Yang, B., 2014. Nanotransfer printing of gold disk, ring and crescent arrays and their ir range optical properties. *J. Mater. Chem. C*, 2 (2014), 2333–2340. doi:10.1039/C3TC31338G. http://dx.doi.org/10.1039/C3TC31338G. (cited on page 64)

Wang, W., 2012. Plasmons and optical excitations in graphene rings. *Journal of Physics: Condensed Matter*, 24, 40 (2012), 402202. http://stacks.iop.org/0953-8984/24/i=40/a=402202. (cited on page 7)

Wessel, J., 1985. Surface-enhanced optical microscopy. *J. Opt. Soc. Am. B*, 2 (1985), 21538–1540. (cited on page 6)

West, P.; Ishii, S.; Naik, G.; Emani, N.; Shalaev, V.; and Boltasseva, A., 2010. Searching for better plasmonic materials. *Laser and Photonics Reviews*, 4, 6 (2010), 795–808. doi:10.1002/lpor.200900055. http://dx.doi.org/10.1002/lpor.200900055. (cited on page 135)

Wu, T. T., 1962. Theory of the thin circular loop antenna. *Journal of Mathematical Physics*, 3, 6 (1962), 1301–1304. (cited on pages 5 and 31)

Xu, T.; Wu, Y.-K.; Luo, X.; and Guo, L. J., 2010. Plasmonic nanoresonators for high-resolution colour filtering and spectral imaging. *Nat Commun*, 1, 5 (2010), 59. (cited on page 63)

Yu, Z.; Raman, A.; and Fan, S., 2010. Fundamental limit of light trapping in grating structures. *Opt. Express*, 18, S3 (Sep 2010), A366–A380. doi:10.1364/OE.18.00A366. http://www.opticsexpress.org/abstract.cfm?URI=oe-18-103-A366. (cited on page 7)

Zhan, T. R. and Chui, S. T., 2014. t matrix of metallic wire structures. *Journal of Applied Physics*, 115, 14 (2014), 144901. doi:http://dx.doi.org/10.1063/1.4870863. http://scitation.aip.org/content/aip/journal/jap/115/14/10.1063/1.4870863. (cited on pages xiv, xvii, 52, 60, 61, 112, 113, and 124)

Zhou, J.; Koschny, T.; Kafesaki, M.; Economou, E. N.; Pendry, J. B.; and Soukoulis, C. M., 2005. Saturation of the magnetic response of split-ring resonators at optical frequencies. *Physical Review Letters*, 95, 22 (11 2005), 223902–. http://link.aps.org/doi/10.1103/PhysRevLett.95.223902. (cited on pages xv, 63, 67, and 68)

Zhou, L. and Chui, S. T., 2006. Eigenmodes of metallic ring systems: A rigorous approach. *Phys. Rev. B*, 74 (Jul 2006), 035419. doi:10.1103/PhysRevB.74.035419. http://link.aps.org/doi/10.1103/PhysRevB.74.035419. (cited on pages xiv, 5, 51, 52, 57, and 59)

Zhu, D.; Bosman, M.; and Yang, J. K. W., 2014. A circuit model for plasmonic resonators. *Opt. Express*, 22, 8 (Apr 2014), 9809–9819. doi:10.1364/OE.22.009809. http://www.opticsexpress.org/abstract.cfm?URI=oe-22-8-9809. (cited on pages 63 and 66)